UNIVERSIDADE FEDERAL DE PERNAMBUCO
CENTRO DE TECNOLOGIA E GEOCIÊNCIAS
DEPARTAMENTO DE ENGENHARIA CIVIL E AMBIENTAL
PROGRAMA DE PÓS-GRADUAÇÃO EM ENGENHARIA CIVIL
TECNOLOGIA AMBIENTAL E RECURSOS HÍDRICOS

JULLIANA MELO PINHEIRO DE ARAÚJO

INFLUENCE OF TEMPERATURE AND DIFFUSION ON AEROBIC GRANULAR SLUDGE FOR MUNICIPAL WASTEWATER TREATMENT: EXPERIMENTAL AND MODELING STUDIES

Recife

2022

JULLIANA MELO PINHEIRO DE ARAÚJO

INFLUENCE OF TEMPERATURE AND DIFFUSION ON AEROBIC GRANULAR SLUDGE FOR MUNICIPAL WASTEWATER TREATMENT: EXPERIMENTAL AND MODELING STUDIES

Thesis presented to the Graduate Program in Civil Engineering at the Universidade Federal de Pernambuco, as a partial requirement for obtaining the title of Doctor in Civil Engineering.

Concentration Area: Environmental Technology and Water Resources.

Supervisor: Prof. Dr. Lourdinha Florêncio
External supervisor: Prof. Dr.-Ing. Marc Wichern

Recife

2022

JULLIANA MELO PINHEIRO DE ARAÚJO

INFLUENCE OF TEMPERATURE AND DIFFUSION ON AEROBIC GRANULAR SLUDGE FOR MUNICIPAL WASTEWATER TREATMENT: EXPERIMENTAL AND MODELING STUDIES

Thesis presented to the Graduate Program in Civil Engineering of the Universidade Federal de Pernambuco, Centro de Tecnologia e Geociências, as a partial requirement for obtaining the title of Doctor in Civil Engineering. Concentration Area: Environmental Technology and Water Resources

Approved on: November 18th, 2022

Supervisor: Prof. Dr. Maria de Lourdes Florencio dos Santos – UFPE
External supervisor: Prof. Dr.-Ing. Marc Wichern – Ruhr-Universität Bochum

COMMITTEE MEMBERS

participation by videoconference
Prof. Dr. Bruna Scandolara Magnus (Chair of the committee)
Universidade Federal de Pernambuco

participation by videoconference
Prof. Dr.-Ing. Tito Augusto Gehring (External examiner)
Ruhr-Universität Bochum

participation by videoconference
Prof. Dr. Tiago Rogerio Vitor Akaboci (External examiner)
Centre de Recherche et d'Expertise pour l'Eau

participation by videoconference
Prof. Dr. Osmar Luiz Moreira Pereira Fonseca de Menezes (External examiner)
The University of Arizona

participation by videoconference
Prof. Dr. Rejane Helena Ribeiro da Costa (External examiner)
Universidade Federal de Santa Catarina

pr'aquele por quem sempre junto a massa,
esquento a massa e levo à praça,
meu avô e maior amor,
Heleno Louro

ACKNOWLEDGMENTS

First, I would like to thank my supervisors, Prof. Dr. Lourdinha Florêncio, Prof. Dr.-Ing. Marc Wichern, and Dr.-Ing. Tito Gehring. I feel deeply fortunate to have found those professors who guide me with kindness, patience, brilliant insights, and joy. Thank you very much for supporting and believing in me. I also want to thank the committee members, Dr. Tito Gehring (again!), Prof. Dr. Rejane da Costa, Prof. Dr. Bruna Magnus, Dr. Tiago Akaboci, and Dr. Osmar Menezes, for their valuable contributions.

Throughout my academic journey, extraordinary people have crossed my path and taught me so much that it is impossible to put into words all my gratitude, but I cannot stop trying. Starting with my great friends from the *Laboratório de Saneamento Ambiental* at UFPE, *o querido* LSA, I want to thank: Poliana Januário, with whom I sized, bought the components, assembled, and operated the first reactors of my life, Lis and Jojo (now Frank). Oucilane Alves, my partner in this Ph.D. since the very beginning, with whom I shared many days in Mangueira, working (hard), smiling, sometimes crying, but in the end, getting excellent results. Also, thanks to the best *ICs* LSA has ever seen: Henrique Campos, Marília Marques, and Luciana Soares (whom I also thank for the countless modeling meetings). Likewise, I am also really grateful to all colleagues and professors at the chair, especially Profs. Lourdinha Florêncio, Mário Kato, Wanderli Rogério, and Bruna Magnus, for all their academic insights; the technicians, Ronaldo Fonseca, Danúbia Freitas, and Iago Silva, for all help in the lab; and the secretaries, Andrea Negromonte, Claudiana Araújo, and Juliana Henriques, for all the paperwork assistance.

Crossing the Atlantic also are so many others to whom I am extremely grateful. First, Professor Wichern, for opening the doors of his warm and professional department and guiding me through this German journey. Tito Gehring, one of the most intelligent and generous people I have ever met, who welcomed me to RUB and Bochum and steered me with such care and zeal. Thank you again, Tito! Stephan Berzio, with whom I assembled the fastest reactors on record (Josefina, Januário, and Joana), and shared so many things, starting with an office, followed by a lot of work, papers, german lessons, a little stress (sorry for that, though), many Kekse and Freitagskuchen ("almost" getting me addicted to sugar!). Max Bremkes, a genius with his camera and so dedicated, thanks for helping us take care of the reactors and sometimes translating German into German. At Ruhr-Universität Bochum, *die liebe* RUB, I've learned so much! Thanks to Stefan Krimmler, Hans-Gerd Berkhoff, Andrea Rademacher, Edith Nettmann, Kaja Nauroth, Lothar Klauke, Carolin Wehrheim, and Tobias Littfinski for all kinds of support and the funny *Feierabende* full of laughs, scientific talks, and perhaps one or two beers.

"'do you have a favorite saying?' asked the boy.
'yes,' said the mole
'what is it?'
'if at first you don't succeed, have some cake.'
'I see, does it work?'
'every time.'"

Charlie Mackesy

ABSTRACT

Influence of temperature and diffusion on aerobic granular sludge for municipal wastewater treatment: experimental and modeling studies

Aerobic granular sludge (AGS) has been widely used in recent decades as an alternative to conventional activated sludge systems for treating domestic sewage. AGS increases biomass retention and sedimentation and enables the simultaneous removal of nutrients and organic matter, making it applicable to a wide range of wastewater types, temperatures, and reactor scales, as evidenced in the literature. However, previous studies investigating the roles of engineering parameters such as volumetric organic load, temperature, and hydraulic retention time in the granulation process in AGS systems show yet no consensus, hindering the development of a precisely predictable system. In this context, the mathematical modeling of these systems may provide valuable insights for a more comprehensive understanding of microbial biochemical conversions in AGS systems. Hence, this work investigates the influence of temperature, cycle configuration, and influent composition in sequencing batch reactors (SBR) systems with AGS of different scales, focusing on understanding sensitive parameters through mathematical modeling. For this purpose, four different methodological strategies were used. Initially, two different cycle configurations in a pilot-scale (PS) SBR (115 L) were used to cultivate AGS without inoculum at approximately 30 °C. Data from these experiments were then used to implement and calibrate the biofilm model proposed by Wanner and Gujer (1986) associated with the activated sludge model n° 3 (ASM3 – GUJER et al., 1999). The model calibration showed high sensitivity of diffusion-associated parameters such as boundary layer thickness. To assess these results, we analyzed diffusion, boundary layer thickness, as well as the presence and size of aerobic/anaerobic layers from O_2 micro-profiles using granules (1.4-2.0 mm diameter) collected from two lab-scale (LS) SBR (9.1 and 11.2 L) operated at 20 and 30 °C. The LS reactors were also monitored to investigate the influence of temperature on AGS formation, morphology, and stability. This approach to model implementation enabled the description of a non-steady state AGS system performance related to solids and COD removal. However, it could not capture the complexity of nitrogen removal processes in AGS (under different redox conditions) by assuming a single diameter for all granules. The temperature, in turn, was a primary factor in determining AGS stability, formation, and morphology in the LS reactors. Granules formed at 30 °C (LS) were larger, more compact, and considerably more stable against system disturbances. In addition, a prolonged anaerobic phase or the insertion of air pulses during slow feeding were configuration strategies for SBR cycles that improved the granulation process. The wastewater composition directly affected microbial diversity and system performance, with lower efficiency observed when lower loads were applied. Finally, implementing mathematical models in non-steady-state systems allowed us to analyze the influence of setting fixed parameters, with the number of granules and boundary layer thickness among the most sensitive parameters.

Keywords: aerobic granular sludge (AGS); mathematical modeling; real municipal wastewater; sequencing batch reactor (SBR); warm climate.

RESUMO

Influência da temperatura e difusão no lodo granular aeróbio para tratamento de esgoto sanitário: estudos experimentais e de modelagem

O lodo granular aeróbio (LGA) vem sendo amplamente utilizado nas últimas décadas como alternativa ao sistema de lodos ativados convencional para o tratamento de águas residuárias domésticas. Essa tecnologia aumenta a retenção de biomassa e sedimentação e permite a remoção simultânea de nutrientes e matéria orgânica, tornando-o aplicável a grande diversidade de águas residuárias, temperaturas e escalas, como evidenciado na literatura. Entretanto, estudos anteriores investigando os papéis de parâmetros de engenharia, como carga orgânica volumétrica, temperatura e tempo de retenção hidráulica no processo de granulação em sistemas LGA ainda não mostram consenso, não sendo ainda possível desenvolver um sistema precisamente previsível. Neste contexto, a modelagem matemática destes sistemas pode fornecer conhecimentos valiosos para uma maior compreensão das conversões bioquímicas microbianas nos grânulos. Sendo assim, esse trabalho teve como objetivo investigar a influência da temperatura, configuração do ciclo e composição afluente em sistemas SBR com LGA de diferentes escalas, concentrando-se na compreensão de parâmetros sensíveis durante a implementação de modelos matemáticos. Para isso, quatro diferentes estratégias metodológicas foram utilizadas. Inicialmente, diferentes configurações de ciclo foram utilizadas em um RBS em escala piloto (115 L) para o cultivo de LGA sem inóculo sob temperaturas próximas a 30 °C. Os dados provenientes destes experimentos foram então utilizados para implementar e calibrar o modelo de biofilme proposto por Wanner e Gujer (1986) associado ao modelo de lodo ativado n° 3 (ASM3 – GUJER et al., 1999). Durante a calibração do modelo, uma alta sensibilidade dos parâmetros associados à difusão, tais como espessura da camada limite, foi observada. Para melhor entender estes resultados, grânulos (diâmetro entre 1.4 e 2.0 mm) provenientes de dois RBS em escala de laboratório (LS, 9,1 e 11,2 L) foram utilizados para analisar difusão de oxigênio, a presença e o tamanho de camadas aeróbias/anaeróbias, bem como estimar a espessura da camada limite através de micro-perfis de O_2. Os reatores LS (operados a 20 e 30 °C, respectivamente) também foram monitorados buscando investigar a influência da temperatura na formação, morfologia e estabilidade do LGA. Esta abordagem de implementação do modelo permitiu a descrição do desempenho de um sistema LGA em estado não estacionário em termos de sólidos e remoção de DQO. Entretanto, não foi possível cobrir a complexidade dos processos de remoção de nitrogênio nos grânulos (e suas diferentes condições redox) assumindo um único diâmetro para todos. A temperatura, por sua vez, foi um fator decisivo na estabilidade, formação e morfologia do LGA nos reatores LS. Os grânulos formados a 30 °C (LS) eram maiores, mais compactos e consideravelmente mais estáveis contra distúrbios no sistema. Além disso, uma fase anaeróbia mais prolongada e/ou a inserção de pulsos de ar durante a alimentação lenta foram estratégias de configuração para ciclos SBR que, de modo geral, melhoraram o processo de granulação. A composição do afluente afetou diretamente a diversidade microbiana e o desempenho nos sistemas, sendo observada menores eficiências quando cargas mais baixas foram aplicadas. Por fim, a implementação de modelos matemáticos em um sistema em estado não estacionário permitiu analisar a influência da configuração de parâmetros fixos, estando o número de grânulos e a espessura da camada limite entre os parâmetros mais sensíveis.

Palavras-chave: clima tropical; esgoto municipal real; logo granular aeróbio (LGA); modelagem matemática; reatores em bateladas sequenciais (RBS).

KURZFASSUNG

Einfluss von Temperatur und Diffusion auf aeroben granulierten Schlamm für die kommunale Abwasserreinigung: Experimentelle Untersuchungen und Modellierung

Aerob granulierter Schlamm (AGS) wurden in den letzten Jahrzehnten häufig als Alternative zu herkömmlichen Belebtschlammsystemen eingesetzt. AGS verbessert den Rückhalt der Biomasse sowie die Sedimentation und ermöglicht die gleichzeitige Entfernung von Nährstoffen und organischen Belastungen, sodass er für ein breites Spektrum von Abwässern, Temperaturbereichen und Größenklassen geeignet ist. Bisherige Studien, welche die Rolle von Ingenieurgrößen wie die organische Raumbelastung, die Temperatur und die hydraulische Verweilzeit im Granulierungsprozess in AGS-Systemen untersucht haben, zeigen jedoch noch keinen Konsens, was die Entwicklung dieser Systeme erschwert. Hier kann die mathematische Modellierung das grundlegende Verständnis der mikrobiellen biochemischen Umwandlungen in AGS-Systemen deutlich verbessern. Mit dieser Arbeit wird der Einfluss der Temperatur, der Zykluskonfiguration und der Zulaufzusammensetzung in Sequencing Batch-Reaktoren (SBR) mit AGS unterschiedlicher Größenordnung untersucht. Insbesondere liegt der Schwerpunkt auf dem Verständnis sensibler Parameter durch mathematische Modellierung. Zu diesem Zweck wurden vier verschiedene Betriebsstrategien erprobt. Hierzu zählen zwei unterschiedliche Zykluseinstellungen in einem SBR (115 L) im halbtechnischen Maßstab, um AGS ohne Inokulum bei etwa 30 °C zu kultivieren. Die Daten aus diesen Versuchen wurden dann zur Implementierung und Kalibrierung des von Wanner und Gujer (1986) entwickelten Biofilm-Modells in Verbindung mit dem ASM3 (GUJER et al., 1999) verwendet. Die Modellkalibrierung zeigte eine hohe Sensibilität der Diffusion im Zusammenhang mit Parametern wie der Grenzschichtdicke. Um diese Ergebnisse zu bewerten, wurden die Diffusion, die Grenzschichtdicke, der Sauerstoff sowie die Größe von aeroben/anaeroben Schichten anhand von O_2-Mikroprofilen untersucht. Hierzu wurden Granula (1,4-2,0 mm Durchmesser) aus zwei SBR (9,1 und 11,2 L) im Labormaßstab (LS) entnommen, die bei 20 und 30 °C betrieben wurden. Anhand der LS-Reaktoren wurde ebenfalls der Einfluss der Temperatur auf die AGS-Bildung, Morphologie und Stabilität untersucht. Hieraus ergaben sich Ansätze für die Modellimplementierung zur Beschreibung der Leistung eines AGS-Systems im Stationärzustand in Bezug auf die Feststoffentfernung und die CSB-Elimination. Allerdings konnten die komplexen Stickstoffentfernungsprozesse in AGS (unter verschiedenen Redoxbedingungen) nicht erfasst werden, da ein einziger Durchmesser für alle Granula angenommen werden musste. Die Temperatur war ein Hauptfaktor für die Stabilität, Bildung und Morphologie von AGS in den LS-Reaktoren. Die bei 30 °C gebildeten Granula (LS) waren größer, kompakter und wesentlich stabiler gegenüber Systemstörungen. Darüber hinaus konnten eine verlängerte anaerobe Phase und die Zufuhr von Luftimpulsen während der langsamen Beschickung die Reinigungsprozesse deutlich verbessern. Die Zusammensetzung des Abwassers wirkte sich dabei direkt auf die mikrobielle Diversität und die Systemleistung aus, wobei eine geringere Effizienz beobachtet wurde, wenn geringere Belastungen vorlagen. Zusammenfassend lässt sich sagen, dass die Anwendung mathematischer Modelle in nicht-stationären Systemen es ermöglicht, den Einfluss der Einstellung fester Parameter zu analysieren, wobei der Granulierungsgrad und die Dicke der Grenzschicht zu den sensiblen Parametern gehört.

Schlüsselwörter: aerober granulierter Schlamm (AGS); mathematische Modellierung; reale kommunale Abwässer; Sequencing-Batch-Reaktor (SBR); warmes Klima.

LIST OF FIGURES

LIST OF TABLES

LIST OF ACRONYMS

AGS	Aerobic granular sludge
AL	Advective link
AS	Activated sludge
ASM1	Activated sludge model n.° 1
ASM2	Activated sludge model n.° 2
ASM2d	Activated sludge model n.° 2d
ASM3	Activated sludge model n.° 3
AZT	Aerobic zone thickness
BAF	Biological aerated filters
BASR	Biofilm airlift suspension reactor
BC	Biofilm compartment
BLR	Boundary layer resistance
BOD	Biological oxygen demand
COD	Chemical oxygen demand
DL	Diffusive link
DO	Dissolved oxygen
DPAO	Denitrifying polyphosphate accumulating organisms
EBPR	Enhanced biological phosphorus removal process
EPS	Exopolymeric substances
f_A	Inert particulate fraction of particulate COD
f_B	Inorganic fraction of total suspended solids
f_S	Inert dissolved fraction of total COD
GAO	Glycolgen accumulating organisms
HSG	Hochschulgruppe
LS	Lab-scale
MBBR	Moving bed biofilm reactor
MC	Mixed compartment
MLSS	Mixed liquor suspended solids
NH_3	Free ammonia
NH_4^+	Ionized ammonia
NO_2^-	Nitrite

NO_3^-	Nitrate
OCR	Oxygen consumption rate
OLR	Organic loading rate
OM	Organic matter
PAO	Polyphosphate accumulating organisms
PHA	Polyhydroxy alkanoates
PS	Pilot-scale
RA	Relative abundance
S_A	Rapidly hydrolyzable COD fraction for ASM2 and ASM2d
S_{Alk}	Soluble alkalinity as carbonic acid (H_2CO_3)
S_F	Easily degradable COD fraction for ASM2 and ASM2d
S_I	Soluble inert COD fraction for ASM series
S_{O2}	Dissolved oxygen
S_{NHx}	Ammonia nitrogen
S_{NO}	Nitrate and Nitrite nitrogen
S_{N2}	Dissolved nitrogen gas (only product of denitrification)
S_S	Easily or rapidly biodegradable COD fraction for ASM series
S_{XS}	Dissolved biodegradable COD fraction of slow degradation by Lange (2018)
SBR	Sequencing batch reactor
SND	Simultaneous nitrification and denitrification
SRT	Sludge retention time (Sludge age)
SVI	Sludge volume index
$th_{biofilm}$	Biofilm thickness
$th_{biofilm,virtual}$	Virtual biofilm thickness
TN	Total nitrogen
TOC	Total organic carbon
TSS	Total suspended solids
tWW	Filtered treated municipal wastewater
UASB	Upflow anaerobic sludge blanket
VSS	Volatile suspended solids
WWTP	Wastewater treatment plant
X_A	Autotrophic microorganisms COD fraction for ASM series

X_H	Heterotrophic microorganisms COD fraction for ASM series
X_I	Particulate undegradable organics
X_{MI}	Particulate mineral fraction in TSS for DWA-A 131 (ATV-DVWK, 2016)
X_{PAO}	Phosphorus accumulating microorganisms COD fraction for ASM2 and ASM2d
X_S	Heavy and slowly degradable COD fraction for ASM series
X_{SS}	Total suspended solids
X_{Sto}	Organic storage products of heterotrophs (but not included in their mass)

CONTENTS

1 INTRODUCTION

The conventional activated sludge (AS) system has been widely used since its first implementation in 1924 (JENKINS & WANNER, 2014). A better understanding of fundamental microbial-driven mechanisms allows for a continuous improvement of this technology leading to better degradation rates and lower resource consumption. For instance, the aerobic granular sludge (AGS), first reported by Mishima and Nakamura (1991) and only recently upscaled (e.g., PRONK et al., 2015 and DE GRAAFF et al., 2020), provides a big step in reducing the AS technology footprint, among other advantages.

Short settling times are required in AGS due to its compact and dense structure. Overall, AGS systems enable about three to five times more biomass per liter of wastewater than conventional activated sludge. Thus, sedimentation tanks become unnecessary for this technology, allowing wastewater treatment plants (WWTP) with smaller reactor volumes and substantially reducing the used area (SARMA et al., 2017). The microenvironments within granules are another advantage provided by diffusion gradients, allowing the growth of bacteria with different metabolic functions and environmental requirements. Therefore, several stages of the conventional aerobic treatment process occur inside the biomass aggregates, allowing the simultaneous biological removal of organic matter and nutrients without high recirculation rates (WINKLER et al., 2013).

This technology is considered a relevant achievement in 21st-century environmental biotechnology (SARMA et al., 2017), as seen in the many studies applied to diverse types of wastewater and temperature ranges. For example, the use of AGS for treating municipal wastewater (KOSAR et al., 2022), high-saline municipal wastewater (THWAITES et al., 2021), industrial wastewater (COSTA et al., 2022), and even influents rich in azo dyes (FAN et al., 2022) and other difficult-to-degrade compounds, as phenol and thiocyanate (TOMAR et al., 2022). Different scales and operating temperatures of the reactors are also reported, e.g., Jiang et al. (2016) monitored a 17 L sequencing batch airlift reactor fed with synthetic sewage at 10-14 °C, Thwaites et al. (2018) a 61.5-63.5 L SBR fed with municipal wastewater at 18.8-27.2 °C, and Bassin et al. (2019) a 1.5 L SBR at temperatures above 28 °C.

However, a straightforward comparison between these temperatures documented in various reports is still very difficult. There are many other important factors, along with these studies mentioned above, such as the influent composition (organic loads, salinity, solids fractions, etc.), reactor scale, operational conditions, or inoculum. Another relevant aspect of AGS is that mass-transfer processes are potential rate-limiting steps for biological conversion

processes and are also temperature-dependent. Diffusion (and the diffusion coefficient, D), for example, depends directly on temperature (T) and inversely on the solution viscosity (μ, which also decreases with increasing temperature) since $D \cdot \mu \cdot T^{-1}$ is constant (STEWART, 2003). Higher operating temperatures result in higher diffusion rates, but the granular structure and density also affect the diffusion rate since they determine the effective diffusion coefficient within the biofilm. Hence, all these factors directly affect the denitrification and phosphorus removal processes. Furthermore, this also significantly limits the transference transferability of findings concerning the effects of different operating temperatures in conventional activated sludge systems on AGS.

For instance, a lower denitrification rate is usually expected at low temperatures due to the reduced anoxic zones, resulting in an increased dissolved oxygen concentration within the granules (DE KREUK et al., 2005). Therefore, the granules sizes are another key parameter regarding oxygen transport e.g., Jiang et al. (2016) reported a high total nitrogen removal efficiency (around 80% after complete granulation) at temperatures between 10 and 14 ∘C with larger granules (the majority ranged from 350 to 1000 μm). At higher temperatures, in turn, a decrease in biological phosphorus removal is expected due to the favoring of the growth of glycogen accumulating organisms (GAOs) over phosphate accumulating organisms (PAOs) (LOPEZ-VAZQUEZ et al., 2009). Still, a total phosphate removal was reported for an SBR fed with synthetic influent at 30°C after the system stabilization (BASSIN et al., 2012).

In this sense, mathematical modeling emerges as a helpful tool while studying AGS systems, considering that it can provide valuable information for a basic understanding of microbial biochemical conversions (WICHERN et al., 2018). The first mathematical models aimed to describe biochemical processes (e.g., organic matter and nutrient removal) during activated sludge wastewater treatment and were developed in the late 1970s (GUJER, 2010). To date, the most notable ones were designed for conventional AS systems, named the activated sludge model series (ASM, HENZE et al., 2000). However, unlike processes in conventional systems, applying these models to describe processes in AGS requires modification or association with biofilm models since substrate concentration gradients are determinants in these processes. For example, Baeten et al. (2018) verified that it was possible to implement activated sludge model n. 2 (ASM2d, GUJER et al., 1995) with modified apparent half-saturation coefficients to lump reaction-diffusion processes within the granules while modeling a 3L-SBR. Nevertheless, most studies in the literature present models exclusively for AGS systems in a steady state (BAETEN et al., 2018; SUN et al., 2019; CHEN et al., 2020a).

The Graduate Program in Civil Engineering (PPGEC), with an emphasis on environmental technology, at the Environmental Sanitation Laboratory (LSA) in the Federal University of Pernambuco (UFPE) has a research line for AGS. Initially, the group's research sought to understand the influence of different effluent volumetric exchanges (ARAÚJO et al., 2016; SILVA, 2017a) and different ascensional airflow velocities (SILVA, 2017a; ALVES, 2017) during the formation of aerobic granules in a pilot-scale (PS) system (115L SBR). However, it was found that despite the presence of microenvironments in the granules, nutrient removal did not occur satisfactorily, indicating that other strategies should be used to ensure adequate oxi-reduction conditions to optimize nitrogen and phosphorus removal.

In this regard, Sales et al. (2018) and Dantas (2018) added an anoxic phase to the operational cycle of their experiments (same SBR), obtaining higher removal efficiencies but with more unstable granules. The need for a better understanding of the processes inside the granules was then even more evident, such as mass transfer, optimal dissolved oxygen concentration, or the influence of temperature and wastewater composition. As mathematical modeling is a tool capable of improving the monitoring of processes in biological reactors and obtaining operational parameters that allow optimizing the operation in effluent treatment systems, this work aimed to initiate research on mathematical models applied to AGS at LSA-UFPE. Moreover, considering the available database composed of experiments in a non-steady state and the literature gap, the proposed model allowed modeling AGS in SBR during the start-up phase. Lastly, additional experiments were performed to directly investigate the influence of temperature as an isolated factor and micro-profiles for analyzing diffusion processes and parameters.

1.1 OVERALL OBJECTIVE

To investigate the influence of temperature, cycle configuration, and influent composition in SBR systems with AGS of different scales, focusing on understanding sensitive parameters while implementing mathematical models.

1.2 SPECIFIC OBJECTIVES

(1). To monitor the formation, stability, and treatment performance of a pilot-scale (PS) AGS system while treating domestic wastewater with low COD and nutrient loadings under high temperatures and different SBR cycle arrangements;

(2). To implement mathematical models of activated sludge (ASM3, GUJER et al., 1999) and biofilm (WANNER & GUJER, 1986) to describe simultaneous nutrient and organic matter removal processes observed experimentally in a PS AGS system during the granulation process (non-steady state);

(3). To elucidate the influence of the operational temperature (20 and 30 °C) on the granule formation, morphology, and stability in lab-scale (LS) SBR treating municipal wastewater and how this reflects in conversion processes and long-term performance;

(4). To evaluate the influence of temperature, structure, and substrate on diffusion aspects of different granules (i.e., presence/absence of anoxic zones, boundary layer resistance) with the aid of microsensors.

2   LITERATURE REVIEW

This chapter covers some principles and applications inherent to the biological treatment of wastewater, emphasizing: the removal of nutrients and organic matter; the use of sequencing batch reactors (SBR); the fundamentals, operational conditions, and particularities of the AGS technology; and a straightforward approach to mathematical modeling and its applications with a focus on biofilm models and software.

2.1   BIOLOGICAL TREATMENT OF WASTEWATER

In natural ecosystems, such as rivers and lakes, different organisms play an essential role in the degradation of various organic pollutants. For example, the organisms involved in the self-depuration processes of water bodies may be attached to surfaces (e.g., stones, aquatic plants) or suspended in the water column, e.g., bacterial flocs, plankton, and crustaceans. Observing these ecosystems, biological wastewater treatment systems emerged, designed to provide an artificial environment favorable for these natural processes to occur in a more accelerated/efficient manner. Namely, the high microbial concentration and the greater availability of energy and substrates of the artificial/designed systems accelerate the biodegradation process, allowing high removal efficiencies in short periods (GEBARA, 1999).

Among the pollutants present in domestic effluents, three can be highlighted: organic matter (OM), nitrogen (N), and phosphorus (P). The organic matter, if discharged in considerable concentration into water bodies (disposal of effluents without treatment or after ineffective treatment), will cause one of the significant problems of water pollution, the rapid consumption of dissolved oxygen (DO), an essential component for aerobic aquatic life. The high concentration of nutrients (nitrogen and phosphorus), in turn, makes the environment conducive to accelerated growth of algae, also promoting a drop in the concentration of DO to critical levels, consumed by the decomposition of dead algae, in a process called eutrophication. Other problems associated with the presence of nitrogenous compounds in effluent discharge are: i) the presence of free ammonia (NH_3), which is toxic to aquatic fauna; and ii) nitrate (NO_3^-), an intermediate product of nitrogen degradation associated with methemoglobinemia disease ("blue baby syndrome") (VON SPERLING, 2005).

The principal organic components of sanitary sewage are carbohydrates, fats, proteins, amino acids, and volatile acids (approximately three-quarters of the organic carbon). Besides, small quantities of hormones, vitamins, surfactants, antibiotics, hormonal contraceptives,

purines, pesticides, hydrocarbons, and pigments can be found. In general, there is no practical need to quantify organic matter in these terms because of the laboratory difficulty arising from the diversity of compounds and the existence of indirect methods for quantifying their polluting potential. Two of the main categories of OM quantification are the measurement of oxygen consumption (Chemical Oxygen Demand – COD, and Biological Oxygen Demand – BOD, considered by many the most critical parameters in characterizing the degree of pollution of a body of water) and the quantification of total organic carbon (TOC) (METCALF & EDDY, 2016).

The primary biological removal of OM is done by heterotrophic microorganisms, which use carbon for energy production and growth. The process starts on the surface of the microbial clusters, where hydrolysis or other enzyme-catalyzed transformation occurs to fractionate complex chain organic molecules (carbohydrates, lipids, and proteins). After this, the cells uptake the fractionated compounds and metabolize them through exogenous respiration, either for synthesizing organic matter (anabolism) or obtaining energy (catabolism). After degrading all biodegradable organic matter, the microorganisms perform endogenous respiration, where the new cells consume their own cellular material to get the energy to be used in cell maintenance (VAN HAANDEL & MARAIS, 1999).

Commonly, organic matter is removed through an oxidative pathway, where an oxidizing agent or electron acceptor (e.g., oxygen, nitrate, nitrite, sulfate) is used during cellular respiration. When there is more than one oxidizing agent available in the medium, the one that produces the higher amount of energy will be used first, thus enabling a greater cellular yield. Since oxygen is usually the most electronegative available element, it will be used preferentially over other receptors. In this way, biological treatment systems can be classified according to the primary electron acceptor used: 1) aerobic: when DO is available; 2) anoxic: when there is no oxygen but oxidized forms of nitrogen or sulfur (e.g., nitrite, nitrate, sulfate); 3) anaerobic: absence of DO or oxidized forms (METCALF & EDDY, 2016).

Among the nitrogenous compounds present in domestic effluents, two forms stand out: organic nitrogen, which can be dissolved or in suspension (urea, amino acids, amino group), and ammoniacal nitrogen (gaseous, free ammonia – NH_3, and ionized ammonia – NH_4^+). On the other hand, the oxidized forms (nitrite, NO_2^-, and nitrate, NO_3^-) have insignificant concentrations under typical conditions. In a nutshell, the biological removal of these compounds can occur through biomass synthesis or biological processes, such as anammox, nitrification, and denitrification (VAN HANDEEL & MARAIS, 1999).

Nitrification corresponds to the biological oxidation process of ammoniacal nitrogen, where aerobic chemoautotrophic bacteria use DO as an electron acceptor. This oxygen consumption is done in two steps and is responsible for converting ammoniacal nitrogen into nitrite (intermediate product) and this nitrate (final product). The biological reduction of nitrate or nitrite can happen in two ways: 1) assimilation, in which, due to the absence of ammoniacal nitrogen, these compounds are reduced from nitrate, or 2) dissimilation (denitrification), where the nitrite and nitrate molecules, under anoxic conditions, are used as electron acceptors for the oxidation of OM, being reduced to nitrogen gas. Mainly, denitrification is performed by facultative heterotrophic bacteria, which modify their enzymatic system when there is no DO available in the medium (METCALF & EDDY, 2016). Figure 1 presents a summary scheme proposed by Winkler and Straka (2019), showing the main biological processes involved in nitrogen removal from wastewater.

Figure 1. Microbial nitrogen transformations for removing ammonia from wastewater, including: nitrification/denitrification, nitritation/denitritation, partial nitritation/anammox, and assimilation. Green arrows indicate autotrophic processes, where the nitrogen species are the electron donor, and brown arrows indicate the need for a non-nitrogen electron donor (organic carbon, or water for photosynthesis).
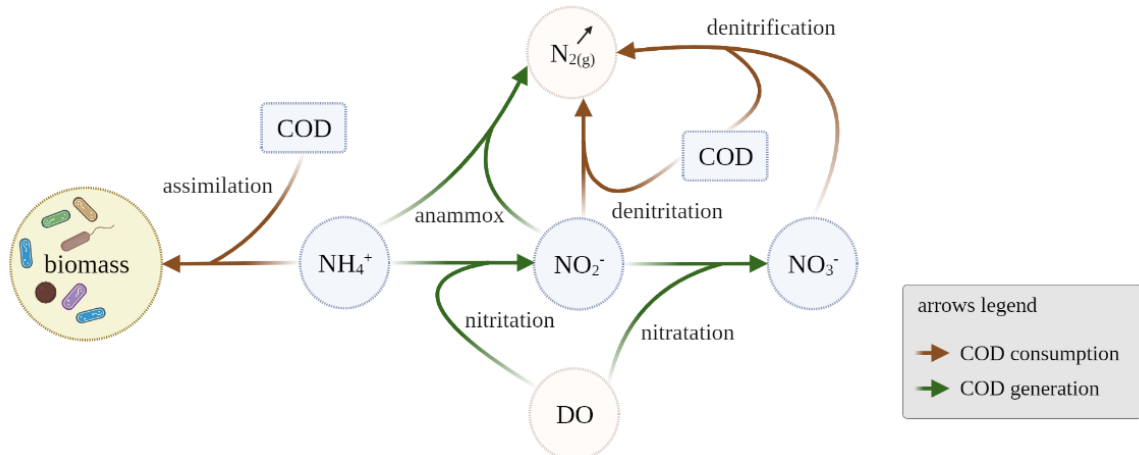
Source: adapted from Winkler and Straka (2019).

Phosphorus is also found in different forms in domestic wastewater; these include organic (e.g., phytin, phospholipids, and nucleic acids), complex inorganic (polyphosphates mainly from detergents), and soluble inorganic orthophosphate (readily available for biological assimilation/consumption). Usually, orthophosphate is the predominant form of phosphorus in effluents undergoing secondary treatment (BLACK, 1980). Phosphorous removal, in its turn, in WWTP, can occur through physicochemical (adsorption and precipitation) or biological processes (METCALF & EDDY, 2016).

Currently, the enhanced biological phosphorus removal process (EBPR) is the most widely used biological treatment. This consists of an activated sludge system adapted for

phosphorus removal by enrichment of polyphosphate accumulating organisms (PAO) and/or denitrifying phosphorus accumulating organisms (DPAO). Such microorganisms are able to store phosphate as intracellular polyphosphate via alternating anaerobic-aerobic conditions. Initially, the organic compounds are converted into orthophosphates or polyphosphates (which, after hydrolysis, are also converted into orthophosphates). Then, under anaerobic conditions, OM is taken up by PAO/DPAO, using glycolysis of glycogen and intracellular polyphosphate cleavage to conserve energy and build up intracellular reserves of polyhydroxyalkanoates (PHA), resulting in the release of phosphate. Hereafter, the same system must be provided with electron acceptors (aerobic environment - PAO, or anoxic environment - DPAO) so that the PAO/DPAO consume the stored PHA and accumulate (intracellularly) glycogen and polyphosphate reserves, effectively removing phosphate from wastewater (MINO et al., 1998).

A similar metabolism to the PAO metabolism is carried out by glycogen accumulating organisms (GAO), utilizing the organic carbon without phosphate transformations. Thus, one should use mechanisms that favor the development of PAO over GAO, such as reducing the accumulation of nitrite in the system and using lower concentrations of dissolved oxygen (SAITO et al., 2004; COMA et al., 2012; CARVALHEIRA et al., 2014).

2.2   SEQUENCING BATCH REACTORS (SBR)
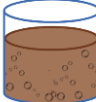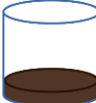
Instructively, biological wastewater treatment systems can be divided into conventional systems (e.g., aeration tanks with activated sludge and stabilization ponds), and compact systems, with the primary difference between them being the reduction of the spaces used by compact system components. The main strategy used for compacting the systems is the development of biological sludge in the form of biofilms, increasing the concentration of biomass and/or improving sedimentation. Among the main compact methods currently used, it can be highlighted: the upflow anaerobic sludge blanket (UASB); the biological aerated filters (BAF); the biofilm airlift suspension reactors (BASR), the moving bed biofilm reactor (MBBR), and sequencing batch reactors (SBR) (BASSIN, 2011).

The SBRs are reactors that operate in intermittent flow (cycle regime). Each system consists of a single tank that, during the operation cycles, assumes the function of a biological reactor and clarifier. The same reactor will be used for biological reaction and settling in a temporal sequence, different from the conventional continuous systems in which these phases occur simultaneously but in separate tanks. Considering the system's versatility, which allows the operation with different oxi-reducer conditions in the same operational cycle, specific

operational conditions are more easily manipulated to optimize the biological removal of organic matter, nitrogen, and phosphorus in the treatment of domestic wastewater (ARTAN & ORHON, 2005).

In general, an SBR cycle is composed of four or five stages (Table 1). Initially (feeding phase), the reactor is fed with influent sewage up to a fixed or variable maximum level, depending on the availability of the influent. In the second stage (reaction), the aerators are turned on, supplying oxygen for the oxidation of organic matter and nitrification. Aeration may be interrupted if the system aims at denitrification, activating an agitation mechanism to guarantee mixing in an anoxic period. Next (settling), the aerators/agitators are turned off for sludge sedimentation. In the last phase (discharge), the clarified effluent is discharged up to the established minimum, and a safety volume should be guaranteed for sludge entrainment. Another phase (standby/adjustment) can be added for eventual system maintenance, cycle changes, or sludge age control (THANS, 2008).

Table 1. The operational cycle in an SBR.

Cycle phase	Image	Phase goal	Aeration setup
1. Feeding	influent	Substrate insertion	on or off
2. Reaction		Substrate biodegradation	on or off with a mixing mechanism added
3. Settling		Treated effluent clarification	off
4. Discharge	effluent	Discharge of the treated effluent	off
(5). Standby/ Adjustment		Time allocation for system maintenance	on or off

Source: Adapted from Santos et al. (2006).

2.3 AEROBIC GRANULAR SLUDGE (AGS)

As in natural ecosystems, some biological wastewater treatment systems use "surfaces" aiming for microorganisms' adhesion to stimulate biomass accumulation. It is a strategy to increase systems biomass retention, such as in biofilters and MBBR. However, these reactors

require support material and preventive/corrective maintenance for clogging (BASSIN, 2011). Aerobic granulation emerges as an alternative to immobilization using a support medium since, under specific operational conditions, biomass self-immobilization can be stimulated and achieved (ADAV et al. 2008).

Aerobic granular sludge (AGS) comprises self-immobilized microbial aggregates under hydrodynamic stresses with higher settling velocity than conventional activated sludge (AGS: 30-70 m.h^{-1}; activated sludge flocs: 8-10 m.h^{-1}, at least three times lower; MUDA et al., 2013). Although there is no consensus in the literature on the minimum aggregate size to be considered an aerobic granule, the minimum diameter of 0.2 mm defined by de Kreuk et al. (2005) is the most widely used. The same authors also describe the aerobic granulation process, which is only considered complete when the granules correspond to 80% of the biomass in the reactor.

The first definition of an aerobic granule formation mechanism, in turn, was proposed by Beun et al. (1999) when operating an SBR fed with synthetic wastewater and with short settling times (2 and 4 minutes). These authors observed the beginning of the granulation process in an immobilizing matrix formed by fungi. In this matrix, the bacteria could grow and form colonies until they reached diameters between 5 and 6 mm when the rupture of these aggregates was observed due to oxygen limitations inside them. After that, bacteria with better sedimentability aggregated again, configuring themselves into the first aerobic granules formed.

For Liu and Tay (2002), however, the granulation process does not require a non-bacterial matrix and can be divided into four steps (Figure 2): i) movements arising from cell motility (through flagella, cilia or pseudopodia), hydrodynamic, thermodynamic, diffusion and/or gravity forces promote contact between the microorganisms; ii) initial attractive forces (proton translocation, surface charge neutralization, hydrophobicity of the cell surface, and Van der Walls forces) keep the surface contact between cells stable, acting as a driving force for the self-aggregation of bacteria; iii) microbial forces favor granule maturation (extensive biosynthesis of exopolymeric substances – EPS – by aggregated microorganisms stimulated by quorum sensing and environmental stresses); iv) finally, the three-dimensional structure of the aggregate becomes stable due to hydrodynamic shear forces. The hydrodynamic shear force shapes the granules to form a particular structured community, and this force is one of the determinants of the outer shape and size of the aggregates. Although many years have passed this proposition, recent studies endorse this formation mechanism, highlighting the importance of selection pressure in increasing the hydrophobicity of the surfaces and EPS-producing organisms in granulation (SARMA et al., 2017; SENGAR et al., 2018).

Figure 2. A conceptual representation of AGS formation processes according to Liu and Tay (2002).

| scattered microorganisms | cell-cell adhesion | micro-aggregate formation | EPS synthesis | maturation |
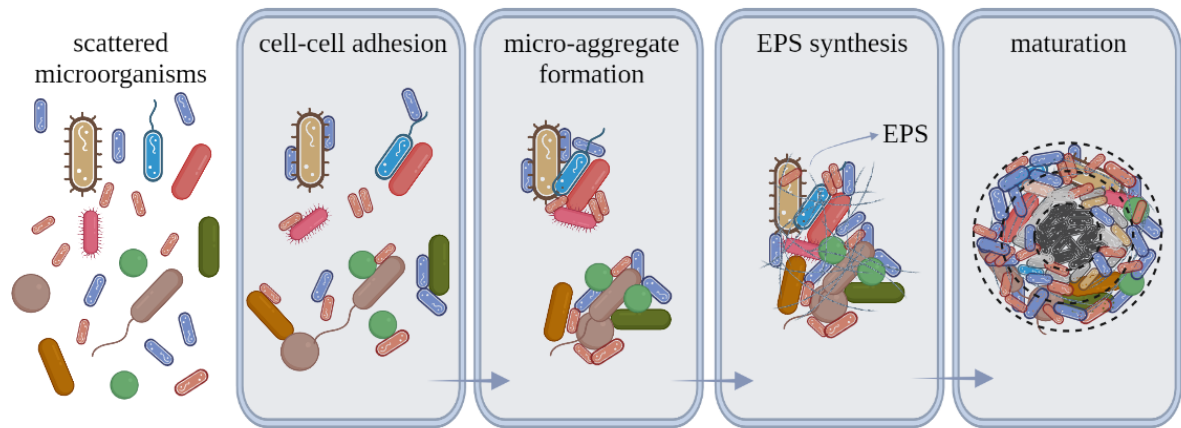
Source: the author (2022).

The microbial population in aerobic granules is similar to that in conventional activated sludge but is differentiated by the biofilm configuration. The heterogeneous structure of granular sludge is a product of the oxygen and substrate gradients (Figure 3) that form between the surface and the interior of the granule, allowing for different "layers" with different oxi-reducer potentials and different microbiological niches (HE et al., 2009).

Figure 3. Conceptual layers in an aerobic granule linked to the pattern of DO/substrate concentration and biological processes. Within the granule, the profile of each zone varies and depends on the bulk concentration.
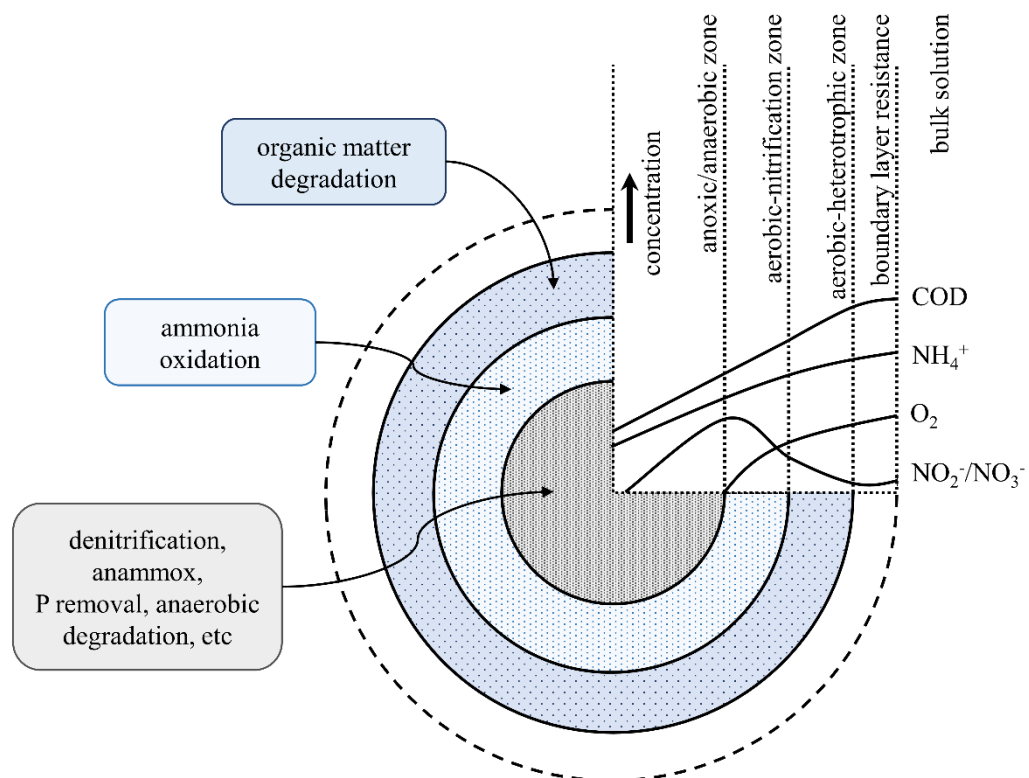
Source: adapted from He et al. (2009) and Gao et al. (2011).

The size of the granules and porosity (greater or lesser resistance to mass transport) define the size of each layer (aerobic, anoxic, and, in some cases, anaerobic), resulting in the stratification of bacteria. The flocculent sludge, however, needs to be subjected to aerobic and anoxic/anaerobic environments, with different substrate concentrations through recirculation in other compartments/tanks. It is thus emphasized that the coexistence of different species of bacteria with different functions is one of the main advantages of AGS, where all conversions can occur in a single tank in different granule layers (GAO et al., 2011; WINKLER et al., 2013; LAYER et al., 2020).

For instance, simultaneous nitrification and denitrification (SND) processes are often reported in AGS systems with significant efficiencies. For example, Li et al. (2022) achieved an SND efficiency of 61.6% during a 142 days operation of an 8L-SBR treating synthetic wastewater. This greater efficiency compared to other systems is justified by the presence of aerobic heterotrophic and autotrophic microorganisms in AGS outer layers, allowing nitrification and much of the oxidation of OM. While the presence of facultative heterotrophic microorganisms in the innermost layers enables denitrification as there is no DO due to its diffusion and consumption in the outer layers (YUAN et al., 2020). Furthermore, with intermittent aeration, biological phosphorus removal, known as EBPR (enhanced biological phosphorus removal), can co-occur with carbon and nitrogen removal in AGS (YUAN et al., 2020).

AGS formation is related to the selection pressure imposed on the system, such as settling time (BEUN et al., 1999), hydraulic shear stress (LIU & TAY, 2002), substrate composition, and organic loading rate (OLR) (GAO et al., 2011), feeding strategy (da SILVA et al., 2021) and cycle type (ROLLEMBERG et al., 2020a). The primary strategy for aerobic granule formation is to increase the selection pressure by applying short sedimentation times, high volume exchange ratios (between 50 and 70%), and a high height-to-diameter ratio in the system. Under these conditions, low-sedimentation flocculent sludge is washed out of the reactor, retaining mainly granular biomass in the system (BEUN et al., 2002; ROLLEMBERG et al., 2020b).

It is also known that high shear force stimulates the formation of compact and denser aerobic granules due to the increased production of extracellular polymeric substances (EPS). The EPS produced increases the hydrophobicity of the cells, thus increasing their adhesion potential. Different studies indicate that EPS production in aerobic granules is twice as high as in flocculent sludge (LIU & TAY, 2002; SCHAMBECK et al., 2021). Deng et al. (2016) found a direct linear relationship between the concentration of EPS and the volumetric index of the

sludge (the sludge showed good sedimentability when EPS concentration was superior to 200 mg.g^{-1} MLSS). However, the role of EPS in granular sludge formation also needs to be further studied, especially concerning its variation in the cultivation process.

There are many advantages of AGS, but granule development and stability – the backbone of this technology – is the aspect that mainly demands elucidation. Zhang et al. (2016) reported that many authors currently consider instability a significant problem for applying AGS technology in large-scale WWTP. Engineering parameters such as volumetric organic load, shear stress, airflow velocity, hydraulic retention time, selection pressure, and microbiological parameters – such as the type of dominant microorganisms and EPS synthesis – have been investigated to establish their roles in the granulation process. However, there is still no consensus among all these data, and it is not yet possible to develop a precisely predictable system (SARMA et al., 2017).

Due to these reasons, further studies are needed on mass transfer within the granules, optimal dissolved oxygen concentration, and the presence of nitrification byproducts when using SBR. Although the installation of larger-scale systems has been reported in the literature (PRONK et al., 2015; DE GRAAFF et al., 2020), the granulation mechanisms still need structural studies at the level of operating conditions. Thereby, mathematical models that describe these mechanisms together with the substrate transport within the granules and their conversion processes might allow for a better interpretation of experimental data and the simulation of different scenarios as an important facilitator.

2.4   MATHEMATICAL MODELLING

Mathematical models for designing and optimizing effluent treatment systems became widespread in the mid-1990s (GERNAEY et al., 2004), seeking greater control of the entire process. Conceptually, a mathematical model can be defined as a mathematical representation of a real system that equates processes, parameters, and variables to obtain responses to different stimuli and/or predict the behavior after modifications/adjustments in the system. The model will then consist of equations that quantitatively represent the hypotheses used in its construction. These can be tested by comparison with experimental data from real systems (WICHERN et al., 2018).

For biological systems, mathematical models are used to understand a microorganism, an ecosystem, the growth and dynamics of a specific population, or the pollutant removal

processes in the case of effluent treatment systems. In such scenarios, modeling can be used for data analysis in complex processes, such as nutrient removal in AGS. The various parameters analyzed in reactors (e.g., COD, NH_4^+, and PO_4^{3-}) result from a series of processes that are often directly interdependent. Therefore, these models allow for a joint analysis of complex phenomena that would otherwise not be possible.

The advances obtained in the computational area have also contributed to greater use and implementation of these models through the development and dissemination of simulation software. Several software packages have been developed in recent years for modeling WWTP, including the most cited in the literature: ASIM®, Aquasim®, and SIMBA®. The simulation software ASIM® (Activated sludge SIMulation Program) was developed by Eawag - Swiss Federal Institute of Aquatic Science and Technology, under the researchers' leaders R. Fankhauser and W. Gujer. Aquasim® is a public-domain software widely used to perform one-dimensional simulation and data analysis of aquatic systems by defining the substances to be modeled in predefined unit blocks with integrated processes (REICHERT, 1994). The SIMBA® software, meanwhile, is a new software with a better-developed visual interface for end users and several new features, namely: a revised and intuitive library structure, web application for alternative user interfaces, support for laboratory testing with a library for script programming, and collection of design models. All three software allow the implementation of biological models for activated sludge and biofilm models, which will be discussed in sections 2.4.1 and 2.4.3.

2.4.1 Activated sludge models (ASM) series

The first models developed for activated sludge systems date back to the early 1980s, highlighting among them the activated sludge model n° 1 (ASM1, HENZE et al., 1987), which is still widely used until the current days (VAN LOOSDRECHT et al., 2015; AMIN et al., 2022; GULHAN et al., 2022; MARTINS JR et al., 2022). This model was developed for conventional activated sludge systems, attempting to describe the removal of organic compounds and nitrogen compounds, considering the simultaneous consumption of oxygen and nitrate as electron acceptors. Since then, several updates have been made, and the model has evolved through the incorporation of new processes, being currently the group of activated sludge models (Activated Sludge Model n° 1, n° 2, n° 2d, n° 3 - ASM1, ASM2, ASM2d, ASM3) most used and with wide dissemination in the scientific and commercial fields. The ASM models, known as white-box models, result from well-defined differential equations based on

engineering principles (general equations of mass balance, bacterial kinetics, and other conservative substances) (HENZE et al., 1987; GUJER et al., 1995; HENZE et al., 1999; GUJER et al., 1999; GERNAEY et al., 2004).

The main differences between these models are summarized below, with the main characteristics highlighted in Table 2:

- ASM1: has 8 biological processes and 13 components, which describe carbonaceous matter removal, nitrification, and denitrification (HENZE et al., 1987).
- ASM2: has 19 biological processes and 20 components, including modeling chemical (precipitation) and biological phosphorus removal processes, in addition to the existing ones in ASM1. In this model, biomass has an internal cellular structure; its concentration is described by the sum of the heterotrophic and autotrophic fractions ($X_{B,H}$ and $X_{B,A}$) (GUJER et al., 1995).
- ASM2d: expands the capacity of ASM2, having 21 biological processes and 20 components, including the denitrifying ability of some phosphorus accumulating organisms (DPAO), allowing a better description of the dynamics of phosphate and nitrate (HENZE et al., 1999).
- ASM3: emerges as a refinement of the first model having 12 processes and 13 components. In this model, bacterial decay is included by the process of endogenous respiration and the internal storage of cellular material (all readily biodegradable substrate is first taken up and stored in an internal cellular component before growth) (GUJER et al., 1999).

Table 2. Comparative summary of the main features of the ASM models.

Model	ASM1	ASM2	ASM2d	ASM3
OM oxidation	X	X	X	X
Nitrification	X	X	X	X
Denitrification	X	X	X	X
Biological phosphorous removal with PAO		X	X	
Biological phosphorous removal with DPAO			X	
Chemical phosphorus removal		X	X	
Processes	8	19	21	12
Components	13	20	20	13

Source: the author (2022).

As discussed previously (section 2.1), due to the laboratory complexity of identifying organic matter precisely, indirect methods are used to quantify its polluting potential, with COD being the most commonly applied method in WWTP. However, the biological processes that occur during the treatment (and therefore are described by ASM) usually use only a fraction of this COD. For example, only the particulate fraction of COD is consumed during hydrolysis, resulting in dissolved COD. Therefore, considering the importance of this parameter and its fractions for simulation, the next topic details each of these fractions and presents methods to determine them.

2.4.2 Influent COD fractionation

The parameter COD comprises different forms of organic carbon that require further differentiation regarding their biodegradation characteristics. Therefore, total influent COD is divided according to its degradability into two main components: biodegradable COD and inert (non-biodegradable) COD in the ASM series. Degradability can then be defined by kinetics mechanisms and enzymatic reactions in the system. That means a substance will be considered biodegradable if the microorganisms have the specific enzymes necessary for the degradation in sufficient quantity during the treatment period (PASZTOR et al., 2009).

A distinction is also made within the biodegradable fraction, which can be easily or rapidly degraded (S_S) or heavy and slowly degraded (X_S). This subdivision depends on the supply of the necessary enzymes and the substance particle size. It should be mentioned that ASM2 and ASM2d separate the rapidly biodegradable COD into two fractions: easily degradable (S_F) and rapidly hydrolyzable (S_A). The inert COD, in turn, can be subdivided into soluble inert COD (S_I) and particulate inert COD (X_I), depending on the size of the particles. Both do not interfere with the treatment's biochemical reactions; however, while the first remains associated with the process effluent, the particulate can be retained and accumulated in the sludge. Other components of COD fractions in the ASM models comprise the microorganisms (autotrophic, X_A, heterotrophic, X_H, and phosphorus accumulating, X_{PAO}). However, X_H has a very high growth rate, and X_A and X_{PAO} constitute only about 1% of the COD influent, so they are usually neglected for the input. (HENZE et al., 1987; GUJER et al., 1995; HENZE et al., 1999; GUJER et al., 1999; PASZTOR et al., 2009). Figure 4 shows a scheme with the main influent COD fractions used as components in ASM models.

Figure 4. Fractions of the influent COD in ASM models.
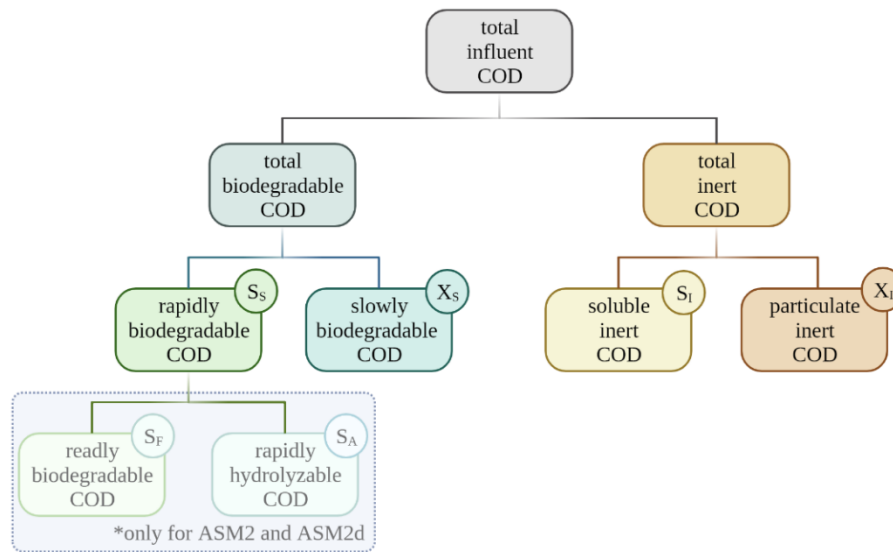
Various methods have been developed for fractionating organic matter using biological and/or physicochemical characterizations. The biological methods, also called respirometric, determine the OM degradability by the biomass response during continuous or batch tests. The electron acceptor's consumption rate is directly related to the amount and degradability of the available substrates. Such methods, although more accurate, often require skilled apparatus and technicians and demand a considerable amount of time.

Meanwhile, the physicochemical methods are based on the assumption that filtration/flocculation processes can separate COD fractions and, hence usually faster. However, the main problem is separating the rapidly and slowly biodegradable because colloidal organic matter (not separable by filtration) can contribute to both (PASZTOR et al., 2009). Therefore, some methods combine the two, such as the one proposed by Roeleveld and van Loosrecht (2002), which includes filtration and flocculation steps, COD, and BOD. Another commonly used methodology is the COD computational fractionation proposed by the German design guideline DWA-A 131 (ATV-DVWK, 2016), based on the COD balance and fractionation coefficients from data of typical German influents. Among the main correlations/coefficients assumed are:

- f_S: soluble inert COD (S_I) corresponds to approximately 5 to 10% of total COD, recommending 5% for municipal wastewater;
- f_A: the particulate inert COD (X_I) amounts to between 20 and 35% of the total particulate COD, and 25% is recommended for municipal wastewater;

- Each gram of volatile suspended solids (VSS) in the wastewater corresponds to 1.45 g of total COD;

- f_B: In addition, this calculates the standard mineral solids fraction (X_{MI}) as a function of total solids (between 20 and 30%), which despite not contributing to COD, is critical data for WWTP design.

However, before applying computational fractionation, it is critical to use a method to characterize the effluent and calculate these correlations/coefficients (such as the one proposed by Lange, 2018). As seen in the examples in Table 3, these fractions vary considerably due to several factors, e.g., population consumption patterns, temperature, and the existence/type of primary treatment.

Table 3. Examples of COD fractions in municipal raw wastewater (%).

Country	S_S	X_S	S_I	X_I	Source
Germany[1]	20	63	3	10	Wichern et al. (2018)
Poland	55	29	4	12	Płuciennik-Koropczuk et al. (2017)
Hungary	10-41	36-66	2-11	11-33	Pasztor et al. (2009)
Netherlands	9-42	10-48	3-10	23-50	Roelevend and van Loosdrecht (2002)
South Africa	20-25	60-65	8-10	5-7	Ekama (1986)

[1]14% corresponding to X_H.

Source: indicated.

2.4.3 Biofilm models

Activated sludge models are considered one-dimensional models, i.e., all component concentrations are calculated in a plane parallel to the substrate. However, some characteristics of the AGS, such as diffusion coefficient, granule size, biomass spatial distribution, and granule density, influence substrate concentration profiles, dissolved oxygen, and, consequently, the biological processes during wastewater treatment. Therefore, multidimensional models (biofilm models) may be more suitable for this system. In these models, the biofilm is modeled as a two-dimensional or three-dimensional structure, and all components can vary in space and time, producing highly detailed and complex results. Consequently, numerical solutions are computationally intensive and require high-level modeling expertise (WANNER et al., 2006).

Wanner and Gujer (1986) developed one of the first analytical mathematical models of microbial interaction in biofilms, "*using a continuum approach and observing conservation principles*." This model predicts changes in biofilm thickness by describing the dynamics and spatial distribution of substrates and microorganisms. Furthermore, it simulates biomass detachment due to shear stress, external mass transfer constraints, and variations in substrate concentrations in the mixed liquor. After that, this research group published a series of works proposing modifications to the previous model, allowing a more flexible description of the transport of dissolved components in the biofilm (GUJER & WANNER, 1990; WANNER, 1994; WANNER, 1995; WANNER & REICHERT, 1996; REICHERT & WANNER, 1997).

Among the additional considerations to the first model are: i) the diffusive transport of particulate components in the solid biofilm matrix, ii) changes in the volume fraction of the liquid phase of the biofilm (porosity), and iii) detachment and the simultaneous attachment of cells and particles to the biofilm surface. Figure 5 shows the primary transport processes in this model. Such modifications associated with the availability of this model in the free software Aquasim® (REICHERT, 1994) have made this one of the most widely used biofilm models to date. A variety of current studies can be found in the literature applied to different biofilm/reactor configurations, e.g., membrane aerated biofilm reactor (MABR, JIANG et al., 2018), CH_4-based membrane biofilm reactor (MBfR, WANG et al., 2019), and moving bed biofilm reactor (MBBR, MOHAMMADI et al., 2022).

Figure 5. Transport processes considered in the mixed-culture biofilm model proposed by Wanner and Reichert (1996) without a substratum. Bigger arrows refer to particulate, and smaller arrows to dissolved components.
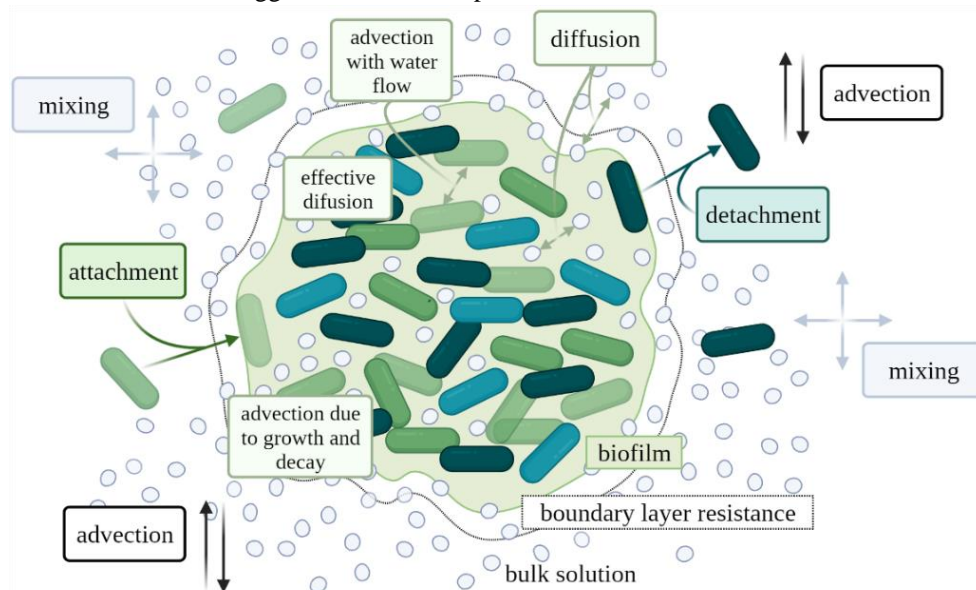
Source: adapted from Wanner and Reichert (1996).

Similarly, many studies have also been conducted with AGS. For example, Akaboci (2013) modified and implemented ASM3 associated with the Aquasim® biofilm compartment to simulate the behavior of COD_S, OCR (oxygen consumption rate), NH_4^+-N, NO_2^--N, and NO_3^--N during an operational cycle in a 116L-SBR with AGS. Zhu et al. (2018) used the biofilm model of Wanner and Reichert (1996) to simulate the variation of granule size distribution and the impact of this variation on nitrification in a reactor with AGS. Baeten et al. (2018) compared results when applying this model with the ones when implementing ASM2d with modified apparent half-saturation coefficients to lump the reaction-diffusion process within granules, verifying its applicability. Other studies, in turn, apply this model to suggest/test control and optimization strategies, e.g., Isanta et al. (2013) focusing on total nitrogen (TN) removal, Sun et al. (2019) on carbon and nitrogen removal, and Chen et al. (2020a) on optimizing the SND process. Table 4 summarizes some of these mentioned works, listing the associated biological process models, objectives, main results, and scale.

Table 4. Examples in the literature using Wanner and Gujer's model for systems with AGS. The models used, their objectives, and main results are also indicated.

Source	Models Biological processes	Biofilm	General aim	Main results	Reactor scale
Isanta et al. (2013)	Adapted from ASM3 (Henze et al., 1999)	Wanner and Gujer (1986); Wanner and Reichert (1996)	Develop a method to estimate the optimal DO for maximum TN removal in an AGS reactor operated as an SBR.	N-removal was enhanced when the applied DO produced a slight ammonium accumulation in the effluent, regardless of granule size, influent C/N ratio, or NLR. Thus, cascade ammonium and oxygen control strategies were proposed.	Lab-scale 1.51 L - SBR
Zhu et al. (2018)	A set of partial differential equations represents solid and soluble components' space and temporal changes.	Wanner and Gujer (1986)	Study the role of particle size distribution in achieving partial nitrification in an aerobic granule reactor.	Nitrite-oxidizing bacteria could be outcompeted in large granules, while it could be present in small granules (preferentially smaller than 50 μm), thereby reducing nitrite accumulation.	Lab-scale 7 L - ALR
Baeten et al. (2018)	ASM2d (Henze et al., 2000) corrected by Hauduc et al. (2010)	Wanner and Gujer (1986)	Understand if apparent half-saturation coefficients could lump the reaction-diffusion process inside granules, which would be applicable in practice.	Macroscale reaction rates in AGS reactors could be approximated in ASM2d using apparent half-saturation coefficients for fixed microbial population distribution. Thus, a single equation model is attractive for full-scale WWTP since it is easier to calibrate using typical monitoring data, enabling process control and identifying rate-limiting substrate.	Lab-scale 3 L - SBR
Sun et al. (2019)	Isanta et al. (2013, adapted from ASM3 – Henze et al., 1999)	Wanner and Gujer (1986); Wanner and Reichert (1996)	Examine and compare two operational and control strategies in AGS technology to identify the optimal one for carbon and nitrogen removal.	The strategy of dividing the SBR cycle into pre-denitrification, high DO aeration, and low DO aeration stages achieved satisfactory TN removal, with or without the high-DO aeration duration control.	Not indicated.
Chen et al. (2020a)	Isanta et al. (2013, adapted from ASM3 – Henze et al., 1999)	Wanner and Gujer (1986); Wanner and Reichert (1996)	Use AGS simulation to test control strategies to promote SND in the AGS-SBR under dynamic influent feeding conditions.	The feedforward control strategy achieved satisfactory TN-removal under SND, while the DO concentration control strategy had its efficiency restricted by a minimum duration of control and aeration. It was also concluded that high DO deteriorates TN removal conditions.	Not indicated.

Sources: indicated.

It is known that granule size, porosity, and substrate diffusion define the size of each layer (aerobic, anoxic, and in some cases, anaerobic, as shown in Figure 3) and the stratification of bacterial colonies. Another critical parameter is a compound's boundary layer resistance (BLR), the zone near the biofilm, where the concentration gradually changes from the bulk to the biofilm surface. Due to this resistance, the substrate concentrations at the biofilm surface can differ considerably from the liquid phase (DE BEER et al., 1993). The thickness of this layer depends on the liquid's hydrodynamics and also the compound's diffusion coefficient. In this sense, neglecting BLR can result in a substantial underestimation of the actual diffusion coefficient (VAN DEN BERG et al., 2020).

Nevertheless, data on how these substrates diffuse within the granules, considering a wide range of sizes and high temperatures, are rarely reported and are still insufficient for proper model calibration. There is no consensus on some boundary parameters, such as the geometry, porosity, granule density, or the boundary layer thickness and diffusion constant – especially considering that most of the literature covers modeling synthetic wastewater treatment operating lab-scale reactors at 20 °C. Another limitation is simulating only systems' in the stationary stage, not considering variations arising from the granulation process. Thus, strategies that enable system simulation during the granulation (start-up) process and studies on granulation process conditions are still needed.

2.5 MICRO-PROFILES

Among the factors influencing microbial processes in biofilms is diffusion because it is directly related to the concentration of substrates, such as oxygen or organic and inorganic nutrients. However, while comparing relatively effective diffusion coefficients of selected solutes in biofilms described in the literature, Stewart (1998; 2003) points out their significant variation, even for the same solutes, e.g., oxygen ranging between 0.4 and 0.75 and nitrate 0.45 and 0.9. This wide variation results probably from the variety of biofilms that exist and is partially attributed to differences in their density. Van den Berg et al. (2020) states that few studies have been done after this review to verify this hypothesis. And such a wide range of values makes mathematical modeling and/or kinetic analyses more laborious. Therefore, methodologies that enable in situ analysis of biofilms are promising to help understand their complex diffusion-reaction processes and the factors that influence them.

Among the methods available for measuring diffusion coefficients in biofilms, one can cite light- or fluorescence-based methods, methods based on mass balance calculations, and

methods based on microelectrode measurements (micro-profiles) (STEWART, 1998). The first ones are generally limited to thin or translucent biofilms that allow analyzing light throughput. Regarding the second one, the uncertainty in calculating granule volume is a major source of inaccuracy in calculating solute uptake and release. And last but not least, the latter, in general, are generally more accurate than mass-balance-based methods but require repeated measurements to average out the spatial heterogeneity (VAN DEN BERG et al., 2020).

The microsensors are valuable tools for investigating microbial ecology since they are minimally invasive while measuring gradients of essential solutes with high spatial resolution. These gradients can also be used to evaluate the size of layers with different oxy-reducer conditions (aerobic/anoxic/anaerobic) and the rates of the measured processes. Like other larger-scale sensors, they are based either on electrochemical or optical principles. Electrochemical sensors can be divided into three groups: i) amperometric sensors, which by having a fixed potential, send faradic current signals proportional to the analyte concentration as a function of electronic processes occurring at the electrode-solution interface; ii) potentiometric sensors, which detect an electrical potential difference generated by charge separation of ions across a membrane; and iii) biosensors, which combine catalysts (as enzymes and cells) with electrochemical sensors. On the other hand, fiber optic microsensors directly measure the light distribution in a sample, or specific chemistry indicator, which changes its luminescence or absorption in response to an analyte (KÜHL & REVSBECH, 2000).

Different types of micro-electrodes are currently available, not only described in the literature – e.g., how to prepare, calibrate, and operate NH_4^+ (DE BEER & VAN DEN HEUVEL, 1988), NO_3^- (DE BEER & SWEERTS, 1989), NO_2^- (DE BEER et al., 1997), but being commercialized (O_2, H_2, H_2S, NO, pH and redox, Unisense®). Several are also uses of microsensors in biofilm studies. Song et al. (2013) used them to help understand the microbiology and ecology within aerobic partial nitrifying (PN) granules. Shanahan and Semmens (2015) calibrate a model developed by the authors in 2004 for a membrane-aerated biofilm using O_2 micro-profiles. More recently, Liang et al. (2021) analyzed oxygen penetration depth into granules under a low temperature (15°C). Littfinski et al. (2022) measured pH in steps of 200μ in single-chamber microbial fuel cells to aid in identifying biological removal pathways and the pH gradient of total ammoniacal nitrogen.

Finally, the use of microelectrodes for micro-profile determination can assist in the study of some parameters inherent to biofilms, of which there is no consensus (or data) in the literature, especially for high temperatures. For example, the boundary layer resistance (BLR) presents a wide range of values in the literature, varying from 0 to 700 μm for aerobic granules,

with 100 μm being the most commonly used typical value estimated based on Horn and Morgenroth (2006) for a biofilm adhered to a membrane under 20-24 °C.

3   MATERIALS AND METHODS

This section presents the systems and operational conditions used to develop this work and the mathematical models implemented. The methods for monitoring these systems and operational cycles, the software (Aquasim®) and parameters used, and model calibration/ validation procedures are also described. It is worth mentioning that this research was conducted at the Federal University of Pernambuco (UFPE, Brazil) in cooperation with the Ruhr-*Universität* Bochum (RUB, Germany). This chapter (3) is divided into four mean subtopics: 3.1 Pilot-scale experimental system; 3.2 Mathematical model; 3.3 Lab-scale experimental system; 3.4 Micro-profiles, as schematically presented in Figure 6 below. Results will also be presented and discussed in chapter 4 according to the same scheme.

Figure 6. Scheme for dividing chapter 3 into four subtopics.

3.1 Pilot-scale

different operational strategies were used in a 115L-SBR to analyze the formation and stability of AGS at around 30 °C.

3.2 Modelling

data from the previous experiments were used to implement and calibrate a biofilm model with ASM3 in Aquasim, observing a high sensitivity for diffusion-associated parameters such as boundary layer thickness.

3.3 Lab-scale

two lab-scale SBRs operated at 20 and 30 °C were used to investigate the influence of temperature on AGS formation, morphology, and stability, also providing granules samples for the next step (micro-profiles).

3.4 Micro-profiles

O_2 micro-profiles were performed at 20/30°C with different COD/NH_4 loads to obtain diffusion gradients (and estimate boundary layer thickness) in granules from both lab-scale SBR

Source: the author (2022).

3.1 PILOT-SCALE EXPERIMENTAL SYSTEM

The first stage of this research was conducted between June 2018 and August 2019 in a pilot-scale experimental system design and assembled by Araújo et al. (2016) and Silva (2017a) at the Mangueira municipal wastewater treatment plant (WWTP), located in Recife, Pernambuco, Brazil. This plant was designed to attend to a population of 18,000 inhabitants, with the capacity to treat an average flow of 31 L.s^{-1} and a maximum flow of 51 L.s^{-1}, and receives municipal wastewater from the area nearby (MORAIS et al., 2013). The Pilot-Scale (PS) experimental system comprised two cylindrical SBRs made of acrylic and had a working volume of 115 L, a liquid height of 2.45 m, and an internal diameter of 24.5 cm. A schematic diagram with reactors' dimensions associated with automation components and a picture of both reactors are shown in Figure 7.

Figure 7. Schematic (left) and photograph (right) of PS reactors used for municipal wastewater treatment. Dimensions and connections with automation components are indicated.
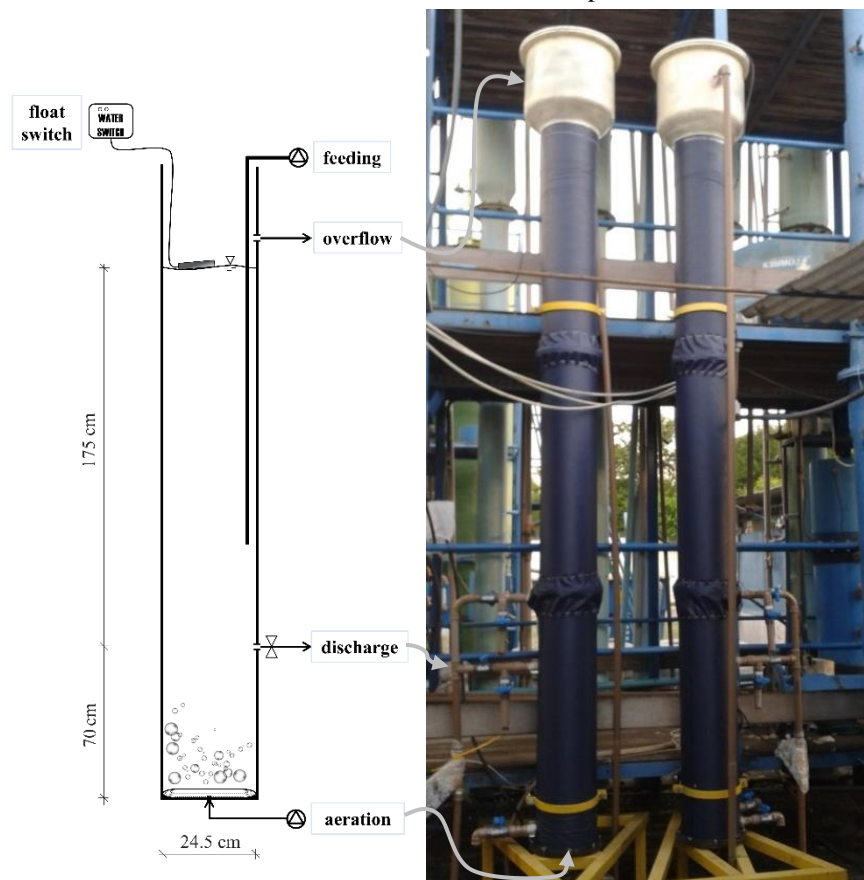
Sources: the author (2022, scheme); Araújo et al. (2016, photo)

A pump (Schneider®, BC 915), an air compressor (Schulz®, CSL 10 100L Pratic air), an air filter (Arprex®, AF1), a rotameter (Dwyer®, DR 200482), a circular membrane diffuser

(Ecosan®, DCM), two pneumatic solenoid valves (for effluent discharge and aeration automation, Asco®, 8210 series), and a float switch (Anauger®, SensorControl) were associated to each reactor. As an accessory component to both systems, a compressor (Schulz®, CSA 8.2 25L Pratic air) was installed to drive the pneumatic solenoid valves to discharge the effluent from both reactors. A Programmable Logic Controller (PLC, Siemens®, Simatic S7 1200) controlled and automated operational cycle phases coupled with a laptop and an electrical panel.

3.1.1 Operational conditions

Two operational strategies were used, totalizing three experiments, E-I, E-II, and E-III. E-III was a repetition of E-I after its interruption due to operational problems. In all experiments, the reactors were not inoculated during the start-up, seeking to stimulate and evaluate biomass growth already acclimated to the affluent characteristics. For each strategy, only one reactor was used, with no parallel operation. The feeding was done with wastewater collected after the grit chamber at Mangueira WWTP and stored in an equalization tank (1 m³).

A typical SBR cycle lasted 240 min (4h) under alternating anaerobic and aerobic conditions to optimize nutrient removal and comprised five phases: (1) a quick descending feeding; (2) an anaerobic/anoxic phase with the introduction of 4 s air pulses every 5 min (continuously measured oxygen during phase lower than 0.2 mg.L^{-1}); (3) an aerobic phase with compressed air supplied to saturation (flow rate 20 L.min^{-1}; ascending velocity 1.0 cm.s^{-1}) through a membrane diffuser attached to the bottom of the reactors; (4) settling; and (5) discharge of the effluent through a solenoid valve located 70 cm from the bottom of the reactors (volumetric exchange around 71%; hydraulic retention time of 5.6 h). The PLC controlled the phase durations and the actuation of the pump, air compressors, and solenoid valves using ladder language in the software provided by the manufacturer. The duration of each phase used for each experiment based on previous findings of the AGS-LSA research group (UFPE, Brazil) is shown in Figure 8 (ARAÚJO et al., 2016; SILVA, 2017a; ALVES, 2017; SALES et al., 2018; DANTAS, 2018).

Figure 8. Operating cycle profiles applied in the three experiments (E-I, E-II, and E-III). The duration of each phase is indicated above each bar. The dissolved oxygen concentration in the anaerobic and aerobic phases is shown in parentheses.
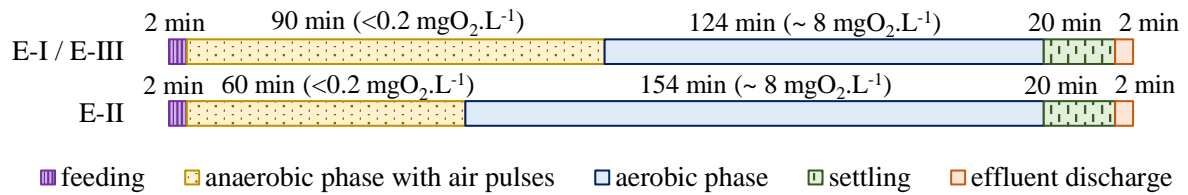
Source: the author (2022).

3.1.2   System Monitoring

In order to follow the performance of the experiments, weekly samplings were made of raw influent (input), mixed liquor immediately after the anoxic/anaerobic phase, mixed liquor at the end of the aerobic phase, and the treated effluent (reactors' outflows). The analyzed parameters and applied methods are listed in Table 5.

Table 5. Analyzed parameters and used methods

Parameter	Method	Source
pH Redox Potential Temperature Conductivity Dissolved Oxygen	Potentiometric	Multi-parameter (HACH CO HQ40d)
Total COD (COD_{total}) Filtered COD ($COD_{filt.}$)	Colorimetric	SM* 5220 D
Total Kjeldahl Nitrogen (TKN-N)	Macro Kjeldahl	SM* 4500 N-org. B
Ammoniacal Nitrogen (NH_4^+-N)	Titrimetric	SM* 4500 N-NH_3 C
Nitrite Nitrogen (NO_2^--N)	Ion chromatography	SM* 4500 NO_2^- B
Nitrate Nitrogen (NO_3^--N)	Ion chromatography	SM* 4500 NO_3^- E
Total phosphorus Orthophosphate	Colorimetric (vanadate-molybdate)	SM* 4500 P D
Alkalinity ($CaCO_3$)	Titrimetric	SM* 2320
Serie of solids	Gravimetric	SM* 2540

* *Standard Methods* (APHA, 2012).

Sources: APHA (2012).

Biomass sedimentability was monitored weekly by the sludge volume index (SVI) using 1.0 L mixed liquor samples obtained after sedimentation at 10 min (SVI_{10}) and 30 min (SVI_{30}) (SCHWARZENBECK et al., 2004). Sludge development and granule formation were monitored using light-field optical microscopy, observing changes in the granules' morphology and identifying the presence of microorganisms that may have contributed to AGS stability, such as rotifers and nematodes. The granules' granulometric distribution in terms of percentage

in the mixed liquor was obtained by particle size analysis according to the methodology proposed by Bin et al. (2011).

3.1.3   Taxonomic analysis of the microbial community

The microbial community characterization in the mixed liquor was performed according to the following protocol for the three experiments:

I.   Mixed liquor samples were collected on days 11, 39, and 138 days for E-I; 41, 80, and 141 days for E-II; and 22, 65, 87, 127, 168, 196, 203, and 247 days for E-III, frozen, and stored until the next step.

II.   Samples' DNA extractions were performed using the Power Soil® isolation kit (MoBio Laboratories Inc., USA) according to the manufacturer's instructions.

III.   After extraction, the samples were metabarcoding using high-performance sequencing of the V3/V4 regions of the 16S rRNA gene by Neoprospecta Microbiome Technologies (Brazil). The primers 341F (CCTACGGGRSGCAGCAG) and 806R (GGACTACH VGGGGGTWTCTAAT) were used for amplification. MiSeq Sequencing System (Illumina Inc., USA) and V2 kit with 300 cycles and single-end sequencing sequenced the libraries. A sentinel pipeline was used to analyze the sequences, and generated files were subjected to low-quality primers and trimming sequences. Taxonomic identifications were performed using the company database. It bears mentioning that clusters with an abundance <2 % (chimeras) were removed from the analyses.

3.2   MATHEMATICAL MODELING

For simulating the experiments E-I and E-III described previously (3.1), the PS reactor's operational conditions and input/output data (affluent/effluent) were used as reference scenarios for the simulations. The current topic thoroughly presents the model implemented in the software Aquasim® (REICHERT, 1994), which comprises a 1D dynamic biofilm model (WANNER & GUJER, 1986) and an activated sludge model (ASM3h) describing the biological reactions. The ASM3h corresponds to the ASM3 proposed by Gujer et al. (1999) with modifications according to the research group Hochschulgruppe (HSG) and the German design guideline DWA-A 131 for activated sludge system (DOHMANN, 1993; ATV-DVWK, 2016).

Furthermore, the methods used for fractionating the inflowing COD and calculating fractionation coefficients are described.

3.2.1 General model description

As mentioned in the literature review, Aquasim's unit block structure simplifies the user experience but also implies some limitations, e.g., it isn't possible to vary the biofilm compartment (BC) volume. Therefore, the total volume of the simulated reactor (115 L) was divided between two compartments: a confined-type BC with a total volume of 33 L and a mixed compartment (MC_2) with a variable volume equal to the volumetric exchange of the system (82 L) and a negligible initial volume (10^{-12} to avoid miscalculations). These two compartments were connected by a diffusive link (DL) with an exchange coefficient of 10^6 m³.d⁻¹ to ensure that the liquid phases (bulk) behave as a perfect mixture without numerical errors (BAETEN et al., 2017).

Additionally, to facilitate the data handling and calibration process, two 50 mL MC were added to the model: one for the influent (MC_1, where the input data was added) and one for the effluent (MC_3, to facilitate obtaining the simulated output data and comparing with the real data). Given that the organic matter input data of the influent were in terms of COD, the fractionation proposed by the German design guideline DWA-A 131 (ATV-DVWK, 2016) was performed. Thus, the total COD was divided into soluble/particulate and biodegradable/inert COD, as described previously in the literature review section 2.4.1 ($COD_{total} = S_I$, S_S, X_I, X_S, X_A, X_H, X_{MI}). The influent transfer from MC_1 to MC_2 was performed through an advective link (AL_1) activated only during the cycle feeding period. The treated effluent discharge (transfer from MC_2 to MC_3) was achieved through another advective link (AL_2), active only during the operational cycle's discharge period.

Finally, to simulate the solids retention in the operational cycle settling stage, a bifurcation (bif.) was added in AL_2 proportional to the solids retention in the real system, which gradually increased as the granulation process stabilized. The schematic shown in Figure 9 presents all the compartments used to implement the model and the links connecting them. A description of all compartment information (volume, variables, process, initial conditions, inputs, outflow) and links (from-to, loadings) is available in Appendix A. The particles' detachment (det.) and attachment (att.) dynamics in BC will be better detailed in topic 3.4.

Figure 9. Compartments and links used in the implemented model. MC₁: Influent compartment (50 mL); MC₂: SBR compartment (variable volume – min. 10^{-12} L; max. 82 L); BC: Biofilm compartment (33 L); MC₃: Effluent compartment (50 mL); DL: diffusive link to ensure complete mixture between both compartments of the simulated reactor; AL₁: advective link active during the cycle feeding period; AL₂: advective link active during the cycle discharge period; bif: bifurcation added in AL₂ for returning the solids (working as the settling phase); det. and att.: particles' detachment and attachment dynamics in BC.
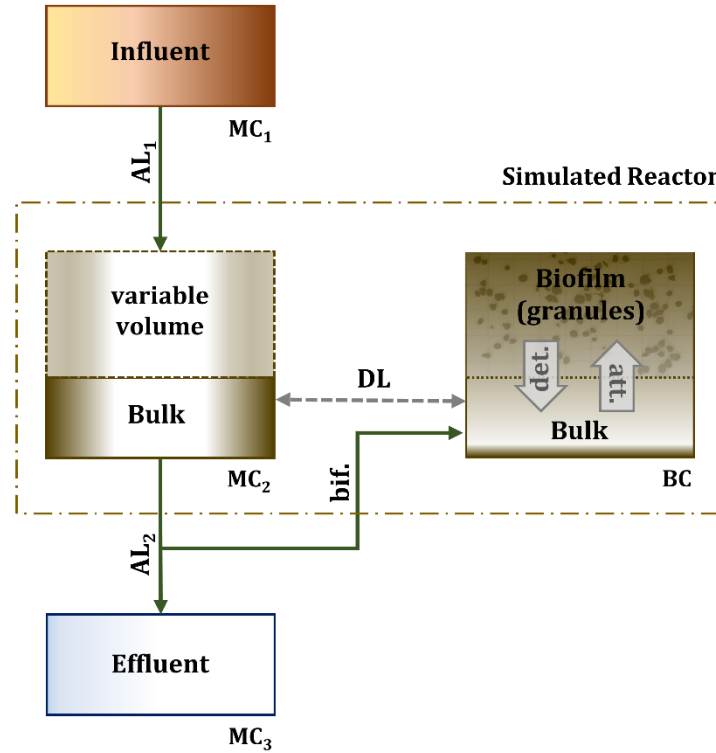
Source: the author (2022).

3.2.2 Influent: estimation of the fractionation coefficients for COD

Specific characteristics were observed in the experiments' influent data, such as low organic matter loads and a high average temperature of 29.5 ± 1.7 °C. Thus, before fractionating the influent COD, the method proposed by Lange (2018) for effluent characterization methodology was adapted to determine three fractionation parameters: f_A, f_B, and f_S, and the COD fractions: S_I, S_S, S_{XS}, X_S, X_I. The introduction of S_{XS} was necessary to compensate for the overestimation of S_S due to using a 0.45 µm membrane filter instead of the filtration through a 0.1 µm membrane after flocculation. This fraction, although dissolved, is of slow degradation, being associated with the XS fraction. The dataset for this influent characterization were from E-I, E-II, E-III, and two more experiments/projects developed in the experimental area of LSA-UFPE at WWTP Mangueira carried out by Morais (2015, Proj. 1) and Silva (2017b, Proj. 2).

The analyses used to characterize the influent in all experiments were: temperature, pH, electrical conductivity, total alkalinity and bicarbonate, total and suspended solids, gross and filtered chemical oxygen demand (COD), TKN, ammoniacal nitrogen, nitrite nitrogen, and

nitrate nitrogen. Total and filtered biological oxygen demand (BOD_5) were performed only in Proj. 1 and 2. As for the filtered COD data after wastewater treatment (necessary for calculating the dissolved inert fraction present in the affluent - S_I), the results from E-I, E-II, E-III, and Proj 2. The system in Proj. 2 was composed of bar grids and grit chamber; an upflow anaerobic sludge blanket (UASB) reactor – total volume 810 m^3, HRT ≈ 8 h, divided into eight cells operated in parallel with 5m-height –; followed by a polishing pond – HRT ≈ 3.5 days. All physicochemical analyses were conducted as recommended by Standard Methods (APHA, 2012). The frequency and sampling period for each characterization was conducted between August/2012 and July/2013, totaling 33 weekly collections for Proj. 1, and between December/2015 and February/2016, counting 05 biweekly samples for Proj. 2.

After data treatment, the gaps were filled with linear interpolation and a moving average of 10 levels for BOD_5 and 50 levels for filtered COD with the aid of Excel® and Matlab® software. The correlation between degradable COD and total BOD was performed after Roeleveld and van Loosdrecht (2002). Finally, the three fractionation parameters (f_S, f_A, and f_B, see section 2.4.2) were calculated using the Matlab® optimization function "*fgoalattain*" for each group of experimental data (comprising a total of 128 samples) based on the methodology proposed by the German design guideline DWA-A 131 (ATV-DVWK, 2016). The Matlab® code used for data treatment and calculation of the coefficients, as well as the graphs from data interpolation and application of the moving average, are available in Appendices B and C.

3.2.3 ASM3h: parameters, processes, and stoichiometry

As mentioned, biological reactions were described with ASM3 proposed by Gujer et al. (1999), modified by HSG and the German design guideline DWA-A 131, the ASM3h (DOHMANN, 1993; ATV-DVWK, 2016). Since the model aims to describe COD and N removal, it expresses the metabolisms of two mean bacteria groups: common heterotrophic organisms (OHO, called X_H in ASM3h) and ammonia-oxidizing organisms (AOO, reported in ASM3h as autotrophic organisms, X_A). In total, the 12 processes of ASM3h (hydrolysis, aerobic and anoxic storage of S_S, aerobic and anoxic growth of X_H, aerobic growth of X_A, aerobic and anoxic endogenous respiration of X_H and X_A, aerobic and anoxic respiration of organic storage products, X_{Sto}) were implemented and activated only in MC_2 and BC. Hence, the following Table 6, 7, and 8 list implemented state variables, the process rate equations, and the stoichiometric matrix. The text in red highlights the adaptations of ASM3h compared to ASM3.

Table 6. State variables used in the model. Changes and additions to ASM3 are in red.

Symbol	Definition	Source
S_{Alk}	Soluble alkalinity as H_2CO_3	mol H_2CO_3.m^{-3}
S_S	Readily biodegradable substrate	g COD.m^{-3}
S_I	Soluble undegradable organics	g COD.m^{-3}
S_{O2}	Dissolved oxygen	g O_2.m^{-3}
S_{NHx}	Ammonia nitrogen ($NH_3 + NH_4^+$)	g N.m^{-3}
S_{NO}	Nitrate and Nitrite nitrogen ($NO_3^- + NO_2^-$) (considered to be NO_3^- only for stoichiometry)	g N.m^{-3}
S_{N2}	Dissolved nitrogen gas (only product of denitrification)	g N.m^{-3}
X_S	Slowly biodegradable substrate	g COD.m^{-3}
X_I	Particulate undegradable organics	g COD.m^{-3}
X_{Sto}	Organic storage products of heterotrophs (but not included in their mass)	g COD.m^{-3}
X_H	Ordinary heterotrophic organisms	g COD.m^{-3}
X_A	Autotrophic organisms	g COD.m^{-3}
X_{MI}*	Particulate mineral fraction	g TSS.m^{-3}

*X_{MI} instead of X_{SS} (Total suspended solids)

Source: Gujer et al. (1999), adapted by HSG (DOHMANN, 1993).

Table 7. Processes' rates used in the model

Process	Definition	Rate
P_1	Hydrolysis	$k_H \left(\dfrac{\frac{X_S}{X_H}}{\frac{X_S}{X_H} + K_X} \right) X_H$
P_2	Aerobic storage of S_S	$k_{Sto} \left(\dfrac{S_O}{S_O + K_{H,O_2}} \right) \left(\dfrac{S_S}{S_S + K_{H,SS}} \right) X_H$
P_3	Anoxic storage of S_S	$k_{Sto} \eta_{HNO} \left(\dfrac{K_{H,O_2}}{S_O + K_{H,O_2}} \right) \left(\dfrac{S_S}{S_S + K_{H,SS}} \right) \left(\dfrac{S_{NO}}{S_{NO} + K_{H,NO}} \right) X_H$
P_4	Aerobic growth of X_H	$\mu_H \left(\dfrac{S_O}{S_O + K_{H,O_2}} \right) \left(\dfrac{S_{NH}}{S_{NH} + K_{H,NH}} \right) \left(\dfrac{S_{Alk}}{S_{Alk} + K_{H,Alk}} \right) \left(\dfrac{\frac{X_{Sto}}{X_H}}{\frac{X_{Sto}}{X_H} + K_{H,Sto}} \right) X_H$
P_5	Anoxic growth of X_H (denitrification)	$\mu_H \eta_{HNO} \left(\dfrac{K_{H,O_2}}{S_O + K_{H,O_2}} \right) \left(\dfrac{S_{NH}}{S_{NH} + K_{H,NH}} \right) \left(\dfrac{S_{Alk}}{S_{Alk} + K_{H,Alk}} \right) \left(\dfrac{S_{NO}}{S_{NO} + K_{H,NO}} \right) \left(\dfrac{\frac{X_{Sto}}{X_H}}{\frac{X_{Sto}}{X_H} + K_{H,Sto}} \right) X_H$
P_6	Aerobic endogenous respiration of X_H	$b_H \left(\dfrac{S_O}{S_O + K_{H,O_2}} \right) X_H$
P_7	Anoxic endogenous respiration of X_H	$b_H \eta_{Hend} \left(\dfrac{K_{H,O_2}}{S_O + K_{H,O_2}} \right) \left(\dfrac{S_{NO}}{S_{NO} + K_{H,NO}} \right) X_H$
P_8	Aerobic respiration of X_{Sto}	$b_H \left(\dfrac{S_O}{S_O + K_{H,O_2}} \right) X_{Sto}$
P_9	Anoxic respiration of X_{Sto}	$b_H \eta_{Hend} \left(\dfrac{K_{H,O_2}}{S_O + K_{H,O_2}} \right) \left(\dfrac{S_{NO}}{S_{NO} + K_{H,NO}} \right) X_{Sto}$
P_{10}	Growth of X_A (nitrification)	$\mu_A \left(\dfrac{S_O}{S_O + K_{N,O_2}} \right) \left(\dfrac{S_{NH}}{S_{NH} + K_{N,NH}} \right) \left(\dfrac{S_{Alk}}{S_{Alk} + K_{N,Alk}} \right) X_A$
P_{11}	Aerobic endogenous respiration of X_A	$b_A \left(\dfrac{S_O}{S_O + K_{A,O_2}} \right) X_A$
P_{12}	Anoxic endogenous respiration of X_A	$b_A \eta_{Nend} \left(\dfrac{K_{A,O_2}}{S_O + K_{A,O_2}} \right) \left(\dfrac{S_{NO}}{S_{NO} + K_{A,NO}} \right) X_A$

Source: Gujer et al. (1999).

Table 8. Stoichiometric matrix of the transformation model. Changes and additions to ASM3 are in red.

Process	S_{Alk}	S_S	S_I	S_{O2}	S_{NHx}	S_{NO}	S_{N2}	X_S	X_I	X_{Sto}	X_H	X_A	X_{MI}
P_1	$(i_{N,X_S} - i_{N,S_I} \cdot f_{S_I} - (1 - f_{SI}) \cdot i_{N,S_S})/14$	$1 - f_{SI}$	f_{SI}		$-(1-f_{SI}) \cdot i_{N,S_S} - i_{N,S_I} \cdot f_{S_I} + i_{N,X_S}$			-1					
P_2	$i_{N,S_S}/14$	-1		$Y_{Sto,aer} - 1$	i_{N,S_S}					$Y_{Sto,aer}$			
P_3	$\frac{i_{N,S_S}}{14} - (Y_{Sto,ano}-1)/40$	-1			i_{N,S_S}	$\frac{Y_{Sto,ano}-1}{40/14}$	$\frac{1-Y_{Sto,ano}}{40/14}$			$Y_{Sto,ano}$			
P_4	$\frac{i_{N,BM}}{14}$			$1 - \frac{1}{Y_{H,aer}}$	$i_{N,BM}$					$-\frac{1}{Y_{H,aer}}$	1		
P_5	$-\frac{i_{N,BM}}{14} + \left(\frac{1}{Y_{H,ano}}-1\right)/40$				$-i_{N,BM}$	$\frac{1 - \frac{1}{Y_{H,aer}}}{40/14}$	$\frac{\frac{1}{Y_{H,aer}}-1}{40/14}$			$\frac{1}{Y_{H,ano}}$	1		
P_6	$(i_{N,BM} - f_{XI} \cdot i_{N,XI})/14$			$f_{XI} - 1$	$i_{N,BM} - f_{XI} \cdot i_{N,XI}$				f_{XI}		-1		$f_{i,SS,BM,prod} \cdot f_{XI} \cdot i_{VSS,BM} \cdot (i_{TSS,VSSBM} - 1)$
P_7	$(i_{N,BM} - f_{XI} \cdot i_{N,XI})/14$				$i_{N,BM} - f_{XI} \cdot i_{N,XI}$	$\frac{f_{XI} - 1}{40/14}$	$\frac{1 - f_{XI}}{40/14}$		f_{XI}		-1		$f_{i,SS,BM,prod} \cdot f_{XI} \cdot i_{VSS,BM} \cdot (i_{TSS,VSSBM} - 1)$
P_8				-1						-1			
P_9	$\frac{1}{40}$					$-\frac{14}{40}$	$\frac{14}{40}$			-1			
P_{10}	$(-\frac{2}{Y_A} - i_{N,BM})/14$			$1 - \frac{64}{14} \cdot \frac{1}{Y_A}$	$-\frac{1}{Y_A} - i_{N,BM}$	$\frac{1}{Y_A}$						1	
P_{11}	$(i_{N,BM} - f_{XI} \cdot i_{N,XI})/14$			$f_{XI} - 1$	$i_{N,BM} - f_{XI} \cdot i_{N,XI}$				f_{XI}			-1	$f_{i,SS,BM,prod} \cdot f_{XI} \cdot i_{VSS,BM} \cdot (i_{TSS,VSSBM} - 1)$
P_{12}	$\frac{i_{N,BM} - f_{XI} \cdot i_{N,XI}}{14} - \frac{f_{XI} - 1}{40}$				$i_{N,BM} - f_{XI} \cdot i_{N,XI}$	$\frac{f_{XI} - 1}{40/14}$	$\frac{1 - f_{XI}}{40/14}$		f_{XI}			-1	$f_{i,SS,BM,prod} \cdot f_{XI} \cdot i_{VSS,BM} \cdot (i_{TSS,VSSBM} - 1)$
	S_{Alk}	S_S	S_I	S_{O2}	S_{NHx}	S_{NO}	S_{N2}	X_S	X_I	X_{Sto}	X_H	X_A	X_{MI}

Source: Gujer et al. (1999), adapted by HSG (DOHMANN, 1993).

Furthermore, an additional aeration process (P$_{13}$) was added and triggered during the aeration phase of the cycles only in bulk MC$_2$ and BC, simulating the addition of dissolved oxygen up to saturation (varying according to the system's temperature).

Finally, to define the values of the parameters applied (stoichiometry and kinetics), a literature review was performed on the range of values used in other works to choose the parameters that best fit during calibration. Table 9 presents applied parameters[1], indicating their sources.

Table 9. Applied parameters.

	Symbol	Unit	Used value	Source
Kinetic parameters				
Hydrolysis rate constant	k_H	d^{-1}	9.0	Koch et al. (2000)
Hydrolysis saturation constant	K_X	$gX_S\ g^{-1}X_H$	1.0	ASM3
Aerobic storage rate constant	k_{Sto}	$gS_S\ g^{-1}X_H\ d^{-1}$	12	Koch et al. (2000)
Anoxic reduction factor for growth/storage	$\eta_{H,NO}$	–	0.5	Koch et al. (2000)
Saturation/inhibition constant for S_O	$K_{H,O}$	$gO_2\ m^{-3}$	0.2	ASM3
Saturation/inhibition constant for S_{NO}	$K_{H,SO}$	$gN\ m^{-3}$	0.5	ASM3
Saturation constant for substrate S_S	$K_{H,S}$	$gCOD\ m^{-3}$	10.0	Koch et al. (2000)
Saturation constant for storage S_{Sto}	$K_{H,Sto}$	$gX_{Sto}\ g^{-1}X_H$	1.0	ASM3
Heterotrophic maximum aerobic growth rate	μ_H	d^{-1}	3.0	ASM3
Saturation constant for ammonium S_{NH}	$K_{H,NH}$	$gN\ m^{-3}$	0.01	ASM3
Saturation constant for bicarbonate S_{Alk}	$K_{H,Alk}$	$mol\ m^{-3}$	0.1	ASM3
Aerobic endogenous respiration rate of X_H	$b_{H,O2}$	d^{-1}	0.3	Koch et al. (2000)
Anoxic endogenous respiration rate of X_H	$b_{H,NO}$	d^{-1}	0.15	Koch et al. (2000)
Aerobic respiration rate of X_{Sto}	$b_{Sto,O2}$	d^{-1}	0.3	Koch et al. (2000)
Anoxic respiration rate of X_{Sto}	$b_{Sto,NO}$	d^{-1}	0.15	Koch et al. (2000)
Autotrophic maximum growth rate	μ_A	d^{-1}	1.12	Koch et al. (2000)
Saturation constant for S_{NH}	$K_{A,NH}$	$gN\ m^{-3}$	1.0	ASM3
Saturation constant for S_O	$K_{A,O2}$	$gO_2\ m^{-3}$	0.5	ASM3
Saturation constant for S_{Alk}	$K_{A,Alk}$	$mol\ m^{-3}$	0.5	ASM3
Aerobic endogenous respiration rate of X_A	$b_{A,O2}$	d^{-1}	0.18	*
Anoxic endogenous respiration rate of X_A	$b_{A,NO}$	d^{-1}	0.09	*
Stoichiometric parameters				
Production of X_I in endogenous biomass respiration	f_{XI}	$gX_I\ g^{-1}X_H$	0.2	ASM3
Aerobic yield of stored products per S_S	$Y_{Sto,aer}$	$gX_{Sto}\ g^{-1}X_S$	0.8	Koch et al. (2000)
Anoxic yield of stored products per S_S	$Y_{Sto,ano}$	$gX_{Sto}\ g^{-1}X_S$	0.8	ASM3
Aerobic yield of X_H growth on X_{Sto}	$Y_{H,aer}$	$gX_H\ g^{-1}X_{Sto}$	0.63	ASM3
Anoxic yield of X_H growth on X_{Sto}	$Y_{H,ano}$	$gX_H\ g^{-1}X_{Sto}$	0.54	ASM3
Yield of X_A per g NO_3^--N	Y_A	$gCOD\ g^{-1}N$	0.24	ASM3
Nitrogen content of S_I	$i_{N,SI}$	$gN\ g^{-1}COD$	0.01	ASM3
Nitrogen content of S_S	$i_{N,SS}$	$gN\ g^{-1}COD$	0.03	ASM3
Nitrogen content of X_I	$i_{N,XI}$	$gN\ g^{-1}COD$	0.04	Koch et al. (2000)
Nitrogen content of X_S	$i_{N,XS}$	$gN\ g^{-1}COD$	0.03	Koch et al. (2000)
Nitrogen content of X_H and X_A	$i_{N,BM}$	$gN\ g^{-1}COD$	0.07	ASM3

Note: The "Heterotrophic organ. (X_H)" grouping spans the rows from "Aerobic storage rate constant" through "Anoxic respiration rate of X_{Sto}". The "Autotrophic X_A" grouping spans the rows from "Autotrophic maximum growth rate" through "Anoxic endogenous respiration rate of X_A".

* intermediate value between the ones proposed by ASM3 and Koch et al. (2000).
Source: indicated.

---

[1] Temperature adjustment was performed for some parameters. The equations can be found at the end of the work (Aquasim code - appendix A).

3.2.4 Biofilm model

As mentioned, biofilm dynamics were simulated in Aquasim® within BC. This compartment has a one-dimensional biofilm dynamics model that calculates the microbial population's distribution over the granule's depth, resulting from competition for space and substrates (WANNER; GUJER, 1986). Hence, granule depth was divided into 10 grid points. Diffusion coefficients in water found in the literature (Table 10) were used to model dissolved substances transport inside the granule, as Aquasim® assumes that diffusion only happens inside the biofilm pores. The temperature correction calculation for diffusion coefficients was performed according to Eq. 1, proposed by Stewart (2003):

$$\theta_D = \mu_{w,25} \frac{(T + 273.15)}{298.15 \mu_{w,T}} \qquad \text{Eq. 1}$$

where θ_D is the temperature correction factor, $\mu_{w,25}$ is water viscosity at 25 °C, T is the operational temperature, and $\mu_{w,T}$ is water viscosity at the operational temperature.

Table 10. Mass transfer parameters.

Symbol	Definition	Diffusion coefficient (10^{-4} m².d⁻¹)	Source
$D_{Alk,25}$	Diffusion coefficient of H_2CO_3 in water at 25 °C*	0.60	Stewart (2003)
$D_{SS,25}$	Diffusion coefficient of S_S in water at 25 °C*	0.60	Stewart (2003)
$D_{SI,25}$	Diffusion coefficient of S_I in water at 25 °C*	0.60	Stewart (2003)
$D_{SO2,25}$	Diffusion coefficient of O_2 in water at 25 °C	2.10	Gmehling et al. (2010)
$D_{NHx,25}$	Diffusion coefficient of NH_4^+ in water at 25 °C	1.70	Stewart (2003)
$D_{NO,25}$	Diffusion coefficient of NO_3^- in water at 25 °C	1.65	Li and Gregory (1974)
$D_{N2,25}$	Diffusion coefficient of N_2 in water at 25 °C	1.62	Stewart (2003)

*Diffusion coefficient of acetate in water at 25 °C used for S_{Alk}, S_S, and S_I.
Source: indicated.

Some significant limitations exist in the biofilm model approach within the Aquasim® for modeling non-steady-state conditions. For example, the number of biofilm particles cannot vary during simulation, just the thickness, which, in turn, must be the same for all in the compartment, varying uniformly only in time. Therefore, to simulate the granulation (start-up) process observed in E-I and E-III, the following approach was used:

1. The data from the granulometric analysis was used to obtain the number of granules for each sample, considering the granule density constant and equal to 40 kg VSS.m⁻³

(WICHERN et al., 2008). It was also assumed that the retained biomass in each particle size range had a diameter equal to the average value of the sieve aperture.

2. The average value calculated for all samples during the operational period was used as the simulated number of granules (n_g). This value was overestimated at the operation start and underestimated at the end because it increases during the actual granulation process.

3. In turn, the used radius for the simulation (virtual biofilm thickness, $th_{biofilm,virtual}$) was calculated from n_g, so the simulated granules mass equaled the actual mass of granular biomass obtained in the TSS analysis. Thus, the simulated radius was calculated for each sample of the experiments. This value was underestimated at the beginning of the operation because as n_g was larger than the actual calculated number of granules, the simulated radius had to be smaller than the average radius to ensure mass conservation. On the other hand, it was overestimated at the operation end because as n_g was smaller than the actual calculated number of granules, it was required to adopt a larger $th_{biofilm,virtual}$ to ensure mass conservation. Figure 10 illustrates the used approach.

4. Finally, to ensure that the simulated biomass presents the desired radius, biofilm thickness ($th_{biofilm}$) was limited by using the surface erosion (u) rate formula proposed by Volcke et al. (2012), $u = \left(th_{biofilm}/th_{biofilm,virtual}\right)^{10}$. Granule surface area ($A$) was described by the equation proposed by Reichert (1994) for biofilms adhered to spherical particles, $A = 4\pi n_g(10^{-9} + z)$, considering a negligible radius for these particles (10^{-9} m), n_g number of particles (granules), and z the depth coordinate relative to the granules' center.

Figure 10. Schematic representation of the simulated granule distribution implemented in Aquasim®. Visualizing over or underestimating the simulated granules concerning the calculated data is possible.
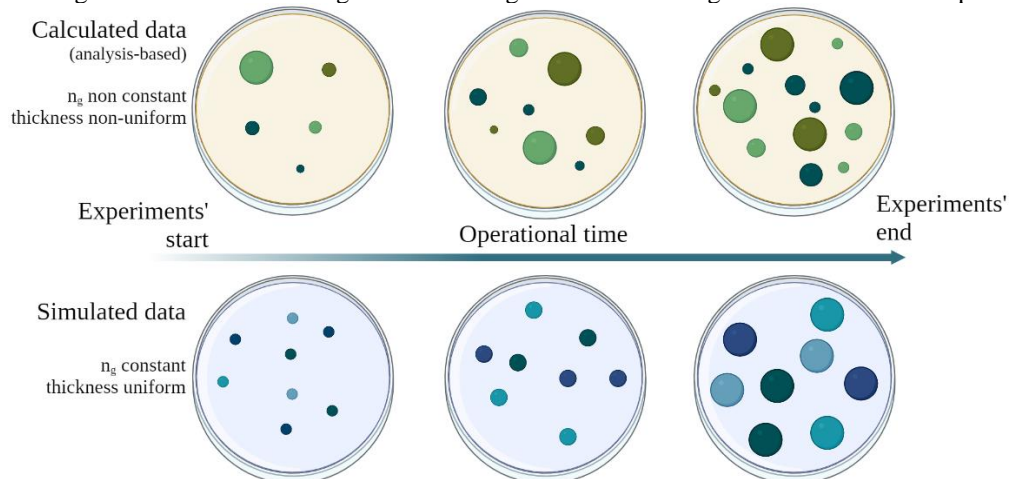
To sum up, the following assumptions were made: (i) granules were described as spherical biofilms adhered to a sphere of minimum size (10^{-9} m); (ii) granule size distribution was uniform throughout the operational time; (iii) MC_2 and BC were thoroughly mixed; (iv) granule density was considered constant throughout its depth; (v) granule depth was divided into 10 grid points; (vi) diffusion was considered constant, varying only with temperature; (v) boundary layer resistance equals to 100μm. All the parameters related to granule characteristics, mass transfer, and reactor operating conditions can also be found in Appendix A.

3.3 LAB-SCALE EXPERIMENTAL SYSTEM[2]

The lab-scale (LS) experiments were carried out in two column-type sequencing batch reactors, SBR_{20} and SBR_{30}, operated at climatized room temperature of 20 ± 1 °C and 30 ± 1 °C, respectively. SBR_{20} had a working volume of 9.1 L, an internal diameter of 14 cm, and a total height of 59 cm. SBR_{30} was slightly larger and had an active volume of 11.2 L, an inner diameter of 15 cm, and a total height of 63.5 cm, noting that both reactors have the same height-to-surface area ratio of 4.2. Figure 11 shows a schematic diagram with reactors' dimensions associated with automation components.

Figure 11. Schematic LS reactors used for municipal wastewater treatment. Dimensions (a. SBR_{20}; b. SBR_{30}) and connections with automation components are indicated.
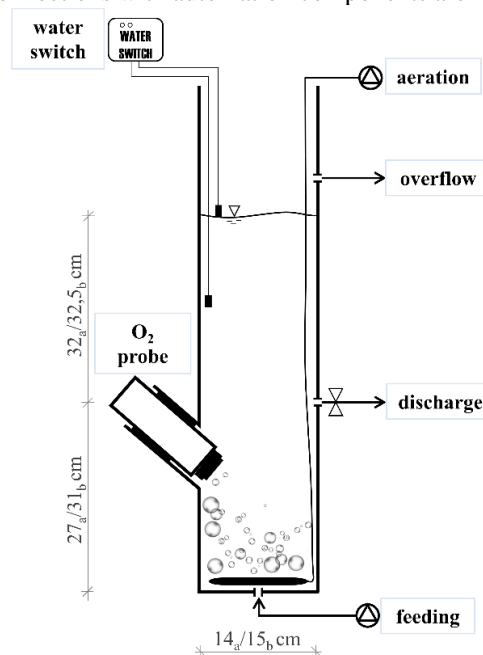
Source: adapted from Bremkes (2020).

---

[2] as similarly described in Araújo et al. (2022).

The materials for the SBRs confection were transparent acrylic for SBR_{20} and polyvinyl chloride (PVC) for SBR_{30}. SBR_{30} temperature was held at 30 °C by pumping warm water through a hose placed around the reactor, as shown in Figure 12.

Figure 12. Photograph of SBR_{20} (left) and SBR_{30} (right).

Sources: Bremkes (2020, left); the author (2022, right).

3.3.1 Operational conditions

Initially, both reactors were inoculated with approximately 2.5 $g.L^{-1}$ activated sludge from a municipal wastewater treatment plant (WWTP – Bochum-Ölbachtal, Germany) for the system start-up. After that, they were operated sequentially in 4.6 h cycles under alternating anaerobic and aerobic conditions to achieve phosphate and nitrogen removal. An SBR cycle comprised an (1) anaerobic/anoxic feeding phase from the bottom by a peristaltic pump (Ismatec, Ecoline v380) through the settled sludge bed, (2) an aerobic phase supplied through an air diffuser placed in the bottom of the reactors (airflow rate around 5 $L.min^{-1}$/ 5.4 $cm.s^{-1}$ air upflow velocity, DO concentration and temperature assessed through an oximeter (Hach LDO2), (3) settling and (4) effluent withdrawal discharged through a solenoid valve at 27 cm and 31 cm above the bottom of SBR_{20} and SBR_{30}, respectively (volume exchange ratio around 49%; hydraulic retention time around 9.2 h). The duration of each phase varied during 290 days of operation (Figure 13) throughout the operation aiming to optimize nutrient removal, mainly nitrate, based on previous research such as Wagner et al. (2015), Guimaraes et al. (2018), Dantas (2018), and Sales et al. (2018).

Figure 13. SBR's cycle profiles. The duration of each phase is indicated above each bar.
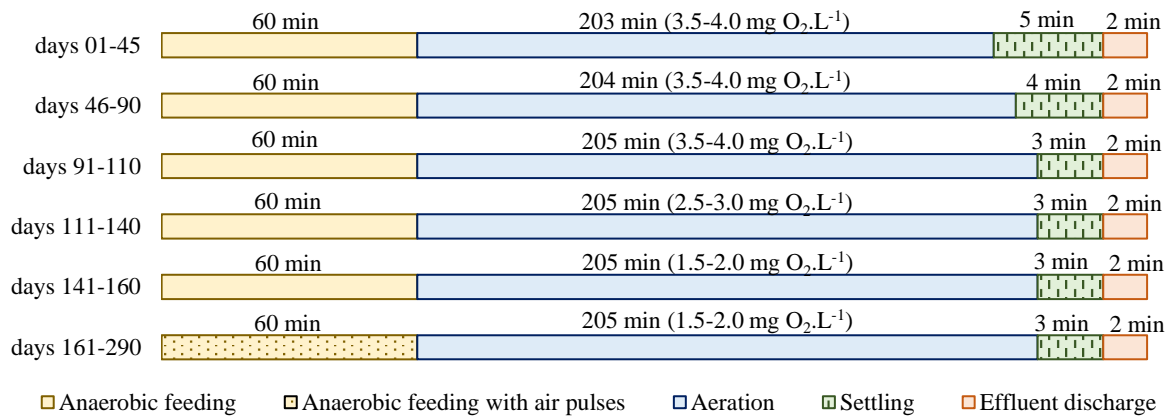
From day 1 to day 130, the settling time was reduced three times (at the end of days 45, 90, and 160), while the aerobic phase was increased correspondingly. Between days 160 and 290, air pulses of 10 seconds were given every 10 minutes during the anaerobic phase to improve the sludge and wastewater influent mixture and, in this way, enhance nutrient uptake/degradation. Phase durations, control of the pumps, air compressors/DO concentration, and valves were controlled by the software InTouch (Invensys Wonderware version 11.0.04) associated with a WAGO I/O system, water switches and a laptop. Reactor walls and probes were cleaned every two days to prevent biofilm growth. The pumped wastewater was taken from a thoroughly mixed equalization tank (1 m³), which receives twice daily municipal wastewater of the effluent of the Grid chamber from WWTP Bochum-Ölbachtal (Ruhrverband, Germany) after a curved screen with a mesh size of 1.5 mm. Total suspended solids (TSS) concentration and pH were measured with online probes inside this mixed tank.

3.3.2 System monitoring

Weekly 24 h composite samples from the inflow and effluent were analyzed. The parameters COD, TN_b (primarily for inflow samples), NH_4^+-N, and NO_3^--N (primarily for effluent samples) were determined photometrically with analytical kits provided by Hach Company. TSS of influent and effluent and mixed liquor suspended solids (MLSS) within the SBRs were determined according to EN 12880:2000 (DIN, 2000). Sludge retention time (SRT) was determined, including the discharged total suspended solids (TSS) within the effluent. Conductivity, pH, and DO concentration were measured weekly with a hand-held probe (WTW Multi 3430).

The sludge volume index (SVI) was determined from samples of the mixed liquor collected weekly (at the beginning 2-3 times a week) to monitor the aerobic granulation process. SVI_5, SVI_{10}, and SVI_{30} were obtained after a 1.0 L mixed liquor probe sedimentation from each reactor at 5, 10, and 30 minutes.

Biomass development was qualitatively monitored throughout the reactor operation using an optical microscope (Olympus BH-2) coupled to a camera (Olympus C-3030). A particle analyzer (Malvern Morphologi G3SE-ID) was used to determine the specific granule size and structure. The size distribution of the granules was quantified with sieves (BIN et al., 2011). Sieves with apertures of 100 µm, 250 µm, 500 µm, 1000 µm, and 2000 µm were used, and the particle size class was obtained from the TSS retained on each sieve. Granules were defined via fractions of d > 250 µm, and flocs, d < 250 µm. De Kreuk et al. (2005) described stable granulation as more than 80% of the granules having a size greater than 212 µm. In this study, the limit was set at 250 µm.

3.3.3 Taxonomic analysis of the microbial community

Mixed liquor samples were collected to characterize the microbial community in both reactors at the end of the operation (day 289) and stored directly at -20 °C until DNA extraction. For DNA extraction, samples were concentrated by successive centrifugation in Eppendorf Safe-Lock Tubes (2 mL) for 5 minutes at 15000°x°g, allowing 260 mg per sample to be used for the DNeasy PowerSoil Kit (Qiagen). DNA extraction was performed according to the manufacturer's instructions. Then, DNA extraction was taken up in 30 µl of elution buffer.

DNA quality and quantity were checked based on optical density (Nanodrop, peqlab) and by separation on 0.8% agarose gel. The microbial communities were taxonomically characterized using high throughput 16S rRNA gene amplicon sequencing, as Maus et al. (2017) described. This sequencing was carried out with Illumina MiSeq sequencer (Illumina, USA) by the Institute for Innovation Transfer (IIT) Biotech GmbH (Germany). The amplification of the hypervariable regions V3 and V4 of the 16S rRNA gene in bacteria and archaea was performed using the primers Pro341F (5'- CCTACGGGNBGCASCAG-3') and Pro805R (5'-GACTACNVG GGTATCTAATCC-3') for a first PCR round (Takahashi et al., 2014). Also, the Institute for Innovation Transfer (IIT) (Biotech GmbH, Germany) performed the first filtering steps of all sequences. PCR products of 460 bp were purified using AMPureXP magnetic beads (Beckman Coulter, USA). Then, Multiplex identifier tags and Illumina-specific

sequencing adaptors were attached to the amplicons in a second PCR using the Nextera XT Index Kit (Illumina Inc.).

Qualitative and quantitative assessments of 16S rRNA gene amplicons were performed using the Agilent 2100 Bioanalyzer system. Constructed 16S rRNA gene amplicon libraries were pooled in equimolar amounts for subsequent Illumina MiSeq sequencing (Illumina, USA), applying the paired-end protocol. A pipeline including different sequence analysis tools was used for amplicon processing, as described recently (WANG et al., 2007; LIEBE et al., 2016). All sequences not merged by FLASH using default settings were discarded during the first filtering step. Sequences with >1N (ambiguous base) and expected errors >0.5 were also filtered out.

The resulting data were processed, and the operational taxonomic units (OTUs) were clustered using USEARCH and taxonomically classified with the RDP classifier in the 16S modus (WANG et al., 2007). Only hits featuring a confidence value of at least 0.8 were considered. Finally, raw sequence reads were mapped onto the OTU sequences to get quantitative assignments.

3.4 MICRO-PROFILES

Micro-profiles were determined inside the granules collected from the LS reactors to investigate oxygen diffusion. For this, from the mixed liquor samples collected on day 180, granules with sizes of 1.5 and 2.0 mm were selected with a particle analyzer (Malvern Morphologi G3SE - ID). They were then acclimated to the medium (filtered treated wastewater with and without substrate addition) for a few hours before the measurements to ensure that steady-state profiles were obtained. The medium composition varied according to the experimental design, as detailed below. 50 μm diameter DO micro-sensors (OX-50, Unisense®) were used to track the local concentration of DO at different depths in the granule. A manual micromanipulator (Unisense®, MM33) was used to finely adjust the position of the electrode tip with a spatial resolution of 10 μm.

In short, the oxygen micro-profile measurements were performed in an experimental setup composed of: i) a flow cell, ii) a mixing tank, iii) a micromanipulator, and iv) a DO microsensor coupled with a transmitter/computer (Figure 14). The flow cell (Figure 15) was made based on the vertical liquid-jet flow system developed by Ploug and Jørgensen (1999) to measure chemical gradients in activated sludge flocs. This cell was made by joining two Plexiglas tubes (5 cm diameter and 10 cm high each) with a nylon net in the middle, glued

together with medical silicone adhesive. The mixing tank corresponded to an acrylic 2 L container comprising an aquarium heater to obtain the desired temperature in the medium (20 or 30 °C), an oxygen probe (WTW Multi 3430, for measurement of oxygen and temperature), and two magnetic stirrers to ensure complete mixing. A peristaltic pump (Ismatec, Ecoline v380) transported the liquid from the mixing tank to the flow cell at an average liquid velocity ranging from 2-3 cm.s^{-1}, ensuring the granules were studied suspended 0.5 to 1 mm above the net. The flow cell was fed upward, and the overflow was collected in a plastic container located underneath the flow cell and returned by gravity to the mixing tank.

Figure 14. Micro-profiles experimental setup (diagram above and photo below) composed of: a flow cell, mixing tank, micromanipulator, and oxygen microsensors coupled with a transmitter/computer.
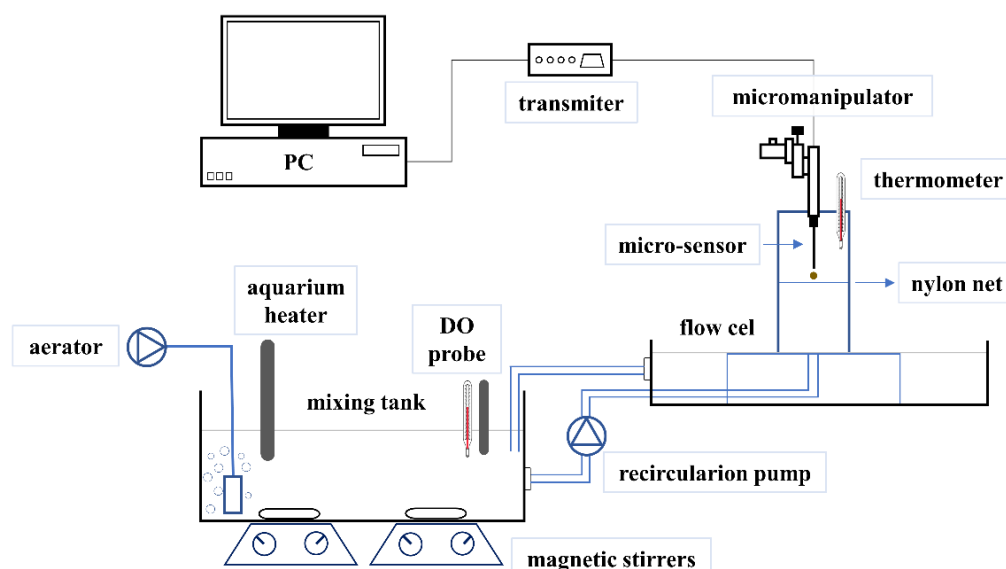
Source: the author (2022).

Before starting the experiments, the DO microelectrodes were polarized and calibrated according to the manufacturer's instructions (Unisense®). Eight (8) sequences were performed in a medium corresponding to treated filtered (20-25 µm) effluent from the WWTP Bochum-Ölbachtal (Bochum, Germany) with or without NH_4^+-N (50 mg.L^{-1}, ammonium chloride) and COD (500 mg.L^{-1}, glucose) addition, as shown in Table 11. For each sequence, two granules (1.5 and 2 mm) from each reactor (SBR$_{20}$ and SBR$_{30}$) were placed in the flow cell a few hours before the first measurement. Profiles were measured in the center of each granule, parallel to the flow, in 20 µm steps. For each granule, at least eight profiles (different medium concentrations and temperatures) were run, with some running in duplicate.

Figure 15. Flow cell photograph.
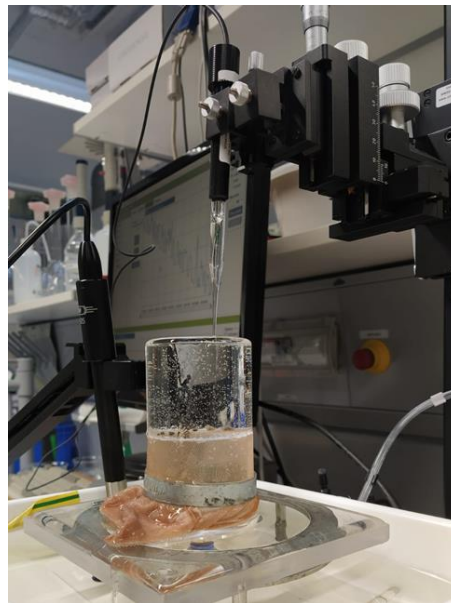
Source: the author (2022).

Table 11. Micro-profiles medium (treated filtered effluent from the WWTP Bochum-Ölbachtal) design.

Microprofile	Granules	Medium Temperature	NH_4^+-N (50 mg.L^{-1})	COD (500 mg.L^{-1})
1	≈ 1.5-2.0 mm from SBR$_{20}$	20 °C	–	–
2			+	–
3			–	+
4			+	+
5	≈ 1.5-2.0 mm from SBR$_{30}$	30 °C	–	–
6			+	–
7			–	+
8			+	+

Source: the author (2022).

4 RESULTS AND DISCUSSION

This section presents the results obtained in this study in the same sequence displayed in the previous chapter (Chapter 3, see Figure 6): 4.1 Pilot-scale experimental system; 4.2 Mathematical model; 4.3 Lab-scale experimental system; 4.4 Micro-profiles.

4.1 PILOT-SCALE EXPERIMENTAL SYSTEM[3]

The results obtained in the three experiments performed at LSA-UFPE (Brazil – E-I, E-II, and E-III) are presented and discussed in this section, focused on the formation and stability of aerobic granules under temperatures around 30 °C. E-I, E-II, and E-III were fed with real wastewater from the WWTP Mangueira at different periods. Table 12 summarizes the influent characteristics for each. The measured parameters' mean and (±) standard deviation were calculated separately and will be mentioned throughout the further discussion. The analysis of the biomass behavior and the observed removal efficiencies of the compounds of interest are presented in the following sub-topics.

Table 12. Influent characteristics (n = number of samples); (mean ± standard deviation).

Parameter	E-I (n = 13)	E-II (n = 14)	E-III (n = 27)
DO (mg O_2.L^{-1})	0.53 ± 0.25	0.41 ± 0.21	0.50 ± 0.22
pH (-)	7.15 ± 0.12	7.21 ± 0.26	7.18 ± 0.21
Temperature (°C)	28.6 ± 1.5	28.1 ± 1.4	29.0 ± 1.7
Conductivity (μS.cm^{-1})	852 ± 64	910 ± 162	885 ± 154
Redox Potential (mV)	-257 ± 50	-297 ± 40	-294 ± 71
Total Solids (mg TS.L^{-1})	439 ± 172	555 ± 152	553 ± 129
Total Suspended Solids (mg TSS.L^{-1})	76.2 ± 29.2	64.3 ± 49.9	61.4 ± 43.7
COD_{total} (mg.L^{-1})	226 ± 62	194 ± 73	201 ± 61
COD_{filt} (mg.L^{-1})	85.8 ± 20.8	68.0 ± 17.3	72.1 ± 15.2
Total Nitrogen (mg TKN-N.L^{-1})	34.6 ± 4.1	29.1 ± 11.3	30.1 ± 10.1
Ammonia Nitrogen (mg NH_4^+-N.L^{-1})	25.2 ± 4.8	22.0 ± 8.4	23.5 ± 6.8
Total Phosphorus (mg PO_4^{3-}-P.L^{-1})	3.94 ± 0.61	3.13 ± 1.17	3.47 ± 1.07
Orthophosphate (mg PO_4^{3-}-P.L^{-1})	1.68 ± 0.17	1.26 ± 0.45	1.44 ± 0.45

Source: the author (2022).

---

[3] Part of the results presented in topic 4.1 (E-III) has been already published in Science of the Total Environment 843 (2022) 156988, entitled: "*Formation and stability of aerobic granular sludge in a sequential batch reactor for the simultaneous removal of organic matter and nutrients from low-strength domestic wastewater*", by Oucilane I.M. Alves, Julliana M. Araújo, Poliana M.J. Silva, Bruna S. Magnus, Sávia Gavazza, Lourdinha Florêncio, and Mário T. Kato.

4.1.1 Development and characteristics of granular biomass

To better discuss the results, the operational period for each experiment was divided into granulation phases (start-up, partial granulation, and complete granulation when achieved) based on granulometry (Figure 16) and SVI (Figure 17) analyses.

Figure 16. Over time, biomass's size distribution in each experiment (E-I, E-II, and E-III). Dashed gray lines demarcate the beginning of the granular period (partial granulation, > 50% of biomass with diameter > 212µm). The dashed gray border rectangle specifies the period with mature granules (complete granulation, > 80% of biomass with diameter > 212µm) observed only in E-III.
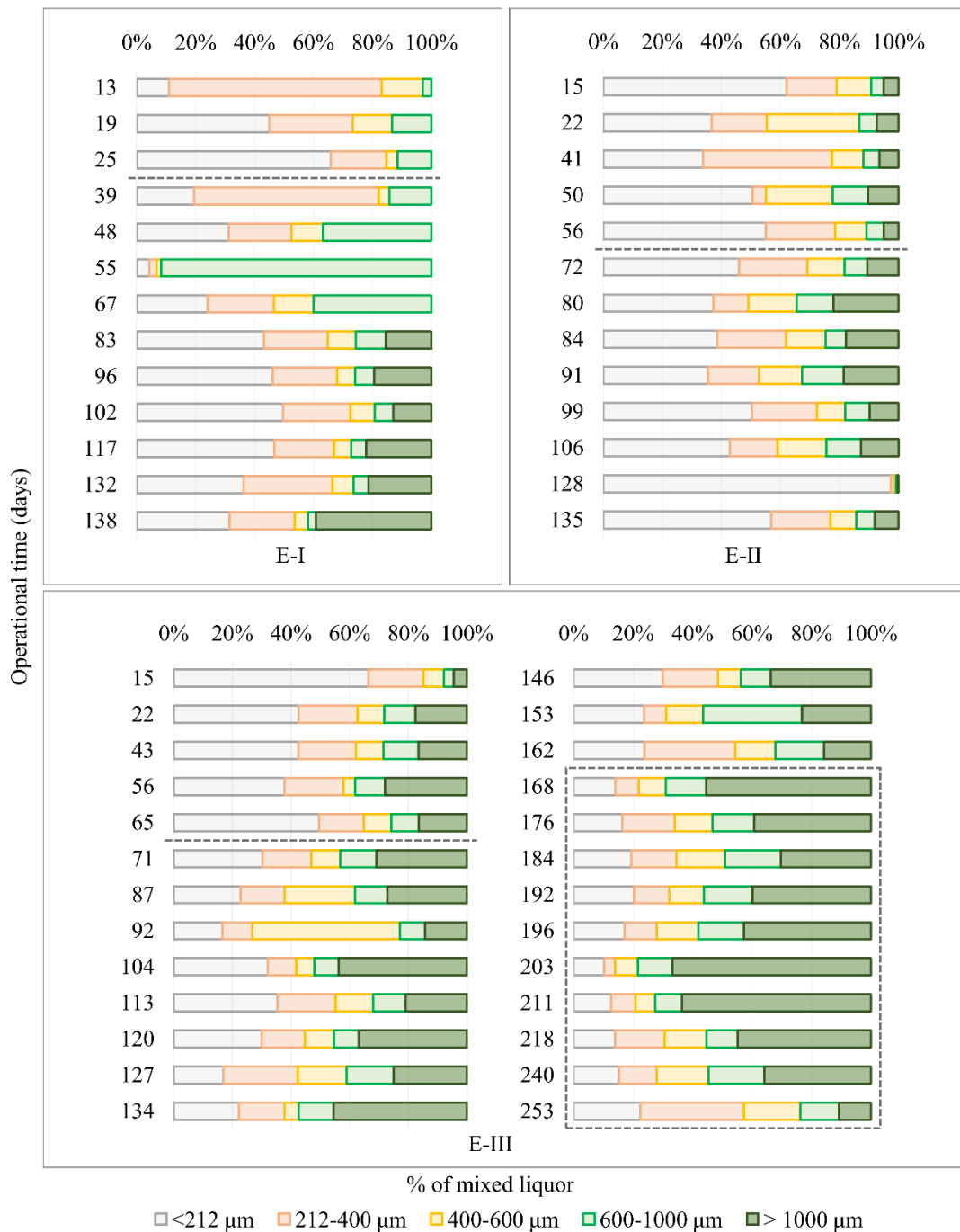
Source: the author (2022).

Figure 17. MLSS (●) and SRT (◊) in E-I (a), E-II (b), and E-III (e); SVI_{10} (■), SVI_{30} (□), and SVI_{10}/SVI_{30} (+) in E-I (c), E-II (d), and E-III (f). The grey and blue area indicate partial granulation and complete granulation, respectively.
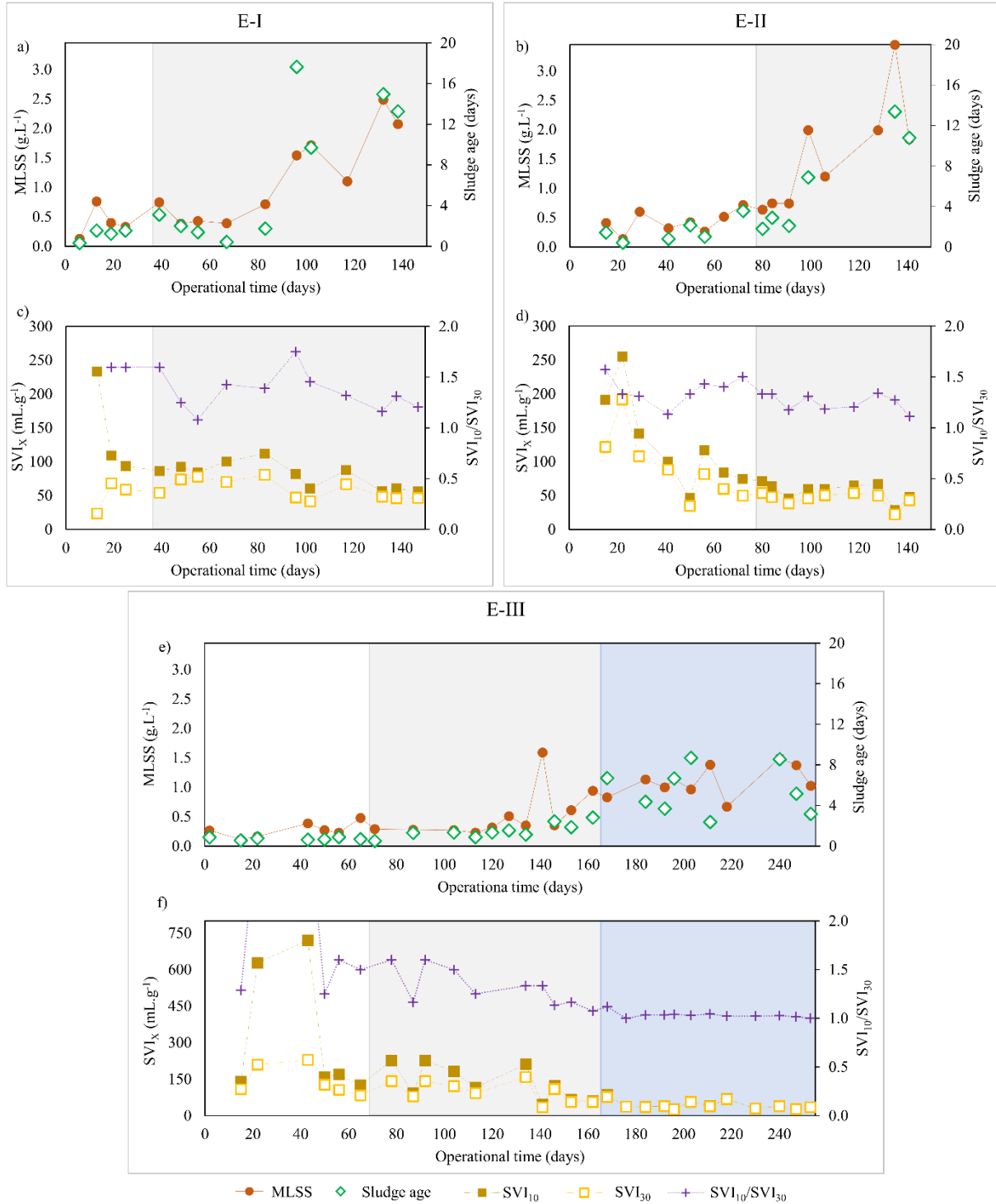
Source: the author (2022).

Observing the particle size distribution (Figure 16), a faster granule formation can be seen in E-I compared to the others. After 39 days, more than 50% of the biomass was composed of granules (diameter greater than 0.2µm). However, until the operation was stopped (due to operational problems on day 147), granules were not retained in sufficient concentration to

characterize as a stable AGS system (more than 80% of the biomass consisting of granules). For E-II and E-III, expressive granule formation was observed after 72 and 87 days of operation, respectively. A complete granulation was only apparent after 168 days in E-III.

Dantas (2018), when operating two experiments with the same experimental system and similar operational conditions (differing in the use of a longer interval between air pulses in the anoxic phase, 20min), obtained granules after a shorter period (58 days for 60-min anoxic phase, similar to E-II, and 79 days for 90-min anoxic phase, analogous to E-III). This fact can be explained by the higher availability of organic matter and nitrogen in this experiments' influent (COD_{total}: 282 ± 52; NH_4^+-N: 32.0 ± 5.7). However, no mature granules were obtained in the reported experimental period (130 days). Related results are commonly found in the literature, e.g., i) Ni et al. (2009) observed the first granules after 80 days of operation treating low-load domestic wastewater (COD_{tot} 95 - 200 $mg.L^{-1}$) in pilot-scale SBR (1 m³), observing more than 80% granular biomass only after 300 days; ii) Liu et al. (2010) verified complete granulation only after 400 days of operation treating sanitary wastewater in bench scale SBR (31.4 L); iii) Akaboci (2013) observed complete granulation after 150 days of operation in pilot-scale SBR (116 L, average OLR of 2.1 kg $COD_{total}.m^{-3}.d^{-1}$); iv) Magnus (2019) while using the same system but fed with a lower OLR (average of 1,3 kg $COD_{total}.m^{-3}.d^{-1}$), observed complete granulation only after 200 days.

In Figure 17, it is possible to observe that biomass development occurred slowly in all experiments. This fact is probably linked to the non-addition of inoculum associated with the short settling time applied from the start of the operation (an operational strategy used to retain biomass of good sedimentability). During partial granulation, average concentrations of mixed liquor suspended solids (MLSS) were 1.16 ± 0.72 g $VSS.L^{-1}$ for E-I, 1.48 ± 0.88 g $VSS.L^{-1}$ for E-II, and 0.85 ± 0.49 g VSS. L^{-1} for E-III. For complete granulation in E-III, it was 1.20 ± 0.38 g $VSS.L^{-1}$. It should be noted that although E-III corresponds to a repetition of E-I operational conditions, it showed lower biomass retention. This matter may be related to the microbial community retained in the system, as discussed in topic 4.1.3. In general, higher average biomass concentrations are reported in the literature[4] of studies with SBR treating low-strength wastewater.

The SRT gradually increased proportionally to the increase in biomass concentration during all experiments (Figure 17). The average results during the partial granular period were 6.6 ± 5.3 days for E-I, 5.9 ± 4.3 days for E-II, and 3.7 ± 0.5 days for E-III. During complete

---

[4] Dantas (2018) 1.67 and 1.70 $g \cdot L^{-1}$ with 130 days of operation; Wagner e Da Costa (2013) 3.4 $g \cdot SSV \cdot L^{-1}$ after 241 days; Liu et al. (2010) 1.3 $g \cdot L^{-1}$ with 70 days.

granulation in E-III, it was 5.6 ± 2.1 days. An SRT between 8 to 10 days is known to benefit nitrogen removal in conventional activated sludge systems (VON SPERLING, 2005); thus, better ammonia removal efficiencies were observed for all experiments after increasing sludge age, as further discussed in topic 4.1.2.

Finally, the SVI results (Figure 17) ratify the results shown by particle size distribution (Figure 16). By analyzing the graphic, it can be ascertained that only during complete granulation in E-III are SVI_{10}/SVI_{30} values lower than 1.1 were observed, as proposed by Liu and Tay (2008) (SVI_{10}/SVI_{30} between 1.0 and 1.1). During partial granulation, E-I and E-II had average SVI_{10}/SVI_{30} ratios of 1.36 ± 0.19 and 1.28 ± 0.11, respectively, confirming that they did not reach complete granulation. As for SVI_{30}, results were similar to those reported in other studies with AGS cultivated with domestic wastewater: Wagner and Da Costa (2013) 53 mL.g TSS^{-1}; Derlon et al. (2016) 80 mL.g TSS^{-1}; Dantas (2018) 61.3 and 63.3 mL.g TSS^{-1}; present study E-I 59 ± 14 mL.g TSS^{-1}, E-II 45 ± 9 mL.g TSS^{-1}, E-III 42 ± 15 mL.g TSS^{-1}.

4.1.2 Reactor Performance

The total influent COD concentrations were quite variable during the experiments, as shown in Figure 18, presenting minimum and maximum values between 156 and 387 mg.L^{-1} for E-I, 85 and 349 mg.L^{-1} for E-II and E-XIII, respectively. COD removal efficiency in Experiments I and II remained little variable throughout the experiment (E-I $76 \pm 5\%$; E-II $75 \pm 9\%$). As for E-III, considerable variations in efficiency were observed even in the period of granular stability ($76 \pm 10\%$ for the entire operational period and $77 \pm 15\%$ for complete granulation). These variations were likely associated with the influent COD fluctuation due to both seasonality and the equalization tank HRT (not controlled). Due to operational problems or maintenance at the WWTP, the influent remained in the equalization tank a few times for more than 12h, resulting in its partial degradation. Thus, the reactor was already fed with partially treated wastewater, and considering the inert fraction of COD, the resulting drop in removal is justified. For example, on day 230 of E-III, the influent had only 79.4 mg COD.L^{-1}, and the effluent (42.9 mg COD.L^{-1}) was within the effluent COD range during the operational period (44 ± 13 mg COD.L^{-1}).

Another critical point to be highlighted is the predominance of particulate organic substrate in the total COD. Layer et al. (2019) concluded that the higher the particulate substrate content, the slower AGS formation occurs. Increasing particulate (non-diffusible) organic substrate decreases the microbial growth potential deep in the granules. Furthermore, non-

diffusible organic substrates do not favor PAOs and GAOs, influencing granule stability (as previously mentioned) and phosphorus removal (further shown – in Figure 20 – and discussed).

Figure 18. Total influent COD (COD_{total}, ●), filtered influent COD (◯), filtered effluent COD (COD_{filt}, △), COD at the anoxic phase end (✲), and COD removal efficiency (+) in E-I, E-II, and E-III. The grey and blue area indicate partial granulation and complete granulation, respectively.
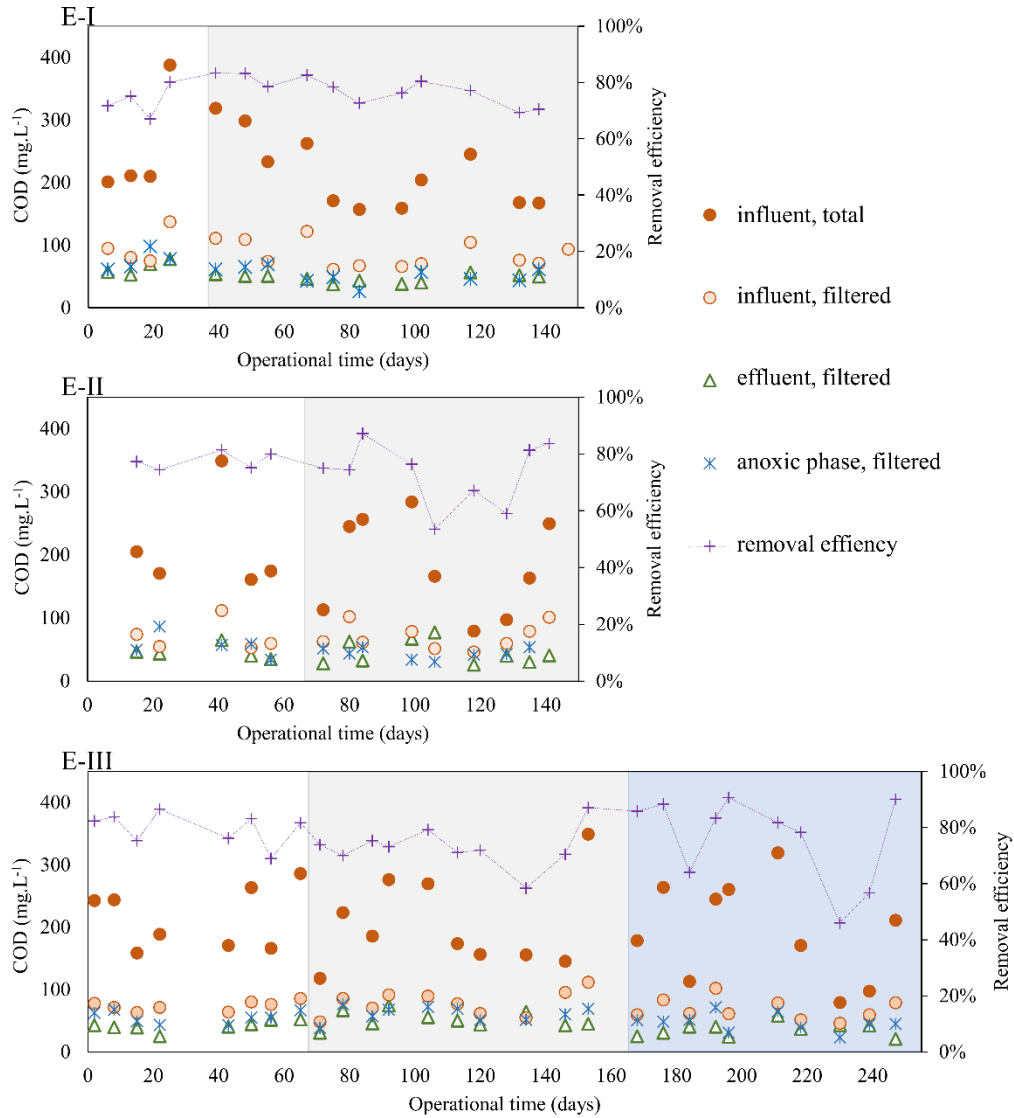
Source: the author (2022).

Figure 19 shows that all experiments showed low ammonia removal efficiency before granulation initiation. This poor performance can be attributed to the gradual development of nitrifying bacteria. These microorganisms are slow-growing and probably frequently washed out of the system due to high selection pressure (DE KREUK & VAN LOOSDRECHT, 2004; ROLLEMBERG *et al.*, 2018). With AGS formation, a nitrification improvement was observed. The average ammonia nitrogen removals were $78 \pm 20\%$ for E-I and $98 \pm 1\%$ for E-II after 100 days of operation and the observed increase in sludge age. However, significant nitrifying

activity only occurred after 134 days of operation for E-III, and during complete granulation, stable ammonia removal fluctuated, which averaged $74 \pm 26\%$.

Figure 19. NH_4^+-N influent (●), NH_4^+-N effluent (○), NO_3^--N effluent (◆), NO_2^--N effluent (□), and NH_4^+-N removal efficiency (+) in E-I, E-II, and E-III. The grey and blue area indicate partial granulation and complete granulation, respectively.
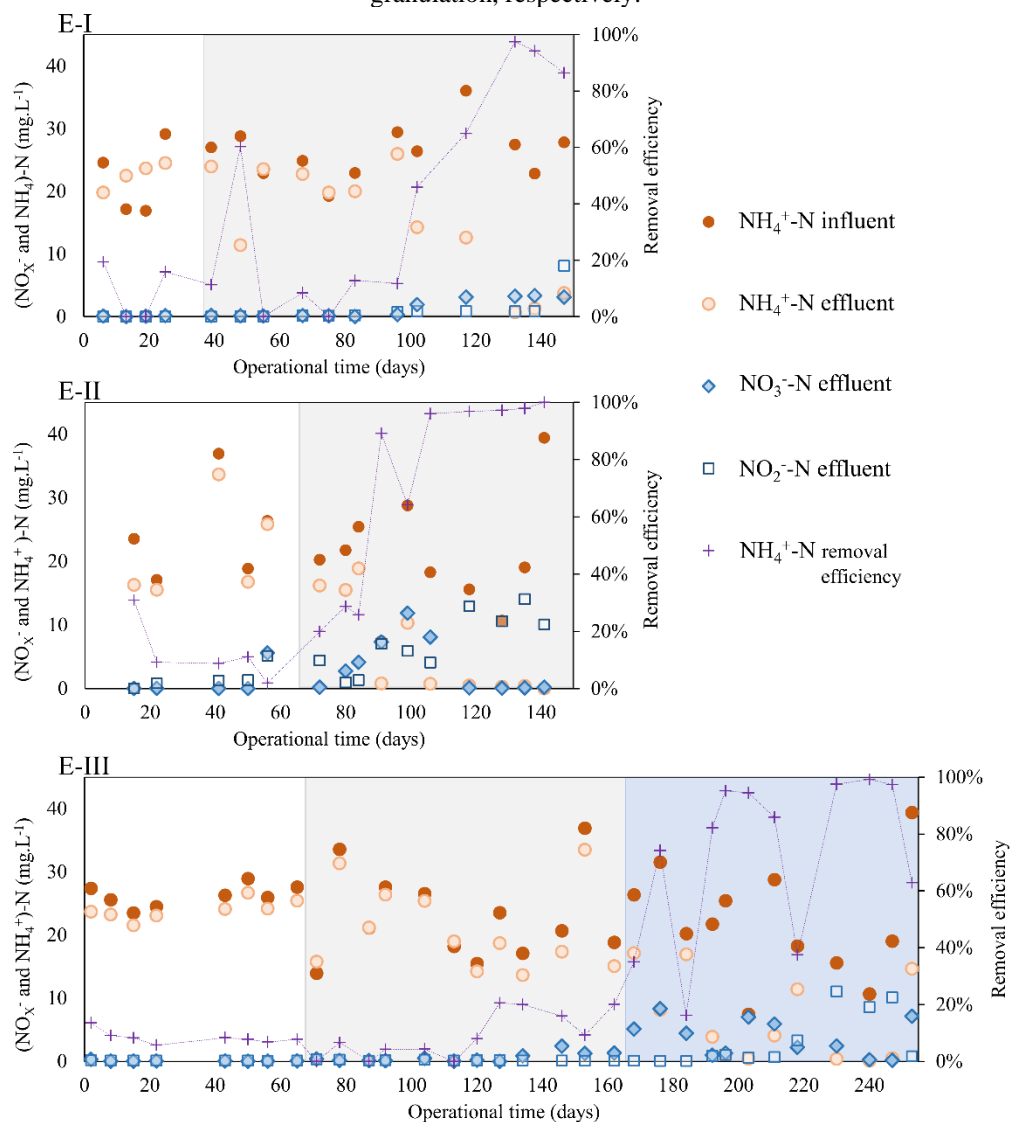
Source: the author (2022).

Since there was no significant intermediate oxidized compounds (nitrite and nitrate) accumulation, SND processes were achieved in all experiments. Dantas (2018), using the same experimental system in two experiments, obtained higher ammonia removals (94 and 95%). However, an accumulation of nitrite and nitrate in the system was observed. Guimarães et al. (2018) also observed high nitrite accumulation (around 16.5 mg NO_2^--N.L^{-1}) when treating domestic sewage in a pilot-scale SBR (98 L). Layer et al. (2020) stated that low-strength municipal wastewater in AGS systems could limit SND processes if constant DO is maintained

during the aeration phase. However, E-III developed larger granules with well-defined aerobic and anoxic zones that enabled the SND processes, even applying near-saturation DO (≈ 8.0 mg $O_2.L^{-1}$, total nitrogen – TN – removal efficiency $31 \pm 30\%$). Furthermore, the main nitrification pathway indicated by microbial diversity (discussed in section 4.1.3) was heterotrophic.

The treatment performances of the experiments assessed in terms of phosphorous removal are shown in Figure 20.

Figure 20. PO_4^{3-}-P influent (●), PO_4^{3-}-P effluent (○), PO_4^{3-}-P at the anoxic phase end (∗), and PO_4^{3-}-P removal efficiency (+) in E-I, E-II, and E-III. The grey and blue area indicate partial granulation and complete granulation, respectively.
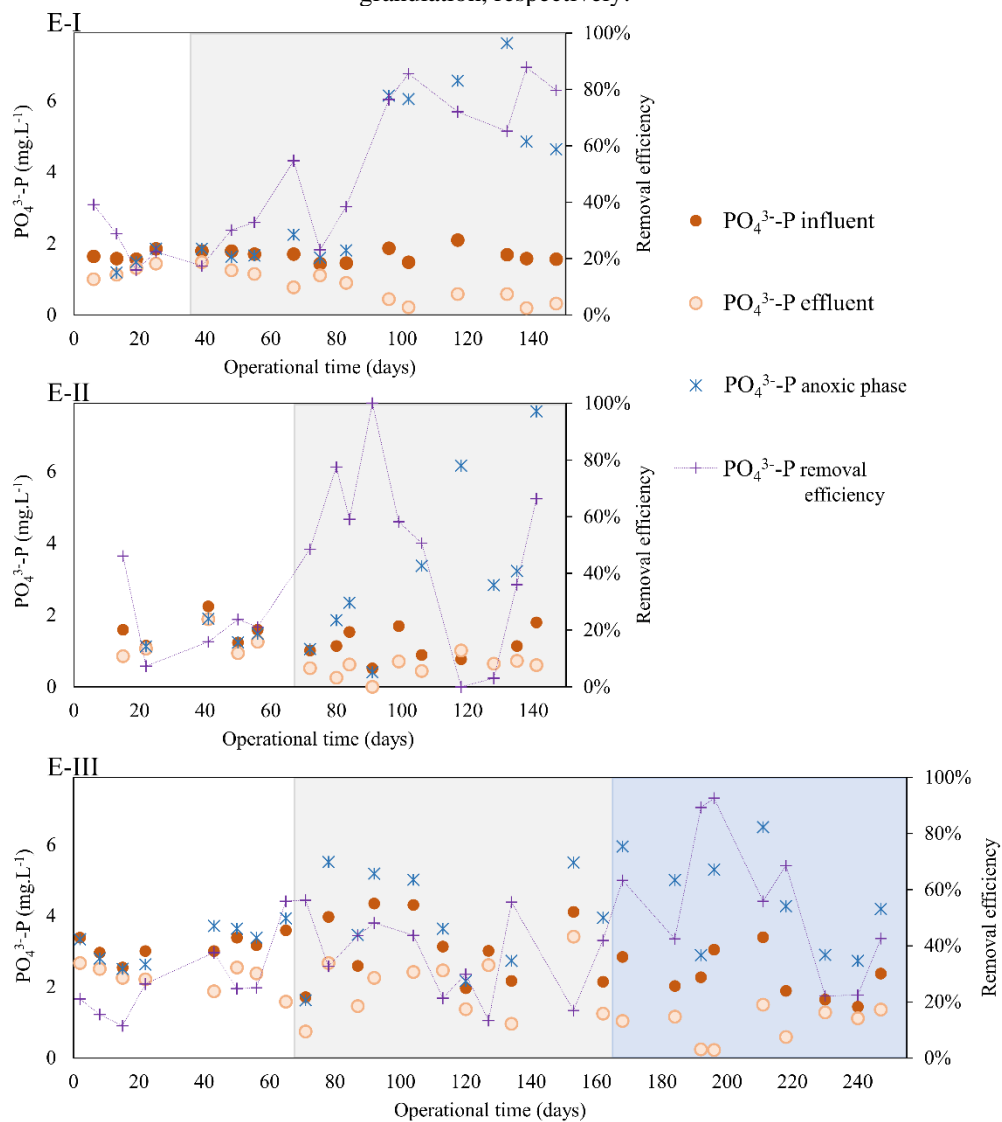
Source: the author (2022).

The low phosphorus removal during the beginning of the experiments is directly associated with the low age of the sludge as the biomass gradually develops (VON SPERLING, 2005; SZABÓ *et al*., 2017; ROLLEMBERG *et al*., 2018). After the start of granulation, an

increase in orthophosphate release and recovery was observed, indicating increased activity of PAO. Although PO_4^{3-}-P removal was unstable even at the complete granulation for E-III, an apparent increase in PAO activity is noticeably visualized. In general, regarding the biological removal of phosphorus, it can be highlighted that they showed similar or slightly higher results than the results found previously for the same experimental system. Namely, Dantas (2018) obtained an average removal of 43% (using a 1h30min-anaerobic phase), and Sales et al. (2018) 57% (40min-anoxic phase). Castellanos et al. (2020) obtained a maximum removal efficiency of only 35% when operating a lab-scale SBR (1.5 L) in a tropical climate (20 ± 3 °C) and with a 20-day SRT for 300 days. In this study, the average phosphorus removals (after 100 days of operation) were 78 ± 8% for E-I and 31 ± 26% for E-II. Whereas for E-III during complete granulation, it was 55 ± 24%. The improved phosphorus removal can be attributed to alternating anaerobic/aerobic conditions followed by granule formation and stability. Alternating anaerobic/aerobic conditions are known to be favorable for beneficial granulation microorganisms, e.g., PAO and GAO, due to the lack of soluble carbon under aerobic conditions (DE KREUK & VAN LOOSDRECHT, 2004). Moreover, after granule formation, the oxygen diffusion gradient promotes the formation of anoxic/anaerobic microzones, which also favors nutrient removal.

Table 13 and Table 14 present an overview of the average results of the parameters found during the experiments after the granulation processes started.

Table 13. Summary of the average results for E-I and E-II (mean ± standard deviation).

	E-I		E-II	
Operational time (days)	**39-99**	**100-147**	**72-99**	**100-141**
MLSS (g.L^{-1})	0.70 ± 0.40	1.84 ± 0.51	0.96 ± 0.52	2.12 ± 0.82
SRT (days)	4.4 ± 6.0	12.6 ± 2.2	3.4 ± 1.8	18.7 ± 9.5
SVI_{30} (mL.g SST^{-1})	67 ± 12	50 ± 9	47 ± 5	44 ± 11
SVI_{10}/SVI_{30}	1.44 ± 0.22	1.29 ± 0.10	1.33 ± 0.10	1.12 ± 0.08
% Granules > 212 µm	72 ± 14	59 ± 7	58 ± 6	50 ± 7
COD_{filt} effluent (mg COD.L^{-1})	43.5 ± 5.4	49.9 ± 7.1	46.8 ± 16.4	33.0 ± 8.6
COD removal (%)	80.1 ± 3.5	75.1 ± 4.2	79.2 ± 5.2	76.6 ± 9.5
NH_4^+-N effluent (mg N.L^{-1})	21.1 ± 4.4	6.3 ± 5.8	12.3 ± 6.4	0.4 ± 0.2
NH_4^+-N removal (%)	15 ± 19	78 ± 20	46 ± 27	98 ± 1
NO_2^--N effluent (mg N.L^{-1})	0.2 ± 0.2	2.3 ± 2.9	5.2 ± 4.0	1.7 ± 3.2
NO_3^--N effluent (mg N.L^{-1})	0.2 ± 0.1	2.9 ± 0.5	3.9 ± 2.4	10.3 ± 3.5
PO_4^{-3}-P effluent (mg P.L^{-1})	1.2 ± 0.2	0.4 ± 0.2	0.4 ± 0.3	0.6 ± 0.1
PO_4^{-3}-P removal (%)	30 ± 11	78 ± 8	69 ± 18	39 ± 3

Source: the author (2022).

Table 14. Summary of the average results for E-III (mean ± standard deviation).

	E-III	
Operational time (days)	**72-167**	**168-247**
MLSS $(g.L^{-1})$	0.52 ± 0.39	1.20 ± 0.30
SRT (days)	1.5 ± 0.7	5.6 ± 2.1
SVI_{30} $(mL.g\ SST^{-1})$	94 ± 39	42 ± 16
SVI_{10}/SVI_{30}	1.24 ± 0.08	1.03 ± 0.01
% Granules > 212 µm	75 ± 6	85 ± 3
COD_{filt} effluent $(mg\ COD.L^{-1})$	63.8 ± 18.4	37.2 ± 10.7
COD removal (%)	68 ± 12	77 ± 15
NH_4^+-N effluent $(mg\ N.L^{-1})$	21.4 ± 6.5	5.8 ± 6.3
NH_4^+-N removal (%)	10 ± 8	74 ± 26
NO_2^--N effluent $(mg\ N.L^{-1})$	0.62 ± 0.72	3.46 ± 2.70
NO_3^--N effluent $(mg\ N.L^{-1})$	0.15 ± 0.06	3.30 ± 4.17
PO_4^{-3}-P effluent $(mg\ P.L^{-1})$	2.1 ± 0.7	0.9 ± 0.4
PO_4^{-3}-P removal (%)	35 ± 13	55 ± 24

Source: the author (2022).

In summary, the 90-min-anoxic phase strategy (E-I and E-III) allowed for faster granule formation and more stable granulation. This strategy also favored phosphorus removal, although nitrogen removal was hampered. Although there was better ammonia nitrogen removal in E-II (60-min-anoxic phase), nitrate accumulation was observed. This is possibly associated with the absence of larger granules in the system, which hindered the SND process. However, it is necessary to study this system in a steady state. In addition, the stress caused by low COD and nutrient loading between days 118 and 128 also caused partial disintegration of the granules (e.g., see day 128 for E-II, Figure 16).

4.1.3 Microbial diversity

The microbial community composition with a relative abundance RA ≥ 1.0% in terms of phyla and taxonomic profiles is shown in Figure 21. The following days were chosen to analyze the changes in the communities: during the pre-granulation period (start-up), days 11 for E-I, 41 for E-II, and days 22 and 65 for E-III; at the beginning of the granulation process, days 39 for E-I, 80 for E-II and days 87 and 127 for E-III; and at the end of the experimental period days 138, 141 and 168 for E-I, E-II and E-III respectively. For the period of complete granulation in E-III, days 196 and 203 were also analyzed. For all three experiments, the identified bacteria primarily belonged to the phylum Proteobacteria (E-I 58-81%, E-II 60-82%,

and E-III 66-83%, data not shown). This phylum is frequently reported in the literature as prevalent in AGS systems (CHEN et al., 2020b; WANG et al., 2021). The second most abundant phylum, Firmicutes, in turn, decreased in E-I (20 → 10%) but increased in E-II (12 → 37%) and increased/decreased in E-III (8 → 32 → 18%).

Figure 21. Microbial community composition for E-I (days 11, 39, and 138), E-II (days 41, 80, and 141), and E-III (days 22, 65, 87, 127, 168, 196, and 203): phyla with RA ≥ 1.0% are shown above, and taxonomic profiles are below. Dashed gray lines demarcate the beginning of partial granulation. The dashed red line specifies the beginning of complete granulation in E-III. [a] Genera related to nitrogen removal. [b] Genera related to PAO's and GAO's. [c] Genera related to EPS production.
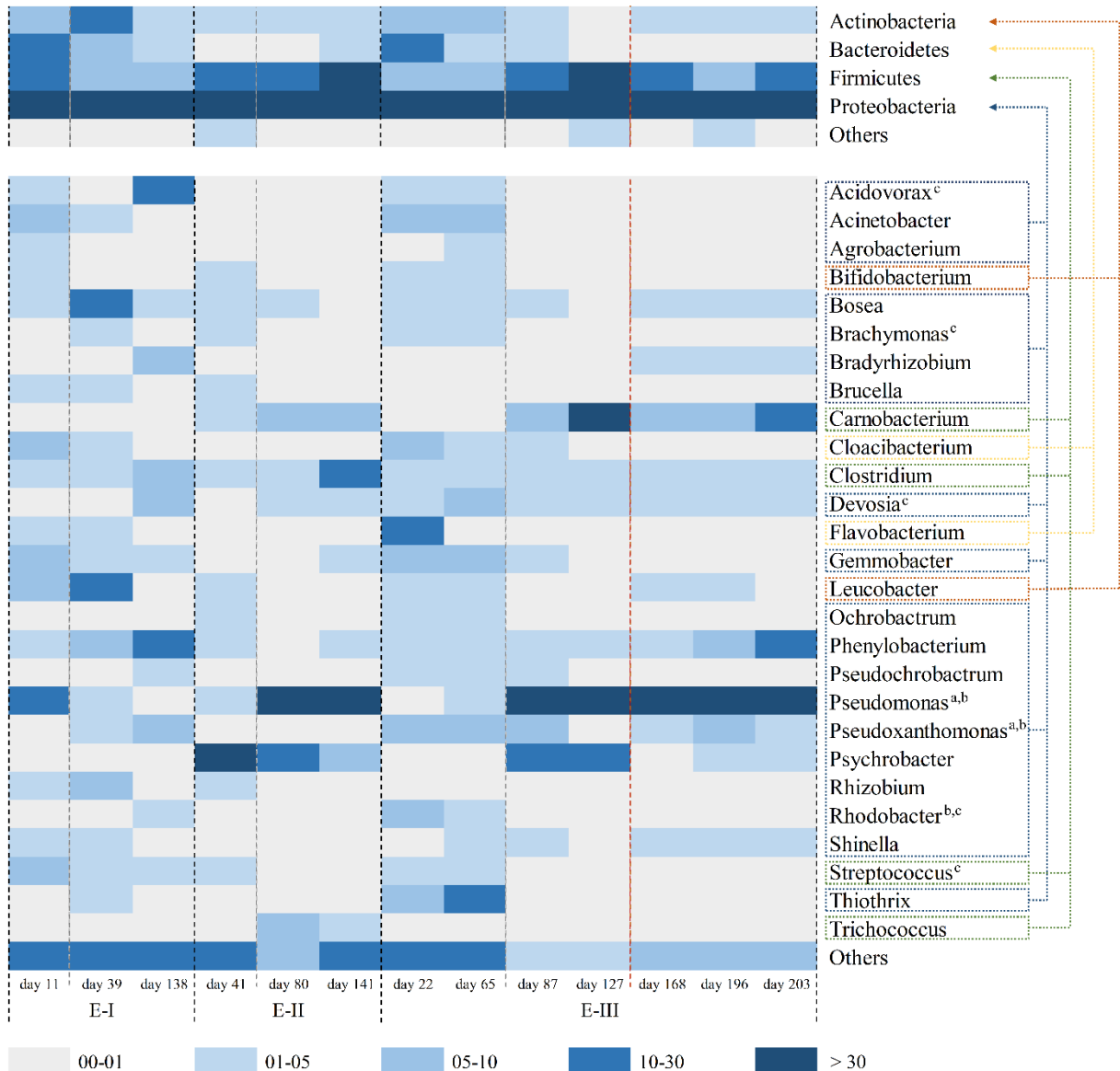
Source: the author (2022).

Analyzing Figure 21, it is notable that the three experiments presented a higher diversity of microorganisms during the initial period, which decreased during the operation. Filamentous bacteria, e.g., the genera *Flavobacterium*, *Acinetobacter*, and *Thiothrix*, showed significant RA

at the beginning of the experiments. Still, after the granulation process started, they were washed out of the system. After granule formation and stability, besides the decrease in microbial diversity, a higher RA of microorganisms known to help in AGS formation and stabilization as well as responsible for EPS production was observed, namely *Devosia*, *Rhodobacter*, *Streptococcus*, and *Brachymonas* (SZABON et al., 2017; XIA et al., 2018; ZHANG et al., 2019).

Microorganisms commonly associated with nitrogen removal – e.g., *Nitrosomonas*, *Nitrospira*, *Nitrobacter*, and *Paracoccus* – were not detected in any sample. However, groups of heterotrophic nitrifying and denitrifying bacteria were identified. Among them, the genus *Pseudomonas* stands out as they are highly abundant (E-I day 11 17%; E-II day 80 58%; E-III complete granulation 44-62%) and capable of heterotrophic nitrification along with aerobic denitrification (WANG et al., 2020a). Meanwhile, *Pseudoxanthomonas* (E-I 8%; E-II not detected; E-III 6-8%) can reduce nitrite and nitrate (LIU et al., 2017).

Also, the main microorganism groups associated with EBPR processes, namely *Accumulibacter* and *Competibacter*, were not identified. Thus, it can be assumed that phosphorus removal was through DPAO, with also the genera *Pseudoxanthomona* (E-I, E-II, and E-III) and *Pseudomonas* (E-II and E-III) standing out. *Pseudomonas* can perform denitrification associated with phosphorus removal using nitrite and nitrate, while *Pseudoxanthomona* preferentially uses nitrite (HE et al., 2020; WANG et al., 2018).

As a final remark, it is noteworthy highlighting the high RA of the genus *Phenylobacterium*, especially at the end of experiments E-I (19% on day 138) and E-III (15% on day 203). This single-species genus (*Phenylobacterium immobile*) has a minimal nutrient spectrum, not utilizing most sugars, alcohols, amino and carboxylic acids, and growing optimally in the presence of complex compounds (chloridazon, antipyrine, pyramid, and L-phenylalanine) (LINGENS et al., 1985). Thus, a strong indication of a possible complex COD source, such as industrial wastewater.

4.2 MATHEMATICAL MODELING

This section presents the results of implementing and calibrating the biofilm model proposed by Wanner and Gujer (1986) associated with ASM3 (Gujer et al., 1999) with Aquasim® aid for the data obtained in E-I and E-III (4.1), since they had the same operational setup. As a matter of organization, these results will be presented in the following sequence:

Influent COD fractionation (4.2.1); Model implementation (4.2.2); Performances in terms of solids (4.2.3), COD (4.2.4), and nitrogen (4.2.5).

4.2.1 Influent COD fractionation

Using a mathematical model requires a correct characterization of the influent since it describes biological processes in wastewater treatment. A greater degree of detail provides more information to the model; thus, higher confidence in the results is possible (PASZTOR et al., 2009). Different components which compose the organic matter in wastewater – degradable or inert, particulate or dissolved – interfere differently in the degradation processes. Among the factors that influence the composition of influent wastewater, it is known that temperature and degradation processes in the sewage network play an important role. Considering the specificities of the experimental data previously obtained at E-I and E-III (low concentrations of organic matter and temperature around 30 °C), the influent characterization methodology proposed by Lange (2018, described in section 3.2.2) was adapted to determine the wastewater characterization parameters according to DWA A-131 (ATV-DVWK, 2016). Figure 22 shows a boxplot summarizing the results.

Figure 22. Fractionation parameters calculated for Mangueira WWTP according to Lange (2018). f_A - inert particulate fraction of particulate COD; f_S - inert dissolved fraction of total COD; f_B - inorganic fraction of total suspended solids (TSS).

	f_A	f_B	f_S
IQR1	0.234	0.153	0.113
IQR3	0.310	0.306	0.217
Mean	0.273	0.236	0.154
Std. dev.	0.044	0.088	0.089
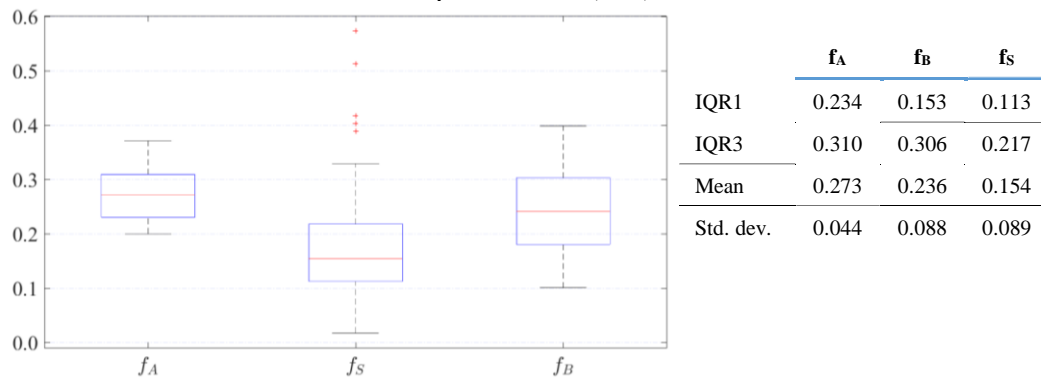
Source: the author (2022).

The wastewater from the experimental site in Recife has a considerably more significant fraction of dissolved inert components (f_S = 11-22%) when compared to the same results in countries with a temperate climate, e.g., Denmark (3-10%), Germany (3-11%) and Poland (4-7%) (ROELEVELD & VAN LOOSDRECHT, 2002; WICHERN, 2010; MAKINIA et al., 2010). This, together with the increased inert particulate COD fraction (f_A = 23-31%) and mineralized inert particles in TSS (f_B = 15-31%), is likely associated with a high degradation

within the sewage collection system due to the higher temperatures in Recife (average wastewater temperature of 29 °C) as well as low organic matter load (WALDER et al., 2013). This calculation of the coefficients with real data provides a much more reliable basis for the model calibration (section 4.2.2). Here, this was especially relevant because such detailed influent COD fractionation is still rare for warm climates.

When calculating the COD fractions using the obtained parameters, it can be seen that the inert dissolved COD (S_I) is significantly higher and contributes up to 22% to the COD of the influent (Figure 23). On the other hand, the relative contribution of the inert particulate fraction (X_I) is somewhat smaller. However, these two fractions summed can reach up to 40%, compared to maximum values of about 30% in the European WWTP (ROELEVELD & VAN LOOSDRECHT, 2002; WICHERN, 2010; MAKINIA et al., 2010). In the degradable fraction, only a minor part is readily available (S_S), as already mentioned. As municipal wastewater usually shows significant seasonal variations, the major degradable fractions oscillate considerably, either in particulate (X_S) or dissolved but hardly degradable (S_{XS}).

Figure 23. COD fractions of Mangueira WWTP. X_I: inert particulate COD; X_S: degradable particulate COD; S_{XS}: dissolved but hardly degradable COD; S_S: degradable dissolved COD; S_I: inert dissolved COD.
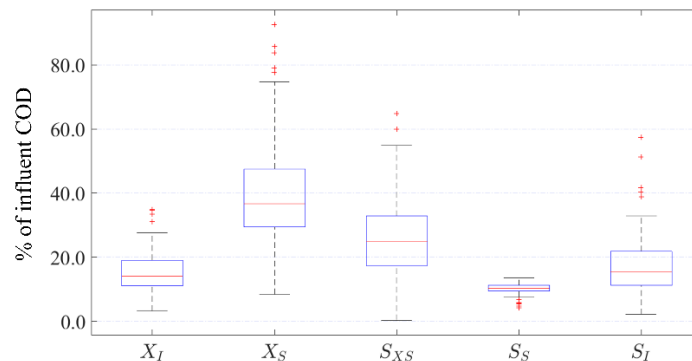
Despite the variations mentioned, it was decided to use a single value for each coefficient during model calibration. The values of 0.3, 0.2, and 0.1 for the coefficients f_A, f_B, and f_S, respectively, were the ones that allowed a great representation of the modeled data group. Figure 24 compares the fractionation results regarding soluble COD (COD_{filt}) and solids (TSS, VSS) with the real data. The fractionation for both experiments showed a good fit for COD_{filt}, but slightly higher values for solids (both TSS and VSS). This fact is first justified by the type of membrane used in the solids analyses in E-I and E-III, a glass fiber membrane (1.20 µm), which has a higher porosity than that adopted by DWA A-131 (0.45 µm), retaining fewer solids than simulated.

Figure 24. Above: Fractionation results obtained for filtered COD (COD$_{filt}$) considering the input data for total COD (COD$_{tot}$). Real COD$_{total}$ data (●); Real COD$_{filt}$ data (○); Simulated COD$_{filt}$ (solid blue line). Below: Fractionation results obtained for TSS and VSS. Real TSS data (■); Simulated TSS data (double purple line); Real VSS data (■); Simulated VSS data (dashed red line).
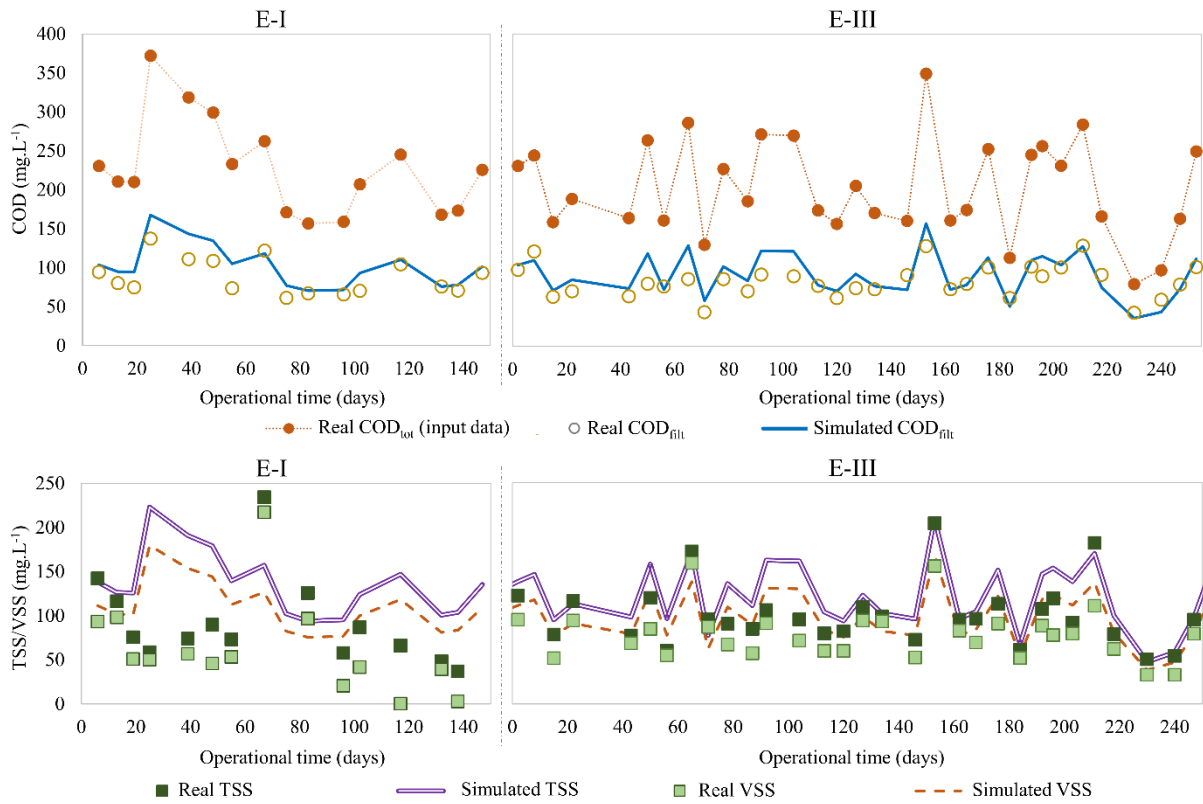
Source: the author (2022).

In addition, it is worth noting also that the composition of the solids in the influent during E-I did not show a clear pattern. Periods with a high COD concentration, for example, between days 19 and 55, did not correspond to high solids concentrations. An alternative would be to use specific fractionation parameters for each sampling point, but it was not used to facilitate the comparison between the experiments. The implications of this difference during the model implementation and calibration are also discussed below.

4.2.2 Model implementation

The ASM3h model and the biofilm model (WANNER & GUJER, 1986) were implemented for the data obtained by experiments E-I and E-III, which were not at a steady state. Thus, initially, the average thickness and the average number of granules were calculated for each sampling point, assuming that the density of the granules was constant and equal to 40 kg VSS.m^{-3} (WICHERN et al., 2008). By having the average number of granules to be used in the simulation (since this should be fixed during the operational period), a virtual thickness was

calculated for each sampling point to obtain the same mass of biofilm existing in the actual system.

Table 15. Strategy used to define virtual radius for E-I and E-III: average radius ($th_{biofilm}$, calculated based on granulometry) and number of granules for each sampling point (calculated with TSS data assuming a density of 40 kg VSS.m^{-3}); mean number of granules for the total period, virtual radius calculated for mass conservation after admitting the average number of granule for each sampling point ($th_{biofilm,virtual}$).

E-I				E-III			
day	$th_{biofilm}$ (mm)	n. of granules	→ virtual $th_{biofilm}$ (mm)	day	$th_{biofilm}$ (mm)	n. of granules	→ virtual $th_{biofilm}$ (mm)
6	0.213	$2.19 \cdot 10^6$	0.165	15	0.313	$1.36 \cdot 10^6$	0.401
13	0.331	$1.44 \cdot 10^7$	0.481	22	0.610	$5.58 \cdot 10^5$	0.580
19	0.330	$3.84 \cdot 10^6$	0.309	43	0.600	$8.73 \cdot 10^5$	0.663
25	0.271	$4.99 \cdot 10^6$	0.277	50	1.141	$1.26 \cdot 10^5$	0.661
39	0.354	$1.15 \cdot 10^7$	0.478	56	0.781	$2.82 \cdot 10^5$	0.592
48	0.461	$3.12 \cdot 10^6$	0.403	65	0.574	$8.65 \cdot 10^5$	0.632
55	0.756	$7.23 \cdot 10^5$	0.405	71	0.865	$2.67 \cdot 10^5$	0.643
67	0.494	$2.16 \cdot 10^6$	0.381	78	0.436	$7.15 \cdot 10^5$	0.450
83	0.572	$1.86 \cdot 10^6$	0.420	87	0.834	$3.23 \cdot 10^5$	0.661
96	0.608	$4.21 \cdot 10^6$	0.586	92	0.662	$6.59 \cdot 10^5$	0.666
102	0.498	$7.42 \cdot 10^6$	0.580	104	1.052	$1.75 \cdot 10^5$	0.680
117	0.646	$2.24 \cdot 10^6$	0.505	113	0.687	$4.53 \cdot 10^5$	0.609
132	0.651	$5.05 \cdot 10^6$	0.668	120	0.947	$2.45 \cdot 10^5$	0.685
138	0.945	$1.93 \cdot 10^6$	0.703	127	0.816	$6.55 \cdot 10^5$	0.819
Mean		$4.69 \cdot 10^6$		134	1.111	$1.89 \cdot 10^5$	0.737
std. dev.		$3.81 \cdot 10^6$		146	0.895	$2.77 \cdot 10^5$	0.674
				153	0.852	$9.05 \cdot 10^5$	0.952
				162	0.644	$2.27 \cdot 10^6$	0.978
				168	1.309	$2.91 \cdot 10^5$	1.002
				176	1.039	$1.02 \cdot 10^6$	1.210
				184	0.914	$1.19 \cdot 10^6$	1.120
				192	1.054	$7.00 \cdot 10^5$	1.081
				196	1.107	$7.92 \cdot 10^5$	1.183
				203	1.495	$2.30 \cdot 10^5$	1.058
				218	1.123	$7.61 \cdot 10^5$	1.184
				240	1.016	$7.61 \cdot 10^5$	1.072
				247	1.257	$5.55 \cdot 10^5$	1.193
				mean		$6.48 \cdot 10^5$	
				std. dev.		$4.54 \cdot 10^5$	

Source: the author (2022).

Analyzing table 15, one can observe the significant variation in the number of granules (std. dev. in a magnitude order between 10^5 and 10^6). Considering that new granules are continuously formed, some granules are washed out of the system, and detachment/attachment happens dynamically, admitting a single granule size and the same quantity during the whole

operational period simplifies the modeling process. Still, such a strategy will always be considered during model calibration and analysis. For example, on day 55 of E-I, the average calculated radius was 0.75 mm; however, since the number of granules ($7.23 \ 10^5$) was less than the average number used ($4.69 \ 10^6$), the virtual radius was 46% smaller (0.405 mm). This adjustment may reflect on processes that depend directly on diffusion, such as denitrification in anoxic zones in the granules' inner layers.

Limiting the simulated radius with the erosion formula proposed by Volcke et al. (2012, see topic 3.2.4) was quite successful, as shown by the simulated radius in Figure 25, which also shows the average calculated and virtual radius.

Figure 25. Modeled biofilm thickness: calculated average radius (th$_{biofilm}$, ●), virtual radius calculated for mass conservation (th$_{biofilm,virtual}$, ○), simulated radius (Simulated th$_{biofilm}$, solid **green** line).
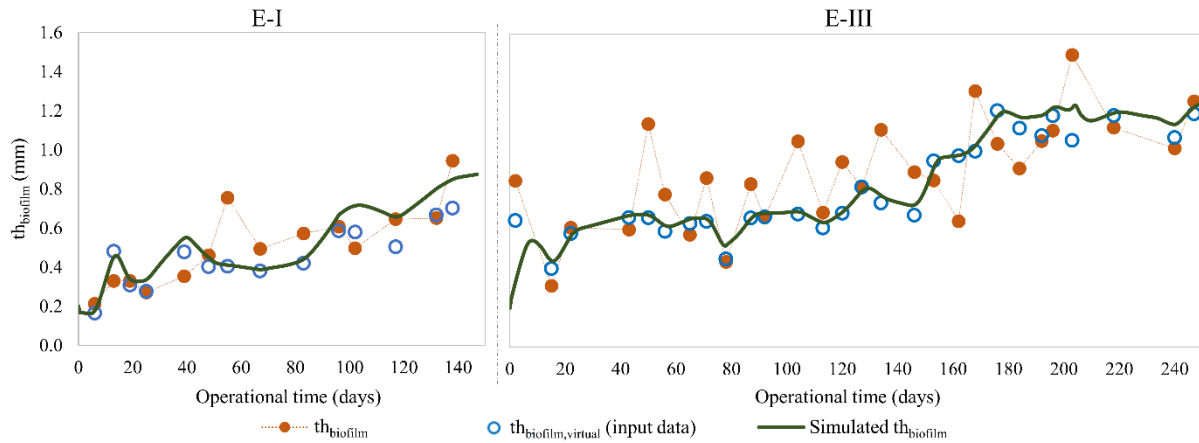
Source: the author (2022).

Thereupon, the model calibration was adjusted in three steps, solids behavior (4.2.3), followed by COD (4.2.4), and at the end, nitrogen (4.2.5).

4.2.3 Solids behavior

As mentioned, the biofilm mass was conserved with the application of the virtual radius strategy. Therefore, the biomass solids calibration was performed only for the suspended solids in the model bulk (flocculent biomass, activated sludge with a diameter < 212 μm). This biomass and the TSS removal efficiency in the settling phase of the cycle were adjusted based on the mixed liquor and effluent solids data with the bifurcation (bif.) of the advective link (AL$_2$). Otherwise, the percentage of solids returning to the system was calculated based on the mass of solids retained and discarded at the sampling points. Table 16 presents the calculated percentage of retained solids for E-I and E-III.

Table 16. Percentage of retained solids calculated for E-I and E-III.

E-I		E-III	
day	% retained solids	day	% retained solids
0	0.0%	0	0.0%
13	26.4%	2	58.7%
19	88.1%	15	57.5%
25	85.2%	22	41.1%
39	80.7%	43	35.0%
48	68.6%	50	0.0%
55	0.0%	56	30.9%
67	0.0%	65	54.3%
83	76.8%	71	0.0%
96	96.5%	87	45.3%
102	95.3%	104	0.0%
117	93.9%	113	47.6%
		120	42.8%
		127	46.9%
		134	32.9%
		146	73.0%
		153	27.8%
		162	66.6%
		168	85.8%
		176	57.0%
		184	77.7%
		192	78.1%
		196	79.1%
		211	0.0%
		240	86.3%

Source: the author (2022).

In turn, Figure 26 shows the behavior of the simulated flocculant biomass (milligrams of TSS per liter of reactor working volume), as well as the concentrations of effluent TSS for E-I and E-III. In periods with higher granule concentration, the solids retention strategy was primarily satisfactory. As the sampling was mainly performed weekly, the solids retention was calculated based on a single cycle for this entire period. On some days, although the simulated flocculated sludge concentration was higher than the real one (e.g., between days 20 and 40 in E-I), the simulated TSS effluent was also higher than the actual data. Therefore, a lower solids retention would lead to an even higher increase of effluent solids. Still, in periods after abrupt system TSS-behavior changes, e.g., between days 60 and 80 for E-I and 140 and 180 for E-III, the fit was not as well satisfied, also affecting system efficiencies (calibration in terms of COD and nitrogen).

Figure 26. Modeled TSS: real flocculated (activated sludge, < 212 μm) TSS (○), simulated flocculated TSS (dashed **brown** line), real effluent TSS (□), simulated effluent TSS (double **green** line).
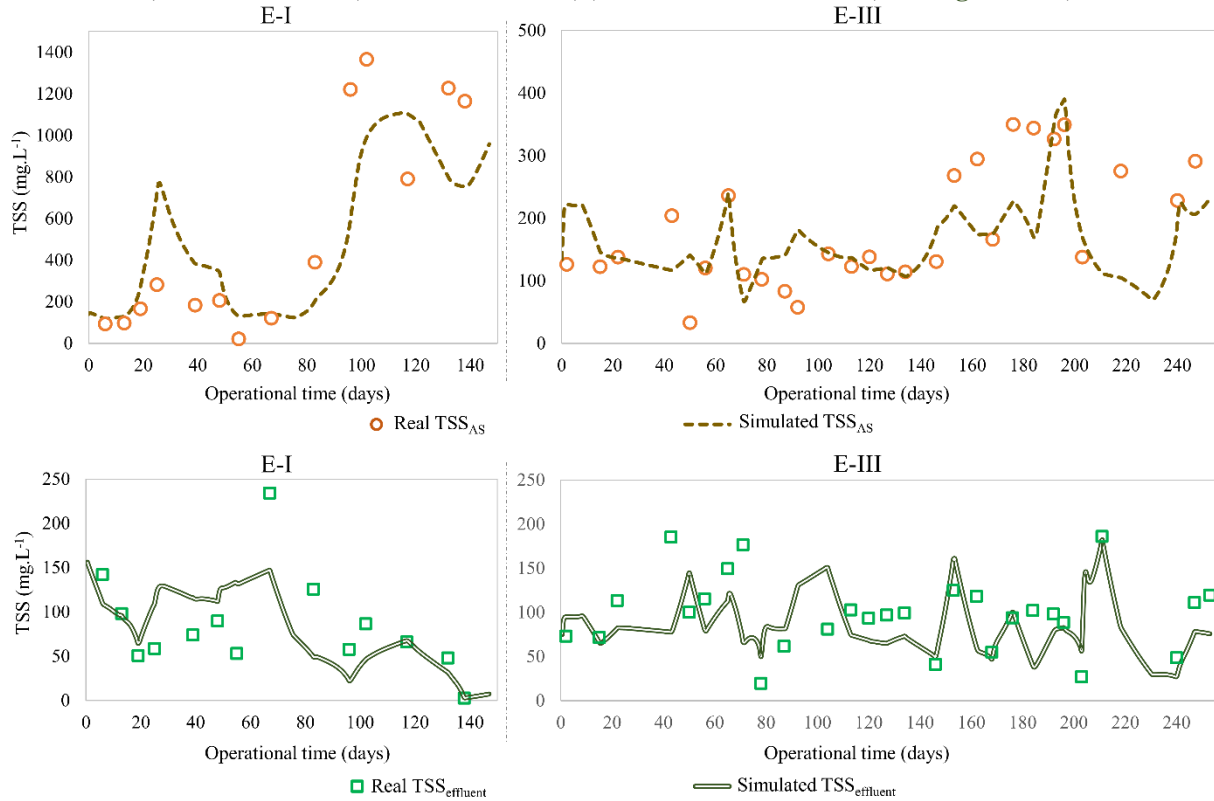
Source: the author (2022).

Besides the factors already mentioned, the difference in solids concentration in the simulated and actual inflow (topic 4.2.1) also contributed to a more significant difference between the real and simulated effluent solids data. This difference will also be reflected in the flocculent biomass concentration (more solids returned to the system in the simulation) and, as discussed in the next topic, in the effluent COD_{total}.

4.2.4 COD performance

When calibrating the removal of organic matter from the system, it was verified that the calibration of influent COD ensured a proper fit without needing to calibrate stoichiometric or kinetic parameters (other than temperature adjustments). The results for effluent COD_{total} and soluble COD ($COD_{filt.}$) are shown in Figure 27. The discrepancies, especially for E-I, are most likely associated with solids calibration during influent COD fractionation. Figure 24 and the discussion in Section 4.2.1 show that after influent COD fractionation, the fraction of solids diverged from the actual input data, especially between days 19 and 55 for E-I. These higher simulated influent solids directly affected solids removal, leading to a higher simulated effluent

concentration. By presenting a better fit in the solids fractionation in the affluent, E-III showed a better fit for COD_{total}. Overall, the simulated values for $COD_{filt.}$ slightly higher than the input data also can be associated with greater membrane porosity than the indicated (1.2 μm instead of 0.45 μm; ATV-DVWK, 2016), increasing the contribution of the colloidal fraction in $COD_{filt.}$.

Figure 27. Modeled COD: real COD_{total} effluent (○), simulated COD_{total} effluent (**purple** line), real $COD_{filt.}$ effluent (●), simulated $COD_{filt.}$ effluent (double **blue** line).
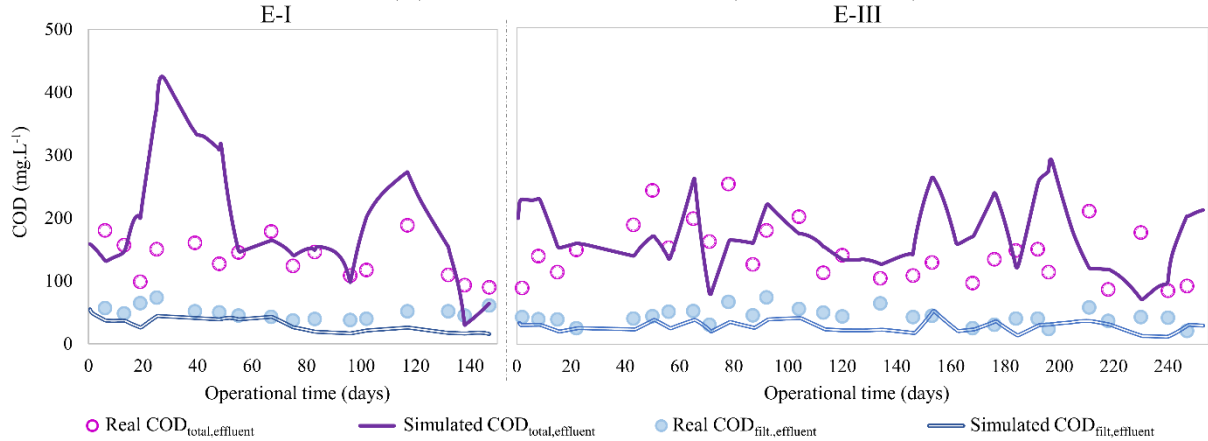
Source: the author (2022).

4.2.5 Nitrogen performance

In turn, the modeling of nitrogen removal presented more significant variations, as already expected, considering the influence of diffusion in its processes. Figure 28 shows the nitrogen simulation dynamics for E-I and E-III.

Figure 28. Modeled nitrogen: real NH_4^+-N effluent (○), simulated NH_4^+-N effluent (**red** line), real NO effluent (NO_2^--N + NO_3^--N, ○), simulated NO effluent (double **green** line), simulated N_2 effluent (dashed **yellow** line).
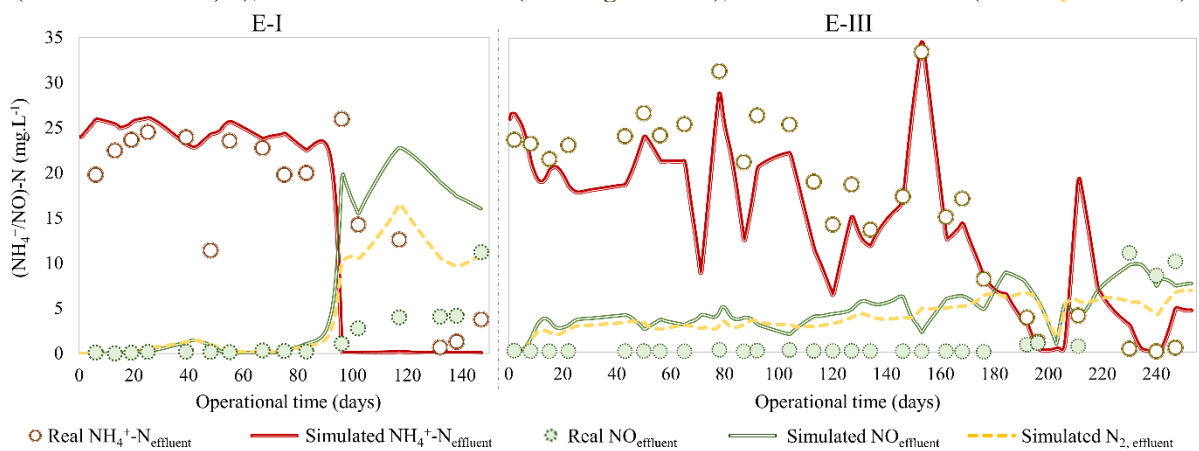
Source: the author (2022).

The calibration process for this parameter was exhaustive and did not significantly change the obtained results, especially considering NO accumulation. During this process, it was realized that the boundary layer resistance thickness was a very sensitive parameter. Since there is no consensus in the literature about its value (VAN DEN BERG et al., 2020), ranging between 0 and 800 μm under 20 °C (DE BEER et al., 1997; ETTERER, 2006; VAN DEN BERG et al., 2020), the influence of different thicknesses on nitrogen removal was verified. Figure 29 presents the ammonium nitrogen and effluent NO range for E-III when varying the BLR thickness between 100 and 500 μm (the actual output values are also indicated).

Figure 29. Modeled nitrogen for E-III when varying the BLR thickness in 100, 200, 300, 400, and 500 μm (n_g = 6.48 10^5). Simulated NH_4^+-N effluent (**red** area), real NH_4^+-N effluent (○), simulated NO effluent (**green** area), real NO effluent (NO_2^--N + NO_3^--N, ◉).
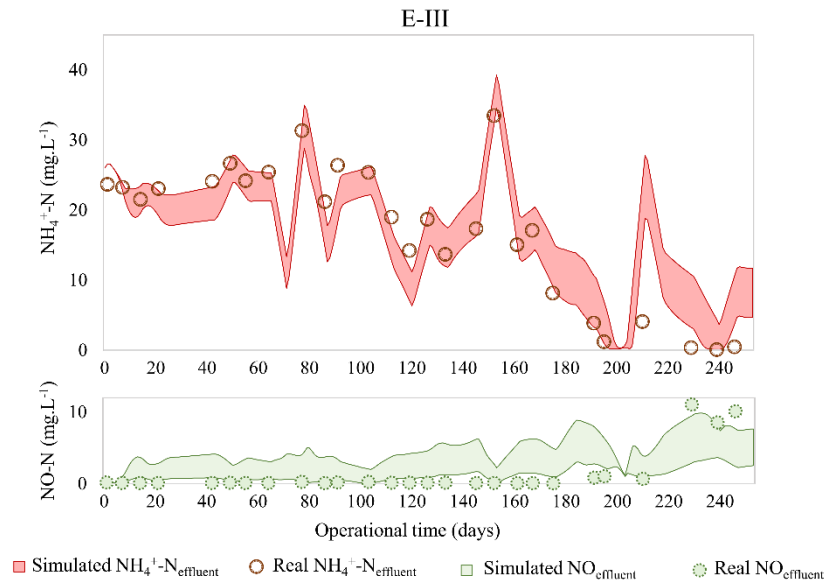
Source: the author (2022).

However, based on the further presented micro-profiles analysis (section 4.4), it was observed that the literature's most typical value of 100 μm (HORN & MORGENROTH, 2006) is reasonable considering the significant reactor turbulence in the real system compared to the flow cell. Hence, increasing the thickness of this layer in the simulation would not set up a realistic approach. Therefore, it was hypothesized that setting a single granule size for the whole system did not represent well the denitrifying activity of larger granules present in the real system. Thus, simulations were run for smaller/larger amounts of granules, aiming to increase/decrease the virtual radius and then test this hypothesis. Figure 30 presents the ammonium nitrogen and effluent NO range for E-III when varying the number of granules between 300,000 and 900,000 (the actual output values are also indicated).

Figure 30. Modeled nitrogen for E-III when varying the number of granules in 100,000, 500,000, and 900,000 (BLR = 100 μm). Simulated NH_4^+-N effluent (**red** area), real NH_4^+-N effluent (○), simulated NO effluent (**green** area), real NO effluent (NO_2^--N + NO_3^--N, ○).
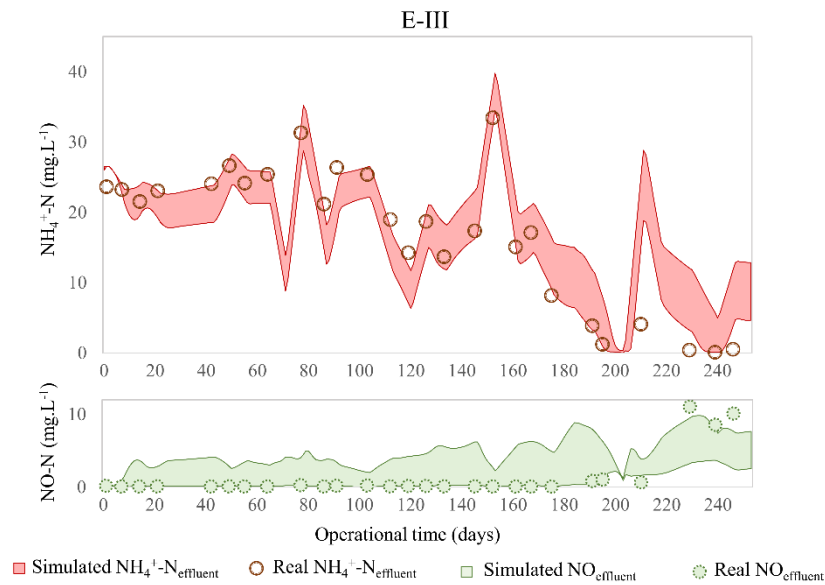
Source: the author (2022).

To sum up, it can be observed that this proposed methodology for simulating reactors in a non-steady state by definition of a fixed number of granules and a single diameter makes it difficult to comprehend the complexity of nitrogen removal processes in AGS. However, although it is hard to describe precisely all the processes, the simulations present more clearly which processes are essential to be investigated in the future. Within a large margin of uncertainty for the analyzed parameters, it was possible to generate approximate results that describe NH_4^+ and NO. Thus, in turn, this considerable uncertainty highlights the importance of these parameters.

4.3   LAB-SCALE EXPERIMENTAL SYSTEM[5]

The results obtained in the two lab-scale SBRs performed at Ruhr Universität Bochum (Germany, SBR_{20} and SBR_{30}) are presented and discussed in this section, which investigates the influence of temperature on AGS formation, morphology, and stability.

---

[5] Results presented in topic 4.3 have been already published in Environmental Research 212 (2022) 113578, entitled: *"Influence of temperature on aerobic granular sludge formation and stability treating municipal wastewater with high nitrogen loadings"*, by Julliana M. Araújo, Stephan Berzio, Tito Gehring, Edith Nettmann, Lourdinha Florêncio, and Marc Wichern.

4.3.1 Development and characteristics of granular biomass

After granulation was established in both reactors (approximately one month from start-up), biomass's size was distributed by sieving regularly, as shown in Figure 31. Exemplary granules microphotographs for day 184 are also presented. The activated sludge used as inoculum for both reactors (Figure 31 - day 0) mainly consisted of flocs, with about 65% of the particles smaller than 250 mm. During the experimental period, both reactors had a considerably higher concentration of granules than the start-up sludge. While SBR_{20} presented more unstable granules with frequent disintegrations and a large flocculent fraction, a complete and stable granulation could be seen after 102 days of operation in SBR_{30}. It is worth mentioning the exception of day 240 for SBR_{30}, where partial disintegration of the granules occurred after an operational disturbance that led to a 24h period without feeding. However, SBR_{30} quickly returned to stability (after around two weeks).

Figure 31. Granular structure on operation day 184 (top left - SBR_{20}; top right - SBR_{30}) with a diameter of approx. 2 mm. The biomass size distribution of both reactors over time is shown at the bottom. The plot on the left (day 0) shows the distribution of the reactor inoculum.
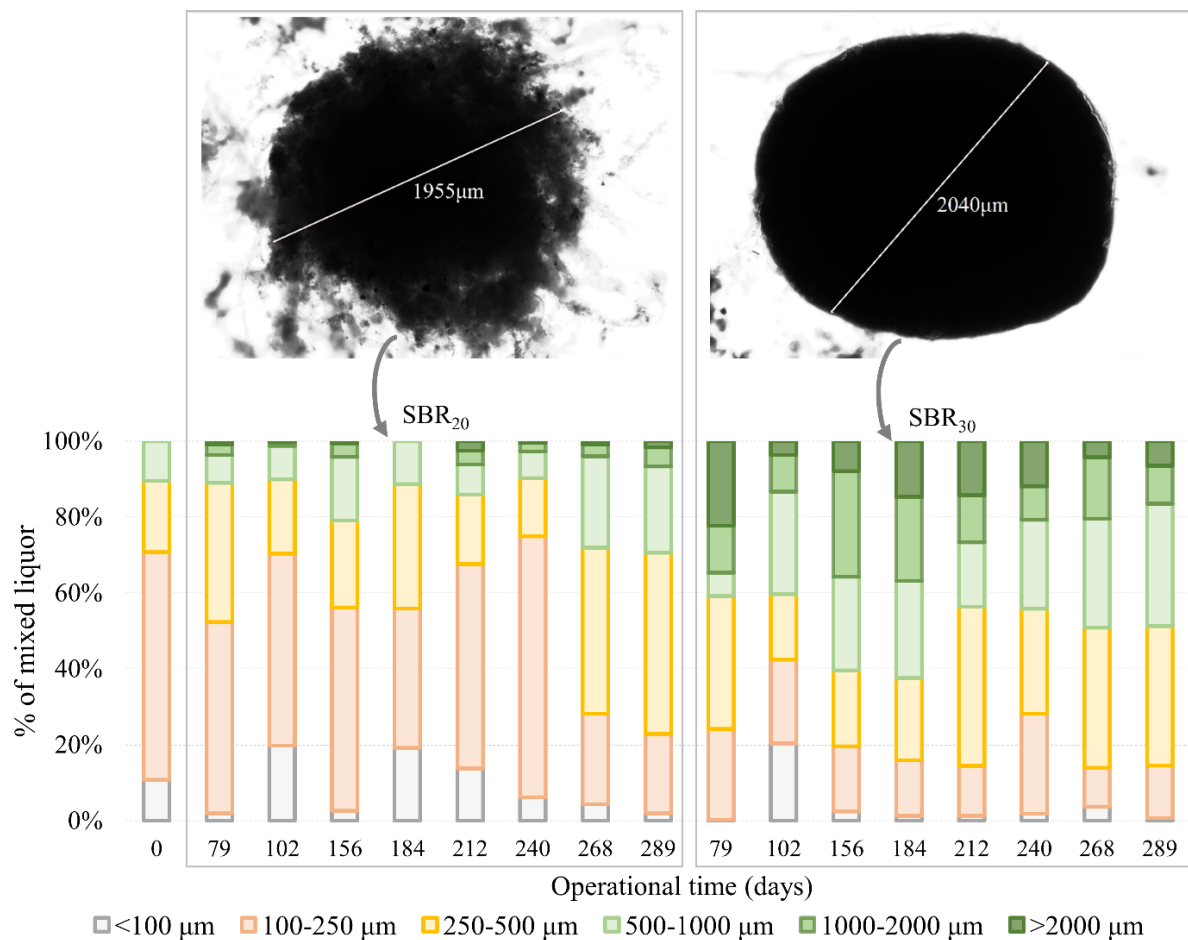
Source: adapted from Araújo et al. (2022).

The temperature significantly influences the formation and structure of the granules under identical operational conditions (e.g., the same wastewater and scale), resulting in striking morphological differences (Figure 31). At higher temperatures (SBR_{30}), granules were larger, more compact, and considerably more stable against system disturbances during all investigations. On the other hand, granules from SBR_{20} usually had a fluffier structure and a higher concentration of filamentous bacteria.

Conversely, in the beginning, the SVI_x and MLSS dynamics (Figure 32) were significantly different at both temperatures. Due to the sludge age control through a selective pressure – i.e., settleability of the biomass – a divergent accumulation of biomass in both reactors was observed. A higher amount of biomass was retained in SBR_{30} (MLSS average of 6.1 ± 1.5 g.L^{-1} after complete granulation on day 102). However, the solids concentration in SBR_{20} was more stable (average of 3.8 ± 0.8 g.L^{-1} during the entire operational period), showing that the biomass growth corresponds on average to the amount of the solids removal through the effluent. A change in this trend can be visualized at the end of the operational period, with the concentration increasing at the three last sample collections.

As for sludge sedimentability, two different aspects stand out in SBR_{30} after day 50: (1) the ratio of SVI_{10}/SVI_{30} in SBR_{30} remained almost constant during the entire operational time (1.08 ± 0.08); (2) the low SVI_{30} values (38.2 ± 11.7 mL.g^{-1}) obtained here are in line with literature values for aerobic granular sludge, e.g., Wagner and Da Costa (2013, 53 mL.g^{-1}) and Giesen et al. (2013, 40 mL.g^{-1}), ratifying the complete and stable granulation. In comparison, the mean values of SVI_{10}/SVI_{30} and SVI_{30} for SBR_{20} were 1.46 ± 0.12 and 49.6 ± 12.6 mL.g^{-1}, indicating that although complete granulation wasn't achieved, the sludge also had good sedimentability.

Figure 32. MLSS (●) and SRT (◊) in SBR$_{20}$ (a) and SBR$_{30}$ (b); SVI$_5$ (■), SVI$_{10}$ (▨), SVI$_{30}$ (□), and SVI$_{10}$/SVI$_{30}$ (+) in SBR$_{20}$ (c) and SBR$_{30}$ (d).
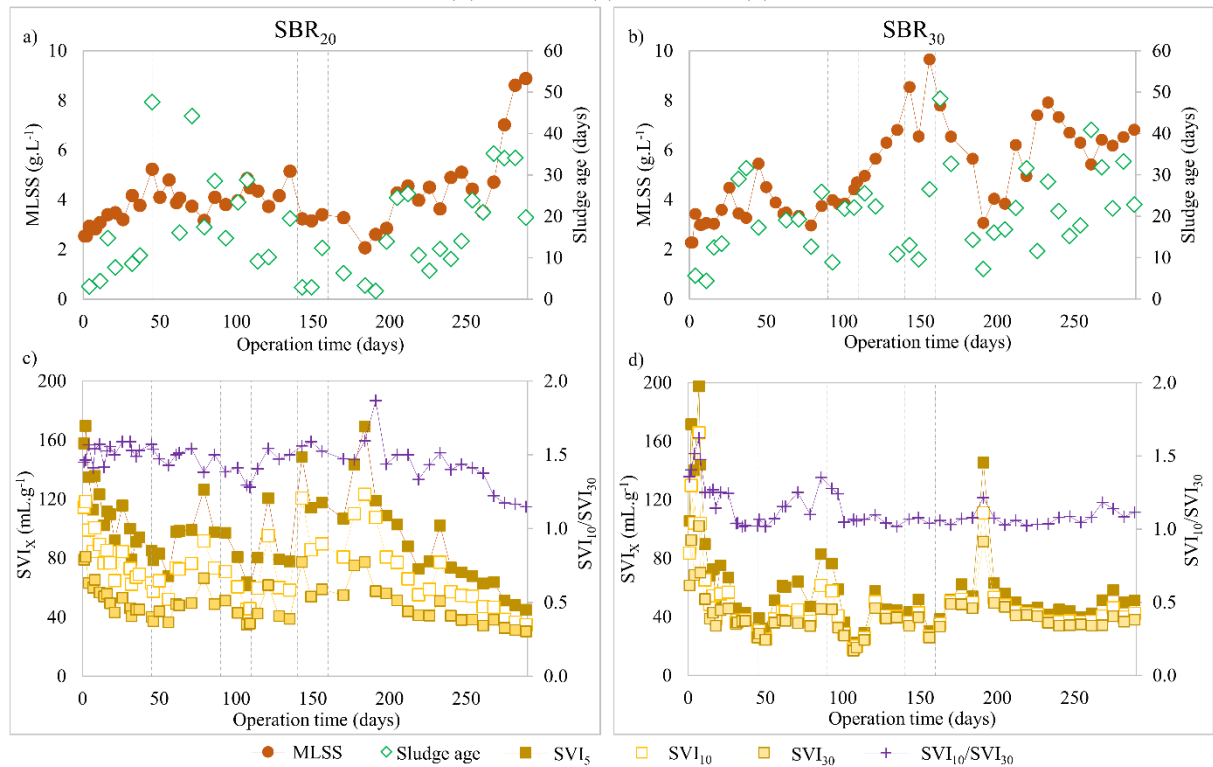
Source: adapted from Araújo et al. (2022).

Generally, AGS systems using real wastewater with low organic loading require a longer operational time to achieve complete granulation, sometimes more than a year (DERLON et al., 2016). Higher temperatures of SBR$_{30}$ provided faster stable granulation (after 102 days) compared to SBR$_{20}$ (complete granulation was not observed within 290 days). This is in line with other published studies using municipal wastewater and operating at approximately 20 °C, e.g., Ni et al. (2009), who obtained 85% of granular biomass after 300 days of operation; Liu et al. (2010), with complete granulation at 400 days of operation; and Derlon et al. (2016), who did not obtain stable granulation even after 1417 days of operation.

In both reactors, more substantial fluctuations in the SVI values could be observed between days 60 and 110. These were possibly caused by a proliferation of *Tubifex* nematodes that, when integrated with the granules (Figure 33), caused their disintegration. De Valk et al. (2017) found that *T. tubifex* predominantly consumed the extracellular polymeric substances (EPS) protein fraction from AGS. Since the EPS plays a crucial role in granulation by providing increased mechanical strength and stability of granules (LI et al., 2020), its degradation can likely disintegrate and worsen sedimentation properties. The problem was solved after two reductions in cycle sedimentation time: from 5 to 4 and 4 to 3 minutes after 90 and 110 days of

operation, respectively. This strategy enabled washing out the nematodes associated with the poorly sedimentable biomass.

Figure 33. Macro photographs of Granules with *Tubifex* from SBR$_{20}$ after 90 days of operation.
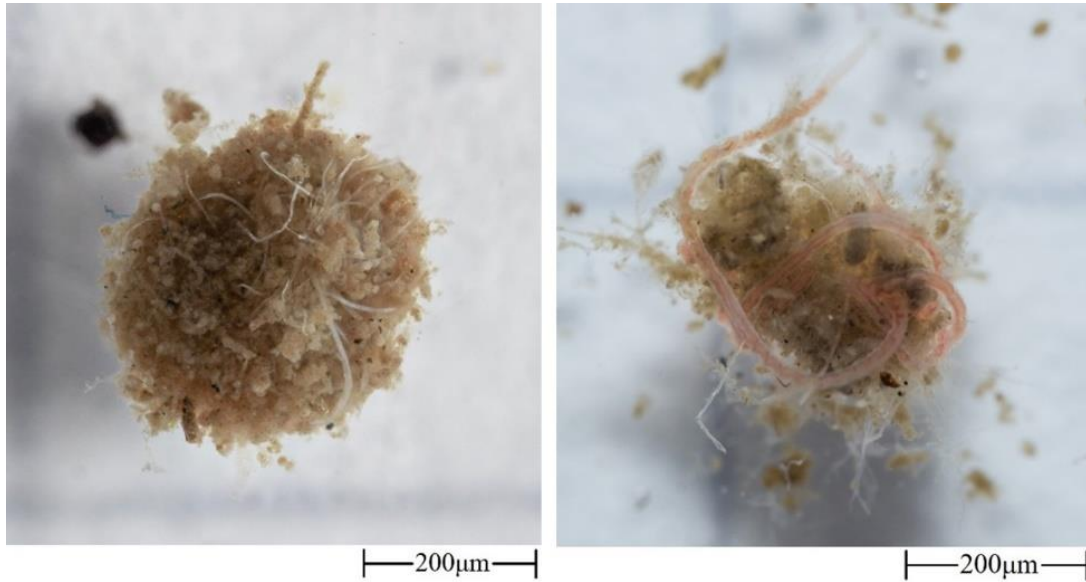
Source: Araújo et al. (2022).

4.3.2 Reactors' Performance

The treatment performances of the SBRs assessed in terms of organic matter and nitrogen removal are shown in Figure 34.

Figure 34. a) Total influent COD (●), filtrated influent COD (○), filtrated SBR$_{20}$ effluent COD (△), filtrated SBR$_{30}$ effluent COD (△); b) total influent TN$_b$-N (◆), influent NH$_4^+$-N (■); c) effluent NH$_4^+$-N (◇) and NO$_3^-$-N (△) in SBR$_{20}$; d) effluent NH$_4^+$-N (◇) and NO$_3^-$-N (△) in SBR$_{30}$.
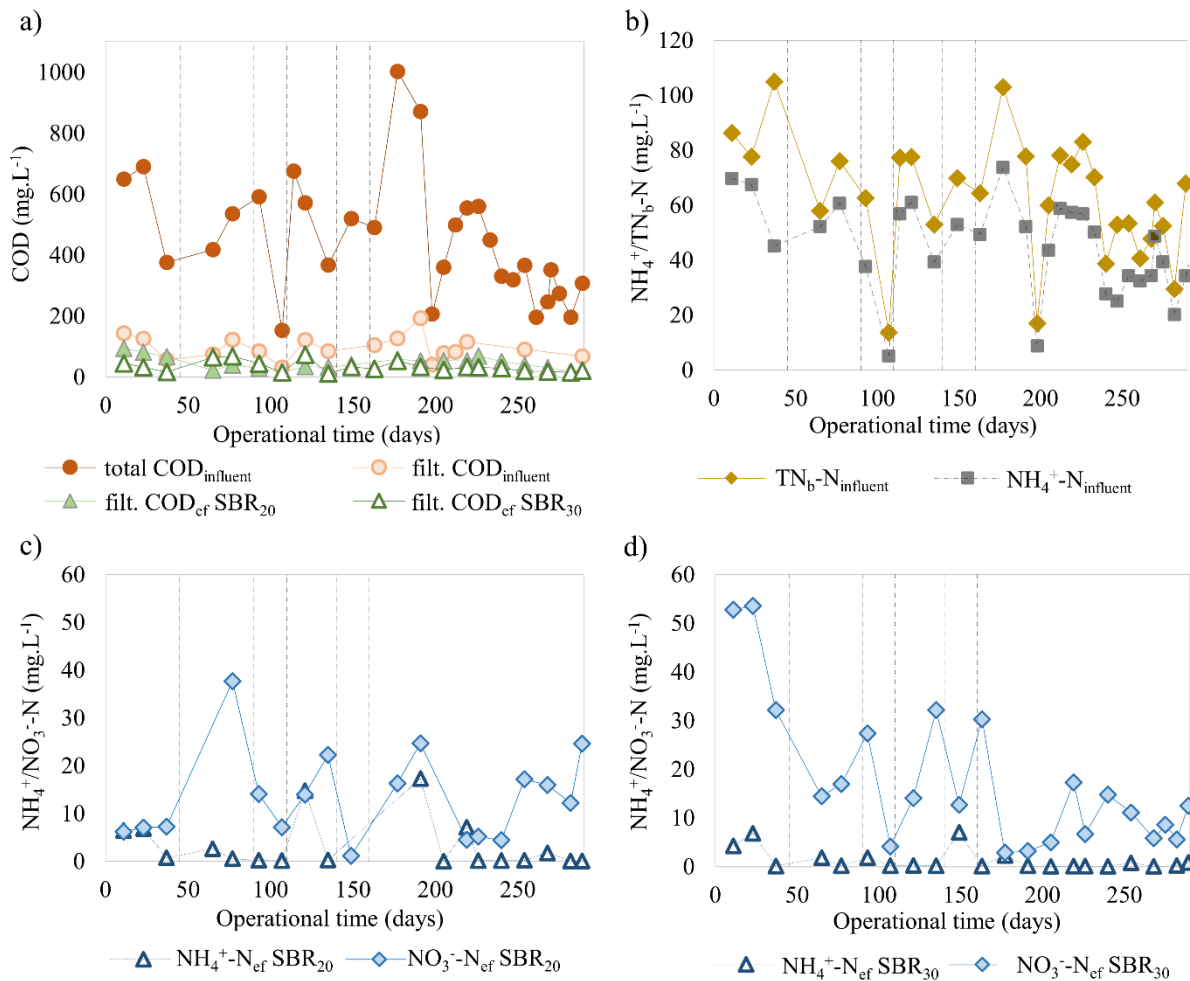
Source: adapted from Araújo et al. (2022).

Initially, it can be seen that the influent values fluctuate noticeably, from a minimum of 153 mg.L^{-1} on day 107 to a maximum of 1,003 mg.L^{-1} on day 177. This resulted in a mean value of 484 ± 160 mg.L^{-1}, leading to a mean organic loading rate (OLR) of 1.3 ± 0.4 kgCOD$_{total}$.m^{-3}.day^{-1}. Also, regarding high particulate COD concentration, Layer et al. (2019) concluded that a higher fraction of non-diffusible particulate COD interferes with granulation. When operating four SBRs in parallel fed with four different types of effluent (100%-VFA synthetic; complex synthetic; primary, and; raw), a higher floc fraction (20-40%) was observed. A 50% higher hydrolysis can be expected from a temperature increase from 20 to 30 °C (GUJER et al., 1999). Hence, this faster kinetics can potentially explain better performance due to the more significant availability of diffusive organic substrates, resulting in faster granulation and excellent granule sedimentability.

The ratio of nutrients is also essential to ensure bacteria's higher and better activity. Typically, the C:N:P ratio associated with municipal wastewater is in the range of 100:5:1 to 100:10:1 (METCALF & EDDY, 2016; HAMZA et al., 2019). However, this ratio was slightly higher in this study, with an average value of 100:15:1.7. Thus, even though larger granules enabled the existence of anoxic zones within the granule core, the denitrification process was limited by the low organic carbon availability. Consequently, nitrate accumulated in both reactors for almost all the investigation period.

Overall, a COD removal efficiency of 90% was observed in both reactors during the entire test period, accompanied by effluent NH_4^+-N concentrations below 0.5 mg $N.L^{-1}$ after 50 days of operation. However, the challenging parameter was nitrate. The initial difference between both reactors (higher accumulation of NO_3^--N in SBR_{30} during the first 100 days of operation) is probably due to increased oxygen diffusion at higher temperatures. According to Stewart (2003), diffusion at 30 °C is about 33% higher than at 20 °C. This potentially explains why in SBR_{30}, nitrate removal is observed concomitant with a stable granulation around day 100 (Figure 31 and Figure 34), as in SBR_{30}, the formation of an anoxic layer within the granules requires larger diameters and/or more compact granule structures than at 20 °C. The reduction of the DO concentration after day 110 further favors nitrate degradation. Gradually decreasing the oxygen concentration and optimizing the filling phase by inserting air pulses decreased the effluent nitrate concentrations (below 20 mg $N.L^{-1}$). In addition to COD and N, the analysis results were complemented by phosphorus (TP) values during the stable test phase. The removal efficiency of approximately 50% was observed for both reactors, indicating increased biological activity.

Although, in theory, simultaneous nitrification-denitrification (SND) is one of the main advantages of AGS systems, results from other investigations suggest that SND during municipal wastewater treatment is limited. For example, Guimarães et al. (2018) observed high nitrite accumulation (mean effluent concentration of 16.5 mg $N.L^{-1}$) when treating domestic wastewater in a pilot-scale SBR.

4.3.3 Microbial diversity

On day 289, Proteobacteria, followed by Bacteroidetes, were the largest phyla (Figure 35) in both reactors. Both reactors include many microorganisms and essential components within the granules and are commonly reported in the literature as predominant phyla in AGS systems (CHEN et al., 2020b; WANG et al., 2021).

Figure 35. Microbial population of mixed liquor samples (day 289) from SBR$_{20}$ (blue) and SBR$_{30}$ (red) at phylum level. Percentages indicate relative abundance.
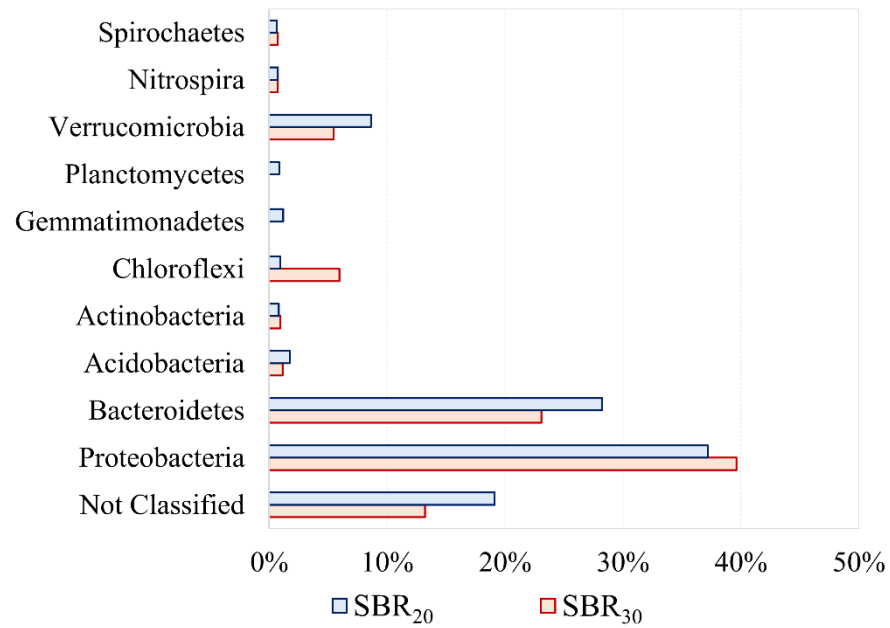
Source: adapted from Araújo et al. (2022).

The taxonomic profiles of the bacterial families identified in both reactors are depicted in Figure 36. Results help to describe the nitrogen and phosphorous removal mechanisms at both temperatures.

Figure 36. Taxonomic profile of the bacteria families identified in SBR$_{20}$ (blue) and SBR$_{30}$ (red). Families related to PAOs and GAOs (⋯). Families related to nitrogen removal (-·-).
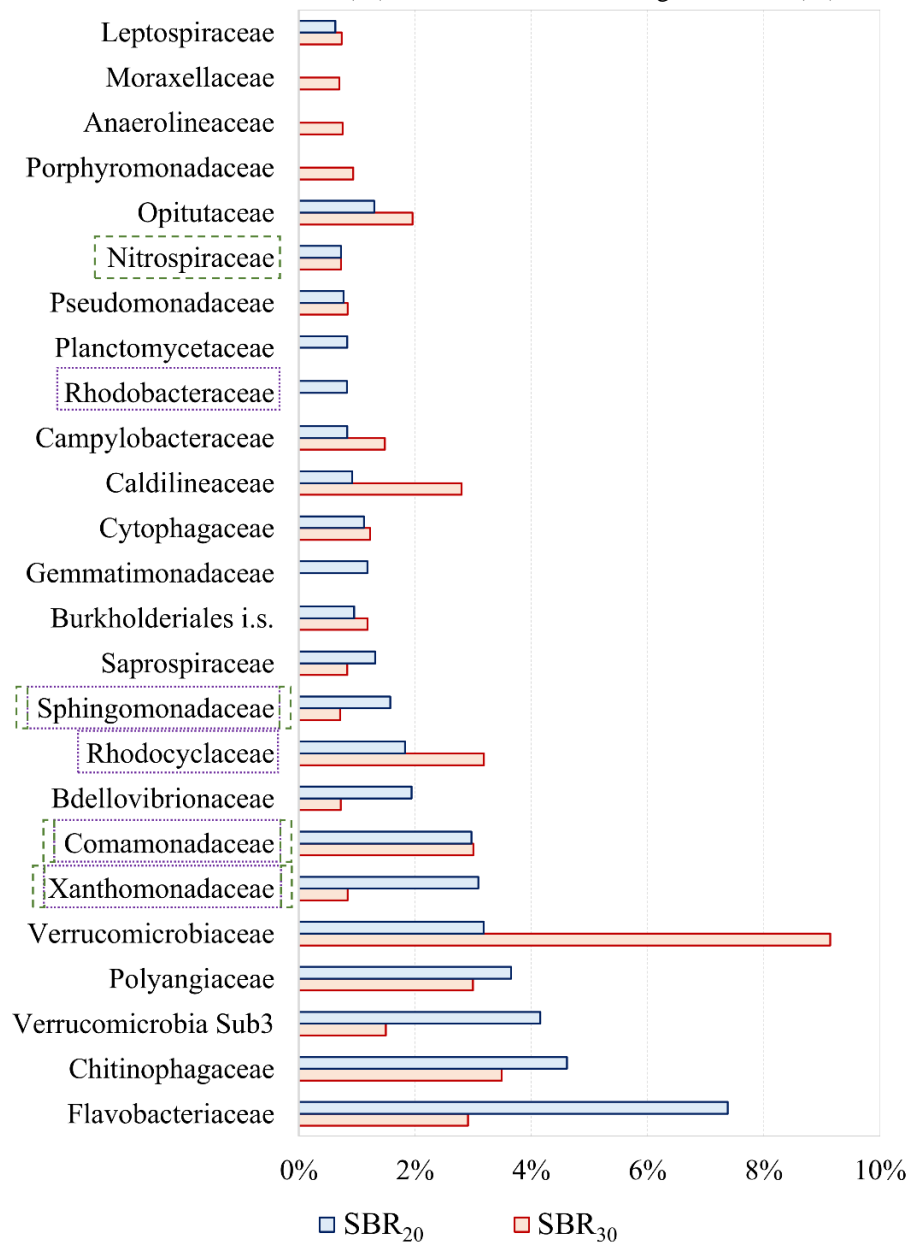
Source: adapted from Araújo et al. (2022).

Several polyphosphate accumulating organisms (PAOs) and glycogen accumulating organisms (GAOs) are listed in the literature within the families *Comamonadaceae*, *Sphingomonadaceae*, *Rhodobacteriaceae*, *Xanthomonadaceae*, and *Rhodocyclaceae*. Such microorganisms are reported to help in the formation and stabilization of AGS. Of note, families known to include both PAO and GAO species (*Rhodobacteraceae* and *Xanthomonadaceae*) were detected at much higher abundance or only in SBR$_{20}$, indicating that a higher temperature does not favor GAO growth. Ong et al. (2016) observed when operating an SBR fed with synthetic sewage at 28 °C that GAOs were detected at a lower abundance (7%) than PAOs

(36%). In addition, the families of *Rhodocyclaceae*, *Xanthomonadaceae*, and *Sphingomonadaceae* are also related to the production of extracellular polymeric substances (EPS) in AGS systems (DE KREUK & VAN LOOSDRECHT, 2004; SZABÓ et al., 2017; ROLLEMBERG et al., 2018).

Remarkably, typical representatives of ammonium and nitrite oxidizers, as well as denitrifiers (e.g., *Nitrosomonas*, *Nitrobacter*, and *Paracoccus*, respectively), could not be detected in the samples. First, regarding common nitrite-oxidizing groups, Luo et al. (2014) observed that *Nitrospira* was favored over *Nitrobacter* with a low COD/N ratio, a similar result was also observed in this experiment. In addition, some detected families and genera are related to nitrification, denitrification, heterotrophic nitrifiers, comammox, anammox, and phosphate accumulation. For example, members of the *Chitinophagaceae* family are known to be heterotrophic AOBs (WANG et al. 2020b, WU et al. 2019) and were detected in both reactors at 18.1% (SBR_{20}) and 13.3% (SBR_{30}), respectively. Representatives of the genus *Hydrogenophaga* (*Comamonadaceae* family) also seem capable of heterotrophic nitrification and aerobic denitrification. *Sphingosinicella humi* (*Sphingosinicella* family) is known, among other compounds, to reduce nitrogen. *Pseudoxantomonas* (*Xanthomonadaceae* family) can reduce nitrite and nitrate and degrade various hydrocarbons (including benzene and toluene) (LIU et al., 2017).

About the most abundant families found in SBR_{30} (*Verrucomicrobiaceae*) and SBR_{20} (*Flavobacterium*), it was already reported that Flavobacterium is located in the granule core of mature granules (ŚWIATCZAK & CYDZIK-KWIATKOWSKA, 2017). However, functions and metabolisms are still not very clear. Verrucomicrobia is a group of microorganisms found mainly in water and soil environments. It is a microorganism that can easily accumulate in AGS systems (WANG et al., 2020a). Recent studies indicate that a lineage within the phylum Verrucomicrobia belongs to methanotrophic bacteria that occur in diverse environments, observed in mesophilic and thermophilic habitats (ROLDÁN et al., 2022). Thus, their higher abundance in SBR_{30} (34.8%) compared to SBR_{20} (12.4%) is justified, strongly indicating the presence of anaerobic zones in the granules. Also, the presence of Verrucomicrobia could suggest a more inorganic core. The family *Anaerolineaceae* found in SBR_{30} includes both mesophilic and thermophilic species. All representatives of this family are strictly anaerobic and chemoheterotrophic (YAMADA & SEKIGUCHI, 2018), confirming the presence of an anaerobic zone in the granules of this reactor. Finally, and by no means least, the family *Bdellovibrionaceae* includes the smallest known predatory organisms. They have gained particular interest due to their ability to attack bacterial pathogens such as *Escherichia coli,*

Salmonella, and *Yersinia* (BRATANIS et al., 2020; LAMBERT et al., 2006). Their significantly higher abundance in SBR_{20} is very likely because the slightly fluffier structure of the granules provides a better "hunting grounds" for these predators than the smoother, more compact surface of the granules in SBR_{30}.

In summary, the main differences are the structure and size of the granules. In SBR_{30}, due to the granules' larger and more compact structure, more facultative anaerobic organisms and archaea can be identified. The results of the 16S rDNA amplicon analysis represent only a snapshot of the microbial community in the AGS at one SBR operating time. It could be shown that the operating temperature impacts the diversity of the biocoenosis and the abundance of individual bacterial groups.

4.4   MICRO-PROFILES

Micro-profiles with the aid of DO micro-sensors (50 μm tip, Unisense®) were performed on granules from SBR_{20} and SBR_{30} between 1.4 and 2.0mm, aiming to analyze diffusion and the boundary layer resistance (BLR) – parameters that showed high sensitivity during model implementation and calibration, topic 4.2. Micro-scale analyses generally have a high spatial resolution, fast response, and minimal perturbation. However, introducing the sensor into deeper layers can lead to considerable disturbance of the micro-sensor axis, and recording multiple concentration profiles at the same location in the biofilm can lead to errors (ETTERER, 2006). Therefore, these study micro-profiles were performed at different locations on a single granule and other granules.

Triplicate analyses on the same granule showed slight variations already expected due to the distribution of other bacterial communities. Although the profiles were performed at different locations, a diffusion pattern could be analyzed, i.e., measurement reproducibility within each granule. Figure 37, for example, shows the triplicate average of the micro-profiles performed on granules from SBR_{20} and SBR_{30} at 20 °C using filtered (20-25 μm) treated municipal wastewater and oxygen at saturation. The lower and upper limits of the granules were estimated based on granule size and diffusion gradients and are indicated by two gray bands (upper and lower) on the graphs.

Figure 37. DO micro-profiles on granules from SBR_{20} and SBR_{30} at 20 °C using filtered (20-25 µm) treated municipal wastewater and oxygen at saturation. The gray band indicates the granules' upper and lower limits.
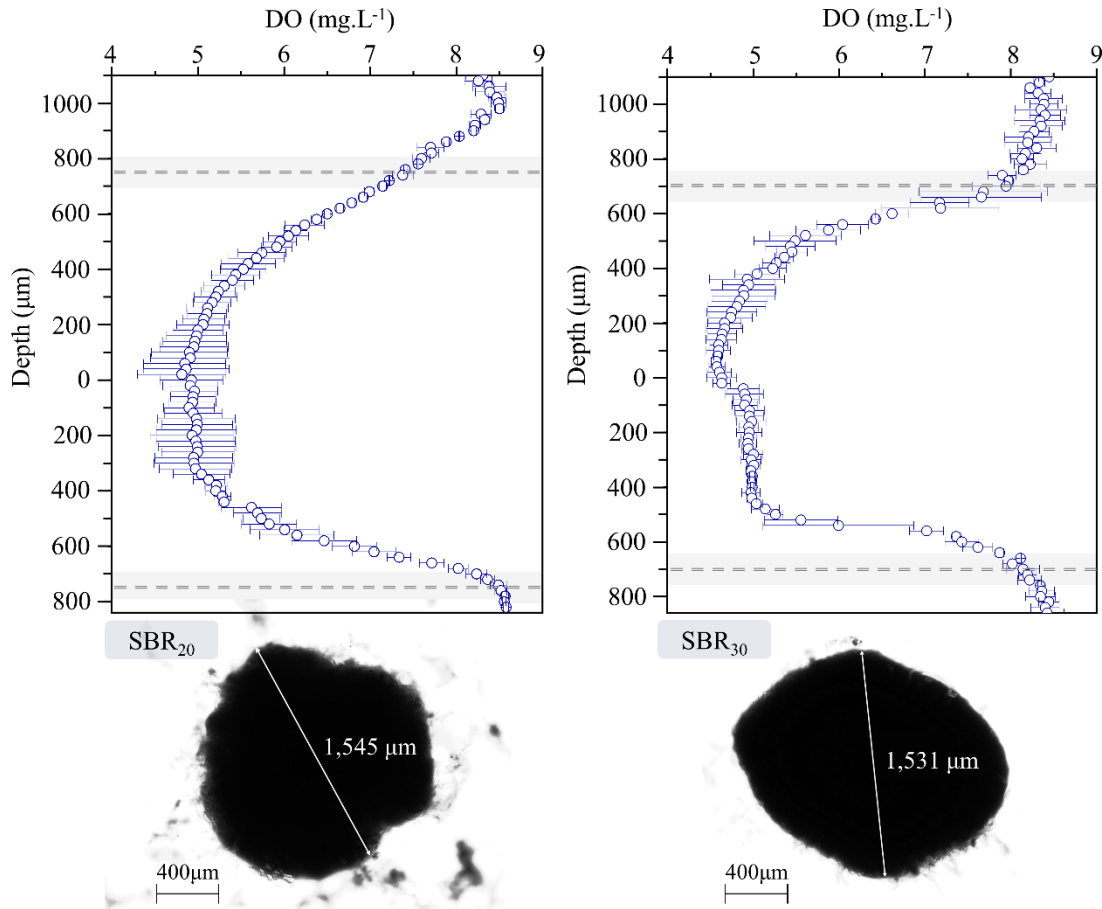
Source: the author (2022).

The designed flow cell (Figure 14) did not feature the same hydraulic conditions as the operated reactors (Figure 12). In addition, even thin electrodes with tip diameters of a few micrometers cause changes in the thickness of the BLR, associated with an apparent higher resistance, especially when introduced from above (KÜHL & REVSBECH, 2000). Hence, the objective of this research step was to qualitatively analyze the influence of different conditions (such as the absence/presence of a substrate and temperature) on the size of the boundary layer resistance and aerobic zone thickness (AZT).

Figure 38 shows representative dissolved oxygen gradients for granules from SBR_{20} (above) and SBR_{30} (below). The dissolved oxygen concentration in the medium (bulk) was at saturation, similar to that used in the pilot-scale experiments (section 4.1), which comprise the modeled ones, E-I and E-III (section 4.2). The profiles were performed for different conditions, including temperature (the left graphs show profiles performed at 20 °C and the right at 30 °C) and substrate concentrations (with and without COD and NH_4^+).
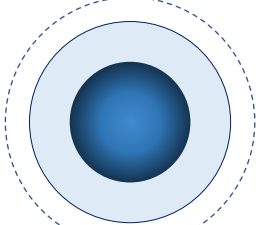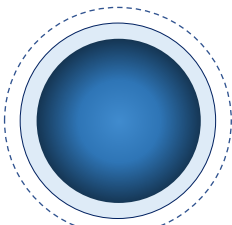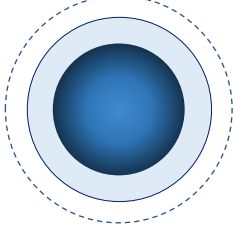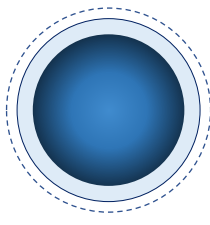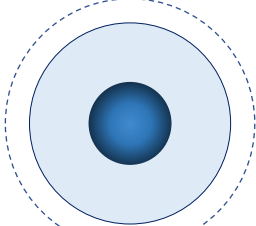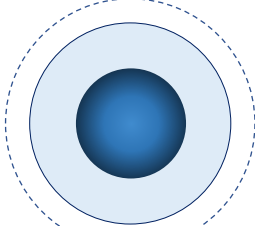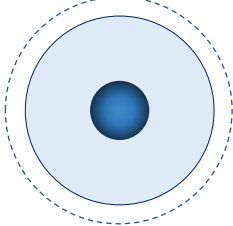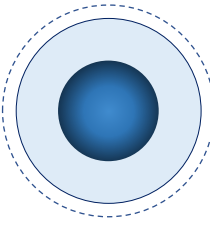
Figure 38. DO micro-profiles on a 1.5 mm granule from SBR_{20} (above) and SBR_{30} (below) at 20 °C and 30 °C and under oxygen at saturation using four different mediums. 1) tWW: filtered treated municipal wastewater; 2) tWW+COD: filtered treated municipal wastewater adding 500 mg $COD.L^{-1}$; 3) tWW+COD: filtered treated municipal wastewater adding 50 mg $NH_4^+-N.L^{-1}$; and 4) tWW+COD+NH4: filtered treated municipal wastewater adding 500 mg $COD.L^{-1}$ and 50 mg NH_4^+-N. The gray band indicates the granules' upper and lower limits.
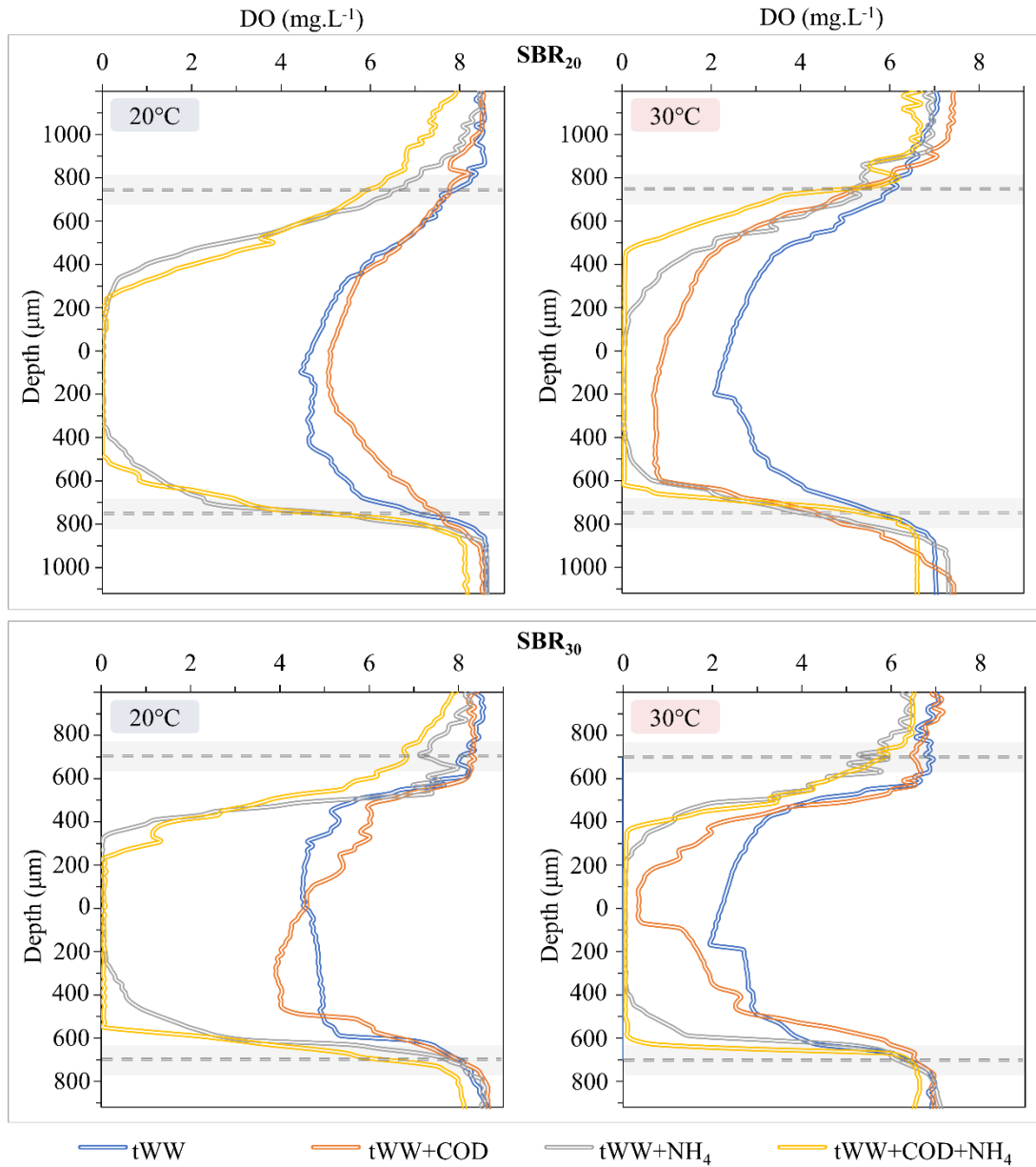
Source: the author (2022).

The granules' lower limit was used during BLR and AZT analysis, as these parameters were more stable considering hydrodynamic conditions (upward flow and downward measurement). DO varied from 5.5 to 7.8 $mg.L^{-1}$ at 20 °C and 4.4 to 6.5 $mg.L^{-1}$ at 30 ° C at granules' surfaces. The BRL, in turn, ranged between 140-180 μm and 80-180 μm for 20 and 30 °C, respectively. Oxygen-free (anaerobic/anoxic) zones were only observed when NH_4^+ or COD with NH_4^+ were added. For ease of discussion, Table 17 summarises BLR and AZT from the micro-profiles with oxygen-free zones (Figure 38).

Table 17. BLR and AZT from micro-profiles with oxygen-free zones. The three layers in the figures from the outside are BLR, AZT, and oxygen-free zone.

Temperature	20 °C	30 °C	Medium
	≈1.5 mm granule from SBR$_{20}$		treated wastewater + COD (500mg.L^{-1}) and NH$_4^+$-N (50 mg N.L^{-1})
BLR (μm)	180	120	
AZT (μm)	300	120	
	≈1.4 mm granule from SBR$_{30}$		
BLR (μm)	160	80	
AZT (μm)	200	120	
	≈1.5 mm granule from SBR$_{20}$		treated wastewater + NH$_4^+$-N (50 mg N.L^{-1})
BLR (μm)	180	180	
AZT (μm)	440	340	
	≈1.4 mm granule from SBR$_{30}$		
BLR (μm)	140	100	
AZT (μm)	480	320	

Source: the author (2022).

In general, higher BLRs were observed for SBR$_{20}$ granules, probably because these granules were more filamentous than SBR$_{30}$ granules, as discussed in section 4.3. However, BLR values were considerably lower than those by Li et al. (2008, 400 μm) when measuring micro-profiles at 25 °C in granules of approximately 5 mm and oxygen at saturation (8.6 mg. L^{-1}). Etterer (2006), using the same flow cell and different substrate conditions at 20 ± 1 °C,

also obtained BLR between 400 and 700µm in granules ranging between 3.6 and 4 mm in diameter. As for AZT, in all granules in Table 17, a decrease was observed with increasing temperature, indicating that even though a higher solute diffusivity was expected, the higher activity of the microorganisms outweighed diffusion. It ranged between 200 and 480 µm at 20 °C and 120 and 320 µm at 30 °C. Ivanov et al. (2005) observed in most granules between 850-1000 µm in diameter the presence of an anaerobic core, which was also observed in this work in a medium with substrates. Chiu et al. (2007) also reported that most of the oxygen was consumed in the first layer (125-375 µm) in profiles performed on a 1.7-mm granule in an oxygen-saturated medium (287 µmol/L) at 25 °C. Wichern (2010), in turn, compared different studies and reported a mean AZT of around 80 µm.

Biofilms are not homogeneous systems but heterogeneous and porous due to the various ways that microorganisms aggregate. Their morphology can be dense or loose with a compact-and-smooth or rough-and-irregular surface (ILTIS et al., 2011). Hence, their structure also has considerable influence on the micro-profiles. Figure 39 presented two micro-profiles obtained from granules with a clear structure difference (linked to Figure 31).

Figure 39. DO micro-profiles on granules from SBR_{20} and SBR_{30} at 20 °C highlighting the difference in diffusional transport due to the granule's structure. In both, filtered (20-25 µm) treated municipal wastewater added 500 mg $COD.L^{-1}$ and 50 mg $NH_4^+\text{-}N.L^{-1}$, and oxygen at saturation were used.
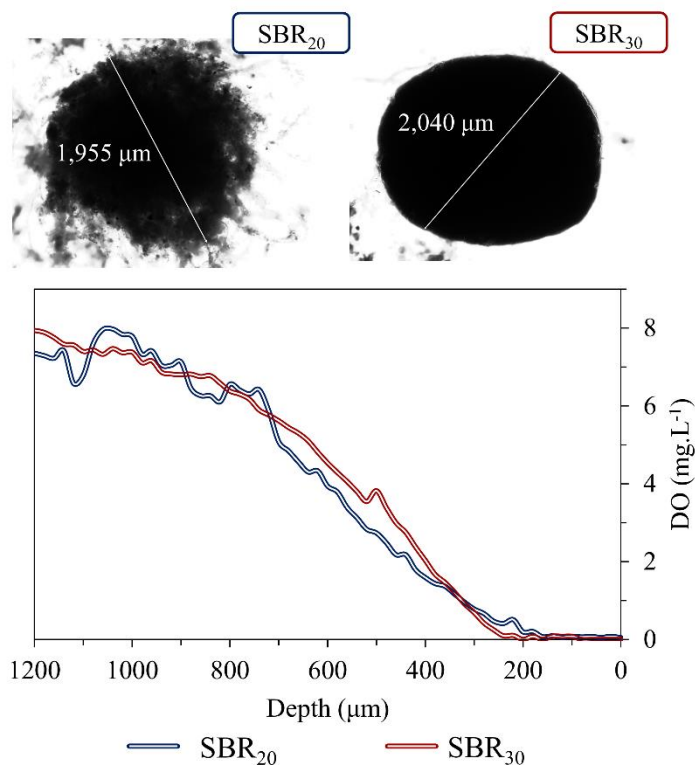
Source: the author (2022).

The differences in DO levels and the changing trends at different locations in the aerobic layer of the biofilm indicate the differences in oxygen diffusion rates and consumption rates, which reflect the amount and density of aerobic biomass and the structure of the aerobic layer of the biofilm (NING et al., 2014). The granule profile of SBR_{30} was typical for most measurements of compact granules, with more or less regular transport associated with diffusion and consumption rates. In the SBR_{20} bead profile, however, because it has a more irregular shape, other forms of oxygen transport into the aggregate through holes connected to the bulk or channels are likely.

5   INTEGRATED DISCUSSION

This chapter discusses integrating the different obtained results considering the diverse experiments and approaches performed during this research.

First, comparing the PS and LS scales operated in the same temperature range (around 30 °C), a faster and more stable granulation was observed in the LS (SBR$_{30}$). The main parameters for both these strategies are summarized in Table 18. While in PS, a complete granulation was observed only in one experiment (E-III) after 168 days, in LS, it was reached after 102 days, remaining stable until the end of the operation (over 180 days). Possible explanations are the non-inoculation in the PS experiments, leading to a slow, gradual accumulation of biomass, and the different influent compositions ensuing in different OLR: PS: 0.88 ± 0.28 kg COD$_{total}$.m^{-3}.day^{-1}; LS: 1.3 ± 0.4 kg COD$_{total}$.m^{-3}.day^{-1}. Although OLR values between 0.5 and 10 COD$_{total}$.m^{-3}.day^{-1} are reported in the literature as reference values for mature granules formation and maintenance, low values (0.54 kg COD$_{total}$.m^{-3}.day^{-1}, PEYONG et al. 2012) can lead to a disintegration of granular biomass (ROLLEMBERG et al., 2018; ADAV et al., 2010). According to Adav et al. (2010), low OLR favors filamentous bacteria and leads to loss of microbial self-aggregation capacity due to reduced protein concentration in the EPS content.

Table 18. Summary of the average results for E-III (PS) and SBR$_{30}$ (LS).

Parameter	PS, E-III	LS, SBR$_{30}$
Working volume	115 L	11.2 L
Inoculum	None (row wastewater)	AS (2.5 g TSS.L^{-1})
Complete granulation after (days)	168	102
Stable operation duration (days)	80	180
OLR (kg COD$_{total}$.m^{-3}.day^{-1})	0.88 ± 0.28	1.3 ± 0.4
NLR (kg NH$_4^+$-N.m^{-3}.day^{-1})	0.10 ± 0.03	0.13 ± 0.5
MLSS[*1] (g TSS.L^{-1})	1.2 ± 0.30	6.1 ± 1.5
SVI$_{30}$[*1] (mL.g SST^{-1})	42 ± 16	38 ± 12
SRT[*1] (days)	5.6 ± 2.1	22 ± 10
COD removal efficiency[*1] (%)	77 ± 15	93 ± 3
NH$_4^+$-N removal efficiency[*1] (%)	74 ± 26	98 ± 2
NO$_3^-$-N effluent[*1] (mg N.L^{-1})	3.3 ± 4.2	13 ± 9

[*1] during complete granulation

Source: the author (2022).

The two strategies also observed different COD and nitrogen removal performances during the operational time. The non-inoculation of PS led to a lower concentration of retained biomass (1.2 ± 0.30 g TSS.L^{-1}, compared to LS, 6.1 ± 1.5 g TSS.L^{-1}). Since ammonia-oxidizing organisms are usually slow-growing, an expressive removal of NH_4^+-N was only observed after complete granulation (Figure 19, E-III, $74 \pm 26\%$). While in LS, NH_4^+-N removal efficiencies greater than 90% were observed during the entire operational period (Figure 34.d, $98 \pm 2\%$ for complete granulation). It is worth pointing out that after the insertion of air pulses during anaerobic feeding after 160 days in LS, an improvement in denitrification was observed, reflected in the reduction of NO_3^--N effluent. The same strategy was used throughout the operational period in PS to ensure mixing during the anaerobic phase, and concentrations below 12 mg.L^{-1} were observed for NO_3^--N effluent.

The lower COD removal observed in PS ($75 \pm 14\%$ compared to $93 \pm 3\%$ in LS) is, in turn, also associated with the influent wastewater characteristics. As seen during the estimation of the influent COD fractions to implement the models for the PS experiments (4.2.1), the wastewater used (from a WWTP in Recife, Brazil) had a more expressive dissolved inert fraction (S_I ranging between 11-22%, Figure 23) when compared to others in the literature (Table 3). Thus, the higher effluent COD concentrations corresponded to this fraction, which could not be removed in the biological treatment. LS, meanwhile, was fed with municipal wastewater from a German WWTP (Bochum-Ölbachtal). In Germany, the inert dissolved fraction has a significantly lower contribution to COD municipal wastewater, as reported by Lange (2018, 4-8%) and Wichern et al. (2018, 3%), enabling higher removal efficiencies.

Regarding microbial diversity in terms of phyla and taxonomic profiles in PS (E-III) and LS (SBR_{30}), the following considerations can be highlighted and are summarized in Figure 40:

a. Proteobacteria, commonly reported as one of the predominant phyla in AGS systems (WANG et al., 2021), were the largest phylum for both, with 80% on day 203 for PS (Figure 21) and 40% on day 289 for LS (Figure 35). Furthermore, the improvement in PS performance is possibly associated with the increase in those of this phylum (53% on day 22, 66% on day 127, and 86% on day 196), the extent to which, according to Cao et al. (2018), this phylum is closely related to nitrogen and phosphorus removal in wastewater treatment systems. Although the second most abundant phyla were not the same (PS: Firmicutes, 17%; LS: Bacterioidetes, 23%), both are listed among the top five phyla with high RA in the sludge granulation process (CHEN et al., 2020b).

b. In PS, the genera commonly associated with nitrogen removal were not detected in any sample, indicating that heterotrophic nitrifying and denitrifying bacteria carried out this process. Among them, the genera *Pseudomonas* (complete granulation 44-62%) and *Pseudoxantomonas* (6-8%) stand out. On the other hand, in LS, the genus Nitrospiraceae associated with nitrogen removal was identified but also with an RA < 1%. The family of genera *Pseudomonas* (*Pseudomonadaceae*) and *Pseudoxantomonas* (*Xanthomonadaceae*) were also found with RA < 1 %. Thus, in this system, nitrogen removal was also performed by the families *Chitinophagaceae* (13%, known to be heterotrophic AOB) and *Comamonadaceae* (3%, the genus Hydrogenophaga can perform heterotrophic nitrification and aerobic denitrification) (WANG et al. 2020b; WU et al. 2019; LIU et al., 2017).

c. Concerning phosphorus removal (EBPR), the genera Pseudoxanthomonas and Pseudomonas were the main groups in PS. Meanwhile, for LS, a higher diversity of PAO was observed. Namely, the families *Comamonadaceae*, *Sphingomonadaceae*, *Xanthomonadaceae*, and *Rhodocyclaceae* have several genera listed as PAO and GAO in the literature (SZABÓ et al., 2017; ROLLEMBERG et al., 2018).

d. Finally, the presence of the families *Verrucomicrobia* and especially *Anaerolineaceae* in LS confirm the presence of an anaerobic zone in the granules of this reactor during all operational cycle phases, a fact not observed in PS, probably hindered by the high DO concentration. On the other hand, the high RA of Phenylobacterium in PS (complete granulation: 15%) indicates the presence of complex COD influent because this is a single species genus (Phenylobacterium immobile) with a minimal nutrient spectrum, as already mentioned (LINGENS et al., 1985).

Figure 40. Comparing microbial diversity in PS (E-III) and LS (SBR$_{30}$).
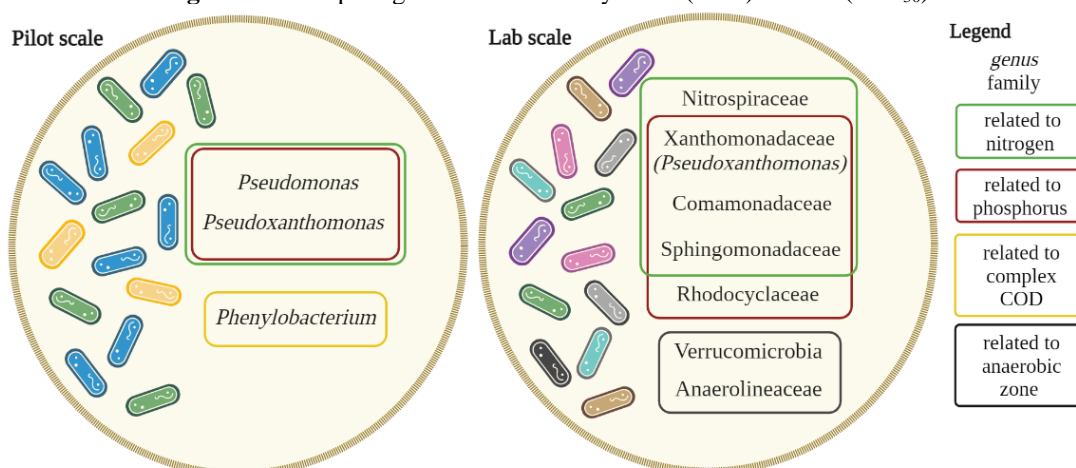
Source: the author (2022).

The characterization of the influent performed for the model implementation (topic 4.2.1) explains the low removal of COD in PS (E-III during complete granulation: $77 \pm 15\%$) compared to other systems with AGS, such as LS ($93 \pm 3\%$) and other systems in the literature (e.g., > 98% KOSAR et al., 2022; > 90% ROLLEMBERG et al., 2019; > 90% JIANG et al., 2016). After fractionation, it was apparent that a significant fraction of the organic matter was found in the inert form (S_I: 11-22%; X_I: 11-18%), thus leading to a higher COD concentration in the effluent. The low microbial diversity and the microorganisms related to complex COD can be linked with the fractionation, considering that such compounds are of slower biodegradation, not covered by the BOD_5 test. Moreover, a performance improvement of the systems after complete granulation could be observed in both the real and simulated results.

Finally, the results obtained in the micro-profiles were decisive for defining the diffusive parameters, especially the thickness of the boundary layer. In the simulation, it was possible to observe the sensitivity of this parameter, considering its importance in defining the concentration of solutes on the biofilm surface. In the micro-profiles, in turn, despite the difficulty of determining the BLR, it was possible to qualitatively analyze that it varies not only with temperature (being lower at higher temperatures) but also with the concentration of the substrate in the medium. Furthermore, the values found (between 80 and 180 μm), even under less stressful hydraulic conditions, corroborate with the most widespread value in the literature (100 μm, HORN & MORGENROTH, 2006); thickness also used during the model implementation (section 4.2).

6   CONCLUSIONS

Considering this study's overall objective[6] and results, it could be stated that temperature was a key factor in AGS's structure, formation, and morphology. Furthermore, a more prolonged anaerobic phase and the insertion of air pulses during the slow feeding were configuration strategies for SBR cycles that generally improved the granulation process. The wastewater influent composition, in turn, directly affected the microbial diversity and system performances, with lower efficiencies observed when lower loads were applied. On the other hand, implementing mathematical models in non-steady-state systems allowed analyzing the influence of the definition of fixed parameters, such as the number and diameter of granules, with effective diffusion coefficients and boundary layer thickness among the most sensitive parameters. To conclude, final considerations about each specific objective are listed below.

(1). To monitor the formation, stability, and treatment performance of a pilot-scale (PS) AGS system while treating domestic wastewater with low COD and nutrient loadings under high temperatures and different SBR cycle arrangements.

Successful granulation was obtained in pilot-scale SBR fed with low-strength domestic wastewater (OLR: 0.88 ± 0.28 kg $COD_{total}.m^{-3}.day^{-1}$; NLR: 0.10 ± 0.03 kg NH_4^+-$N.m^{-3}.day^{-1}$) at around 30 °C without inoculation. However, applying a more extended anaerobic phase (90 minutes compared to 60 minutes) provided a faster and more stable granulation. Complete and stable granulation was observed in one of the experiments (E-III) after 168 days and lasted until the end of the operation (day 247). In this period, the average SVI_{30} was 42 ± 16 $mL.g^{-1}$ TSS and the SVI_{10}/SVI_{30} ratios were smaller than 1.1, indicating great sedimentability.

System performance showed that, after complete granulation, stable performance and increased COD, nitrogen, and phosphorus removal efficiencies were obtained, 75 ± 14, $83 \pm 20\%$, and $55 \pm 24\%$, respectively. SND was observed even without DO control and concentration near saturation (≈ 8.0 $mg.L^{-1}$), indicating that the dominance of granules larger than 0.6 mm (approx. 61% of the biomass) enabled the establishment of anoxic/anaerobic zones within the granules. No common organisms responsible for nitrogen (e.g., *Nitrosomonas*, *Nitrospira*, *Nitrobacter*, and *Paracoccus*) and phosphorus (*Accumulibacter* and *Competibacter*)

---

[6] To investigate the influence of temperature, cycle configuration, and influent composition in SBR systems with AGS of different scales, focusing on understanding sensitive parameters while implementing mathematical models.

removal could be detected regarding microbial diversity. At the same time, the dominant genus was Pseudomonas (44-62%), which is associated by the literature with the SND process and phosphorus removal (WANG et al., 2020b; WU et al., 2019; SZABÓ et al., 2017; ROLLEMBERG et al., 2018; LIU et al., 2017). It can be concluded that nutrient removal occurred mainly heterotrophically, highlighting the contribution of denitrifying phosphorus-accumulating organisms.

(2). To implement mathematical models of activated sludge (ASM3, GUJER et al., 1999) and biofilm (WANNER & GUJER, 1986) to describe simultaneous nutrient and organic matter removal processes observed experimentally in a PS AGS system during the granulation process (non-steady state).

The proposed methodology could describe the system performance in terms of solids and COD removal in a non-steady state SBR by using a fixed number of spheres with variable radius to conserve the mass. Therefore, it enabled the implementation of mathematical models for systems with AGS during the start-up phase, which is so far unreported in the literature. During the model implementation, the following considerations can be highlighted: i) the municipal wastewater at Mangueira WWTP was composed of a sizeable inert fraction (S_I: 11-22%; X_I: 11-18%), justifying the low COD removal efficiency – these results are especially relevant as long as detailed fractioning of influent COD is still rare for warm climates; ii) the calibration of the inflowing solids directly affected the results of effluent solids and COD_{total}; iii) it was not possible to cover the complexity of nitrogen removal processes in AGS (different redox conditions) by assuming a single diameter for all granules.

(3). To understand and quantify the influence of the operational temperature (20 and 30° C) on the granule formation, morphology, and stability in lab-scale (LS) SBR treating municipal wastewater and how this reflects in conversion processes and long-term performance.

By focusing on temperature, a single operational variable, the study of the LS reactors made it possible to state that this parameter directly affects AGS's structure, formation, and morphology. The granules formed at a higher temperature, 30 °C (SBR_{30}), had a more compact structure and reached complete granulation after 102 days. At 20 °C (SBR_{20}), complete granulation was not observed until the end of the experiment, and the granules were less

compact with a more filamentous structure. In addition, these granules reacted more sensitively to operational fluctuations. Overall, the SVI_{10}/SVI_{30} ratios were about 30% lower in SBR_{20} (~ 1.5) than in SBR_{30} (~ 1.1), proving the better sedimentability of the sludge.

Despite the different granulations and a significantly increased nitrogen loading in the influent ($COD_{total}:TN_b:TP$ 100:15:1.7), exceptional efficiencies for the parameters NH_4^+-N (98 ± 2%) and COD (93 ± 3 %) were achieved in both reactors. Successively reducing the oxygen concentration from four to two milligrams per liter and using pulse aeration during anaerobic feeding, it was also possible to keep the effluent value for nitrate-nitrogen below 20 $mg.L^{-1}$. The microbiological tests at the end of the investigated period showed similar compositions in both reactors. The primary differences were possibly attributed to the size and structure of the granules in SBR_{30}.

(4). To evaluate the influence of temperature, structure, and substrate on diffusion aspects of different granules (i.e., presence/absence of anoxic zones, boundary layer resistance) with the aid of microsensors.

When investigating boundary layer resistance and aerobic zone thicknesses in the different granules of SBR_{20} and SBR_{30}, two primary considerations were made: i) in general, larger thicknesses of BLR were observed within granules grown under lower temperature (SBR_{20}), likely due to their structure – these granules were more filamentous and less compact, leading to a higher bacterial activity at their border; ii) qualitatively measuring, after increasing temperature, a decrease in BLR was observed in all granules from both reactors in the presence of substrate, indicating that the increase in microorganism activity outweighed the increase in diffusion – ranging between 200 and 480 μm at 20 °C and 120 and 320 μm at 30 °C.

Finally, based on the results, discussions, and conclusions of this research, the following recommendations and/or suggestions are proposed for further studies:

- Add a recirculation system in the PS-SBR anaerobic phase aiming to increase hydrolysis and improve the performance while treating low-strength domestic wastewater with a high particulate fraction;
- Set a control solution for the excess sludge, handling SRT, since MLSS was not controlled but monitored in both PS and LS;
- Assemble a DO control in PS to improve nutrient removal;

- Investigate the optimal HRT for the different temperatures in LS-SBR since the temperature is a critical factor in biological processes;

- Conduct the experiments for a more extended period to test whether both systems achieve stable granulation over time since few studies cover long-term experiments;

- Perform specific tests to determine the kinetic and stoichiometric parameters used in the model;

- Implement the other models of the activated sludge series (ASM1, ASM2, ASM2d) associated with the biofilm model proposed by Wanner and Gujer (1986), comparing the different results;

- Apply the proposed methodology to describe AGS during the non-stationary period but using multiple compartments with varying thicknesses of biofilm and number of granules to represent the different granule sizes and distribution better;

- Perform redox and DO micro-profiles applying different DO concentrations, temperatures (e.g., colder than 20 °C), and over a more comprehensive granule diameter range;

- Design a flow-cell or measurement system that allows micro-profiling under the same hydrodynamic conditions as the real system.

REFERENCES

Adav, S.S., Lee, D-J., Show, K-Y., Tay, J-H., 2008. Aerobic granular sludge: recent advances. Biotechnology Advances. 26. 411-223. https://doi.org/10.1016/j.biotechadv.2008.05.002.

Akaboci, T.R.V., 2013. Tratamento de esgoto sanitário em reator em bateladas sequenciais: desempenho do processo e modelagem matemática. Master thesis. 169 p. Federal University of Santa Catarina (UFSC): Florianópolis.

Alves, O.I.M., Araújo, J.M., Silva, P.M.J., Magnus, B.S., Gavazza, S., Florêncio, L., Kato, M.T., 2022. Formation and stability of aerobic granular sludge in a sequential batch reactor for the simultaneous removal of organic matter and nutrients from low-strength domestic wastewater. Sci. Total Environ. 843, 156988. https://doi.org/10.1016/j.scitotenv.2022.156988.

Alves, O.I.M., 2017. Aspectos microbiológicos do tratamento de esgotos sanitários em reatores em batelada sequencial com lodo granular. Master thesis. 95 p. Federal University of Pernambuco (UFPE): Recife.

American Public Health Association (APHA). Standard Methods for the examination of water and wastewater. 22 ed. United Book Press: Washington, 2012.

Amin, L., van der Steen, P., López-Vázquez, M., 2022. Expanding the activated sludge model no.1 to describe filamentous bulking: The filamentous model. Journal of Water Process Engineering, 48, 102896. https://doi.org/10.1016/j.jwpe.2022.102896.

Araújo, J.M.P., Silva, P.J.M., Alves, O.I.M., Gavazza, S., Kato, M.T., Florêncio, L., 2016. Formation of aerobic granules in sequencing batch reactors applied for diluted domestic wastewater. The Fifth International Symposium on Environmental Biotechnology and Engineering. Anais. Buenos Aires, Argentina.

Araújo, J.M., Berzio, S., Gehring, T., Nettmann, E., Florêncio, L., Wichern., M., 2022. Influence of temperature on aerobic granular sludge formation and stability treating

municipal wastewater with high nitrogen loadings. Environ. Res. 212, 113578. https://doi.org/10.1016/j.envres.2022.113578

Artan, N., Orhon, D., 2005. Mechanism and design of sequencing batch reactor for nutrient removal. Scientific and Technical Report. n. 19. 116 p. London: IWA Publishing.

ATV-DVWK, Deutsche Vereinigung für Wasserwirtschaft, Abwasser und Abfall, 2016. Arbeitsblatt DWA-A 131. Bemessung von einstufigen Belebungsanlagen. Hennef: ATV-DVWKRegelwerk Arbeitsblatt, A 131.

Baeten, J.E., van Loosdrecht, M.C.M., Volcke, E.I.P., 2017. Improving the Accuracy of Granular Sludge and Biofilm Reactor Simulations in Aquasim Through Artificial Diffusion. Biotechnology and Bioengineering. v. 114. n. 9. p. 2131-2136. https://doi.org/10.1002/bit.26323

Baeten, J.E., van Loosdrecht, M.C.M., Volcke, E.I.P., 2018. Modelling aerobic granular sludge reactors through apparent half-saturation coefficients. Water Res. 146, 134-145. https://doi.org/10.1016/j.watres.2018.09.025.

Bassin, J.P., Tavares, D.C., Borges, R.C., Dezotti, M., 2019. Development of aerobic granular sludge under tropical climate conditions: the key role of inoculum adaptation under reduced sludge washout for stable granulation. J. Environ. Manag. 230, 168–182. https://doi.org/10.1016/j.jenvman.2018.09.072.

Bassin, J.P., Kleerebezem, R., Dezotti, M., van Loosdrecht, M.C.M., 2012. Simultaneous nitrogen and phosphate removal in aerobic granular sludge reactors operated at different temperatures. Water Res. 46 (12), 3805–3816. https://doi.org/10.1016/j.watres.2012.04.015.

Bassin, J.P., 2011. Tecnologia de granulação aeróbia (Lodo granular aeróbio). In: Processos biológicos avançados para tratamentos de efluentes e técnicas de biologia molecular para o estudo da diversidade microbiana. Org: Dezotti, M., Sant'anna Jr., G.L., Bassin, J.P. 1 ed. Editora Interciência: Rio de Janeiro.

Beun, J.J., van Loosdrecht, M.C.M., Heijnen, J.J., 2002. Aerobic granulation in a sequencing batch airlift reactor. Water Res. 36 (3), 702-712. https://doi.org/10.1016/S0043-1354(01)00250-0.

Beun, J.J., Hendriks, A., van Loosdrecht, M.C.M., Morgenroth, E., Wilderer, P.A., Heijnen, J.J., 1999. Aerobic granulation in a sequencing batch reactor. Water Res. 33, 2283-2290. https://doi.org/10.1016/S0043-1354(98)00463-1.

Bin, Z., Chen, Z., Zhigang. Q., Min, J., Zhiqiang, C., Zhaoli, C., Junwen, L., Xuan, W., Jingfeng, W., 2011. Dynamic and distribution of ammonia-oxidizing bacteria communities during sludge granulation in an anaerobic-aerobic sequencing batch reactor. Water Res. 45(18), 6207-6216. https://doi.org/10.1016/j.watres.2011.09.026.

Black, S.A., 1980. Experience with phosphorus removal at existing Ontario municipal wastewater treatment plants. In: Loehr, R.C., Martin, C.S., Rast, W. Phosphorus management strategies for lakes. Ann Arbor, Michigan: Ann Arbor Science Publishers, Inc. chap.13. 329-353.

Bratanis, E., Andersson, T., Lood, R., Bukowska-Faniband, E., 2020. Biotechnological Potential of Bdellovibrio and Like Organisms and Their Secreted Enzymes. Front. Microbiol. 11, 1-14. https://doi.org/10.3389/fmicb.2020.00662.

Bremkes, M., 2020. Untersuchung zur Etablierung von aeroben Granula vom SBR- in den kontinuierlichen Betrieb. Bachelorarbeit. Chair of Urban Water Management and Environmental Engineering, Ruhr-Universität Bochum.

Cao, C., Huang, J., Yan, C., Liu, J., Hu, Q., Guan, W., 2018. Shifts of system performance and microbial community structure in a constructed wetland after exposing silver nanoparticles. Chemosphere 199, 661–669. https://doi.org/10.1016/j.chemosphere.2018.02.031.

Carvalheira, M., Oehmen, A., Carvalho, G., Eusébio, M., Reis, M.A.M., 2014. The impact of aeration on the competition between polyphosphate accumulating organisms and

glycogen accumulating organisms. Water Res. 66, 296-307.
https://doi.org/10.1016/j.watres.2014.08.033.

Castellanos, R.M., Dias, J., Bassin, I.D., Dezotti, M., Bassin, J.P., 2020. Effect of sludge age
on aerobic granular sludge: addressing nutrient removal performance and biomass
stability. Process Saf. Environ. Prot. 149, 212-222.
https://doi.org/10.1016/j.psep.2020.10.042

Chen, W., Lu, Y., Jin, Q., Zhang, M., Wu, J., 2020a. A novel feedforward control strategy for
simultaneous nitrification and denitrification (SND) in aerobic granular sludge
sequential batch reactor (AGS-SBR). Journal of Environmental Management. 260,
110103. https://doi.org/10.1016/j.jenvman.2020.110103.

Chen, Y., Ge, J., Wang, S., Su, H., 2020b. Insight into formation and biological
characteristics of Aspergillus tubingensis-based aerobic granular sludge (AT-AGS) in
wastewater treatment. Sci. Total Environ. 739, 1-10.
https://doi.org/10.1016/j.scitotenv.2020.140128.

Chiu, Z.C., Chen, M.Y., Lee, D.J., Wang, C.H., Laic., J.Y., 2007. Oxygen diffusion in active
layer of aerobic granule withstep change in surrounding oxygen levels. Water Research
41. 884-892. https://doi.org/10.1016/j.watres.2006.11.035.

Coma, M., Verawaty, M., Pijuan, M., Yuan, Z., Bond, P.L., 2012. Enhancing aerobic
granulation for biological nutrient removal from domestic wastewater. Bioresour.
Technol. 103, 101-108. https://doi.org/10.1016/j.biortech.2011.10.014.

Costa, J.G., Paulo, A.M.S., Amorim, C.L., Luís Amaral, A., Castro, P.M.L., Ferreira, E.C.,
Mesquita, D.P., 2022. Quantitative image analysis as a robust tool to assess effluent
quality from an aerobic granular sludge system treating industrial wastewater.
Chemosphere. 291 (2), 132773. https://doi.org/10.1016/j.chemosphere.2021.132773.

Da Silva, V.E.P.S.G., Rollemberg, S.L.S., dos Santos, A.B., 2021. Impact of feeding strategy
on the performance and operational stability of aerobic granular sludge treating high-

strength ammonium concentrations. J. Water Process. Eng.
https://doi.org/10.1016/j.jwpe.2021.102378

Dantas, B.K.S.F., 2018. Formação de lodo granular aeróbio em reatores em bateladas
sequenciais para o tratamento de esgoto doméstico de baixa carga visando à remoção de
nutrientes. Master thesis. 81 p. Federal University of Pernambuco (UFPE): Recife.

De Beer, D., Schramm, A., Santegoeds, C.M., Kühl, M., 1997. A nitrite microsensor for
profiling environmental biofilms. Appl. Environ. Microbiol. 63, 973-977.
https://doi.org/10.1128/aem.63.3.973-977.1997

De Beer, D.; Sweerts, J.-P.R.A., 1989. Measurement of nitrate gradients with ion-selective
microelectrode. An. Chim. Acta. 219, 351-356. https://doi.org/10.1016/S0003-
2670(00)80369-4.

De Beer, D.; Van den Heuvel, J.C., 1988. Response of ammonium-selective microelectrodes
based on the neutral carrier nonactin. Talanta. 35, 728-730.
https://doi.org/10.1016/0039-9140(88)80171-1.

De Graaff, D.R., van Dijk, E.J.H., van Loosdrecht, M.C.M., Pronk, M., 2020. Strength
characterization of full-scale aerobic granular sludge. 41, 13, 1637-1647.
https://doi.org/10.1080/09593330.2018.1543357

De Kreuk, M.K., Mcswain, B.S., Bathe, S., Tay, S.T.L., Schwarzenbeck, N., Wilderer, P.A.,
2005. "Discussion Outcomes ". In: Bathe, S., De Kreuk, M.K., Mcswain, B.S,
Schwarzenbeck, N. (Eds.). Aerobic Granular Sludge. IWA Publishing, pp. 155-169.
ISBN: 9781780402055.

De Kreuk, M.K., Van Loosdrecht, M.C.M., 2004. Selection of slow growing organisms as a
means for improving aerobic granular sludge stability. Water Sci. Technol. 49, 11-12. 9-
17. https://doi.org/10.2166/wst.2004.0792.

De Valk, S., Khadem, A., Foreman, C.M., Van Lier, J.B., De Kreuk, M.K., 2017. Physical and biochemical changes in sludge upon Tubifex tubifex predation. Environ. Technol. 38, 12, 1524-1538. https://doi.org/10.1080/09593330.2016.1236150.

Deng, S., Wang, L., Su, H., 2016. Role and influence of extracellular polymeric substances on the preparation of aerobic granular sludge. Journal of Environmental Management. 173, 49-54. https://doi.org/10.1016/j.jenvman.2016.03.008.

Derlon, N., Wagner, J., Da Costa, R.H.R., Morgenroth, E., 2016. Formation of aerobic granules for the treatment of real and low-strength municipal wastewater using a sequencing batch reactor operated at constant volume. Water Res. 105, 341-50. https://doi.org/10.1016/j.watres.2016.09.007.

DIN EN 12880:2000, 2000. Characterization of sludges – determination of dry residue and water content. ICS: 13.030.20.

Dohmann, M., 1993. Bemessung der Belebungsbecken nach dem Ansatz der Hochschulgruppe (HSG-Ansatz). KA Korresp. Abwasser, 8, 1240.

Ekama, G.A., Dold, P.L., Marais v., G.R., 1986. Procedures for determining influent COD fractions and the maximum specific growth rate of heterotrophs in activated sludge systems. Water Sci. Technol. 18, 91-114. doi:10.2166/wst.1986.0062

Etterer, T.J., 2006. Formation, structure and function of aerobic granular sludge. Technische Universität München.

Fan, J., Li, W., Zhang, B., Shi, W., Lens, P.N.L., 2022. Unravelling the biodegradation performance and mechanisms of acid orange 7 by aerobic granular sludge at different salinity levels. Bioresource Technology. 357, 127347. https://doi.org/10.1016/j.biortech.2022.127347.

Gao, D., Liu, L., Liang, H., Wu, W-M., 2011. Aerobic granular sludge: characterization, mechanism of granulation and application to wastewater treatment. Critical Reviews in Biotechnology. 31(2), 137-152. https://doi.org/10.3109/07388551.2010.497961.

Gebara, F., 1999. Activated sludge biofilm wastewater treatment system. Water Res. 33, 230-238. https://doi.org/10.1016/S0043-1354(98)00210-3.

Gernaey, K.V., van Loosdrecht, M.C.M., Henze, M., Lind, M., Jorgensen, S.B., 2004. Activated sludge wastewater treatment plant modelling and simulation: state of the art. Environmental Modeling & Software. 19 (9), 763-783. https://doi.org/10.1016/j.envsoft.2003.03.005

Giesen, A., De Bruin, L.M.M., Niermans, R.P., Van Der Roest, H.F., 2013. Advancements in the application of aerobic granular biomass technology for sustainable treatment of wastewater. Water Pract. Technol. 8 (1), 47-54. https://doi.org/10.2166/wpt.2013.007.

Gmehling, J., Menke, J., Krafczyk, J., Fischer, K., Fontaine, J.C. and Kehiaian, H.V., 2010. Handbook of chemistry and physics. Haynes, W.M. (ed), p. 247, Taylor & Francis, Boca Raton.

Guimarães, L.B., Wagner, J., Akaboci, T.R.V., Daudt, G.C., Nielsen, P.H., Van Loosdrecht, M.C.M., Weissbrodt, D. G., Da Costa, R. H. R., 2018. Elucidating performance failures in use of granular sludge for nutrient removal from domestic wastewater in a warm coastal climate region. Environ. Technol. 41, 15, 1896-911. https://doi.org/10.1080/09593330.2018.1551938.

Gujer, W., 2010. Nitrification and me – A subjective review. Water Res. 44, 1-19. https://doi.org/10.1016/j.watres.2009.08.038.

Gujer, W., Henze, M., Mino, T., Van Loosdrecht, M.C.M., 1999. Activated sludge model no. 3. Water Sci. Technol. 39, 183-193. https://doi.org/10.1016/S0273-1223(98)00785-9.

Gujer, W., Henze, M., Mino, T., Matsuo, T., Wentzel, M.C., Marais, G.v.R., 1995. Activated Sludge Model No. 2: Biological phosphorus removal. Water Sci. Technol. 31(2), 1-11. https://doi.org/10.1016/0273-1223(95)00175-M.

Gujer, W., Wanner, O., 1990. Modeling mixed population biofilms. In: Characklis, W.; Marshall, K. (ed.). Bioflms. p. 397-443. John Wiley & Sons, New York.

Gulhan, H., Dereli, R.K., Ersahin, M.E., Koyuncu, I., 2022. Dynamic modeling of a full-scale membrane bioreactor performance for landfill leachate treatment. Bioprocess and Biosystems Engineering. 45, 345–352. https://doi.org/10.1007/s00449-021-02664-x.

Hamza, R.A., Zaghloul, M.S., Iorhemen, O.T., Sheng, Z., Tay, J.H., 2019. Optimization of organics to nutrients (COD:N:P) ratio for aerobic granular sludge treating high-strength organic wastewater. Sci. Total Environ. 650, 3168–3179. https://doi.org/10.1016/j.scitotenv.2018.10.026.

He, Q., Wang, H., Chen, L., Gao, S., Zhang, W., Song, J., Yu, J., 2020. Elevated salinity deteriorated enhanced biological phosphorus removal in an aerobic granular sludge sequencing batch reactor performing simultaneous nitrification, denitrification and phosphorus removal. J. Hazard. Mater. 390, 121782. https://doi.org/10.1016/j.jhazmat.2019.121782

He, S., Xue, G., Wang, B-z., 2009. Factors affecting simultaneous nitrification and de-nitrification (SND) and its kinetics model in membrane bioreactor. Journal of Hazard. Mater. 168. n. 2-3. p. 704-710. 2009. https://doi.org/10.1016/j.jhazmat.2009.02.099.

Henze, M., Gujer, W., Mino, T., van Loosdrecht, M.C.M., 2000. Activated Sludge Models ASM1, ASM2, ASM2d and ASM3. IWA Publishing, London, UK. https://doi.org/10.2166/9781780402369.

Henze, M., Grady Jr., C.P.L., Gujer, W., Marais, G.v.R., Matsuo, T., 1987. Activated sludge model no. 1. Scientific and technical report No. 1. IAWPRC (IWA). 1987.

Henze, M., Gujer, W., Mino, T., Matsuo, T., Wentzel, M.C., Marais, G.V.M., van Loosdrecht, M.C.M., 1999. Activated sludge model No. 2d, ASM2D. Water Sci. Technol. 39(1), 165-182. https://doi.org/10.1016/S0273-1223(98)00829-4.

Horn, H., Morgenroth, E., 2006. Transport of oxygen, sodium chloride, and sodium nitrate in biofilms. Chemical Engineering Science, 61, 1347–1356. https://doi.org/10.1016/J.CES.2005.08.027.

Iltis, G.C., Armstrong, R.T., Jansik, D.P., Wood, B.D., Wildenschild, D., 2011. Imaging biofilm architecture within porous media using synchrotron-based X-ray computed microtomography, Water Resour. Res. 47. https://doi.org/10.1029/2010WR009410.

Isanta, E., Figueroa, M., Mosquera-Corral, A., Campos, L., Carrera, J., Pérez, J., 2013. A novel control strategy for enhancing biological N-removal in a granular sequencing batch reactor: A model-based study. Chemical Engineering Journal. 232, 468-477. http://dx.doi.org/10.1016/j.cej.2013.07.118.

Ivanov V., Tay S. T. L., Liu Q. S., Wang X. H., Wang Z. W. and Tay J. H., 2005. Formation and structure of granulated microbial aggregates used in aerobic wastewater treatment. Water Sci. Technol., 52(7), 13-19. https://doi.org/10.2166/wst.2005.0175.

Jenkins, D., Wanner, J. (eds.), 2014. Activated Sludge – 100 Years and Counting, first ed. The International Water Association (IWA).

Jiang, Y., Shang, Y., Wang, H., Yang, K., 2016. Rapid formation and pollutant removal ability of aerobic granules in a sequencing batch airlift reactor at low temperature. Environ. Technol. 37 (23), 3078–3085. https://doi.org/10.1080/09593330.2016.1176075.

Jiang, X., Xu, B., Wu, J., 2018. Sulfur recovery in the sulphide-oxidizing membrane aerated biofilm reactor (MABR): experimental investigation and model simulation. Environ. Technol. 40 (12), 1557-1567. https://doi.org/10.1080/09593330.2018.1426638.

Koch, G., Kühni, M., Gujer, W., Siegrist, H., 2000. Calibration and validation of activated sludge model no. 3 for swiss municipal wastewater. Wat. Res. Vol. 34, No. 14, pp. 3580-3590. https://doi.org/10.1016/S0043-1354(00)00105-6.

Kosar, S., Isik, O., Cicekalan, B., Gulhan, H., Kurt, E.S., Atli, E., Basa, S., Oygun, H., Koyuncu, I., van Loosdrecht, M.C.M., Ersahin, M.E., 2022. Impact of primary sedimentation on granulation and treatment performance of municipal wastewater by aerobic granular sludge process. Journal of Environmental Management. 315, 115191. https://doi.org/10.1016/j.jenvman.2022.115191.

Kühl, M., Revsbech, N.P., 2000. Microsensors for the study of interfacial biogeochemical processes. In: Boudreau, B.P.; Jørgensen, B.B. (ed.). The Benthic Boundary Layer. Chapter 8. Oxford University Press, New York, ISBN 0195118812.

Lambert, C., Morehouse, K.A., Chang, C-Y., Sockett, R.E., 2006. Bdellovibrio: growth and development during the predatory cycle. Curr. Opin. Microbiol. 9(6), 639-644. https://doi.org/10.1016/j.mib.2006.10.002.

Lange, J., 2018. Unsicherheitsanalyse bei der Bestimmung der Zusammensetzung von Zulaufwerten für die Bemessung von Abwasserbehandlungsanlagen-Bauingenieurwesen. Masterarbeit. Chair of Urban Water Management and Environmental Engineering, Ruhr-Universität Bochum.

Layer, L., Adler, A., Reynaert, E., Hernandez, A., Pagni, M., Morgenroth, E., Holliger, C., Derlon, N., 2019. Organic substrate diffusibility governs microbial community composition, nutrient removal performance and kinetics of granulation of aerobic granular sludge. Water Res. 4, 1-15. https://doi.org/10.1016/j.wroa.2019.100033.

Layer, M., Villodres, M.G., Hernandez, A., Reynaert, E., Morgenroth, E., Derlon, N., 2020. Limited simultaneous nitrification-denitrification (SND) in aerobic granular sludge systems treating municipal wastewater: Mechanisms and practical implications. Water Res. X 7, 100048. https://doi.org/10.1016/j.wroa.2020.100048.

Li, D., Guo, W., Liang, D., Zhang, J., Li, J., Li, P., Wu, Y., Bian, X., Ding, F., 2022. Rapid start-up and advanced nutrient removal of simultaneous nitrification, endogenous denitrification and phosphorus removal aerobic granular sequence batch reactor for treating low C/N domestic wastewater. Environ. Res. 212, 113464. https://doi.org/10.1016/j.envres.2022.113464.

Li, Z., Lin, L., Liu, X., Wan, C., Lee, D-J., 2020. Understanding the role of extracellular polymeric substances in the rheological properties of aerobic granular sludge. Sci. Total Environ. 705, 1-7. https://doi.org/10.1016/j.scitotenv.2019.135948.

Li, Y., Liu, Y., Shen, L., Chen, F., 2008. DO diffusion profile in aerobic granule and its microbiological implications. Enzyme and Microbial Technology. 43, 349-354. https://doi.org/10.1016/j.enzmictec.2008.04.005

Li, Y.H.; Gregory, S., 1974. Diffusion of ions in sea-water and in deep-sea sediments. Geochimica et Cosmochimica Acta 38(5), 703-714, https://doi.org/10.1016/0016-7037(74)90145-8.

Liang, D., Li, J., Zheng, Z., Zhang, J., Wu, Y., Li, D., Li, P., Zhang, K., 2021. Rapid start-up of the aerobic granular reactor under low temperature and the nutriment removal performance of granules with different particle sizes. Water, 13, 3590. https://doi.org/10.3390/w13243590

Liebe, S., Wibberg, D., Winkler, A., Pühler, A., Schlüter, A., Varrelmann, M., 2016. Taxonomic analysis of the microbial community in stored sugar beets using high-throughput sequencing of different marker genes. Fems Microbiology Ecology, 92 (2), 1-12. http://dx.doi.org/10.1093/femsec/fiw004.

Lingens, F., Blecher, R., Blecher, H., Blobel, F., Eberspächer, J., Fröhner, C., Görisch, H., Görisch, H., Layh, G., 1985. Phenylobacterium immobile gen. nov. sp. nov. a Gram-Negative Bacterium That Degrades the Herbicide Chloridazon. Int. J. Syst. Bacteriol. 35 (1), 26-39. https://doi.org/10.1099/00207713-35-1-26.

Littfinski, T., Beckmann, J., Gehring, T., Stricker, M., Nettmann, E., Krimmler, S., Murnleitner, E., Lübken, M., Pant, D., Wichern, M., 2022. Model-based identification of biological and pH gradient driven removal pathways of total ammonia nitrogen in single-chamber microbial fuel cells. Chemical Engineering Journal. 431, 133987. https://doi.org/10.1016/j.cej.2021.133987.

Liu, J., Li, J., Wang, X., Zhang, Q., Littleton, H., 2017. Rapid aerobic granulation in an SBR treating piggery wastewater by seeding sludge from a municipal WWTP. Int. J. Environ. Sci. Technol. 51, 332–341. https://doi.org/10.1016/j.jes.2016.06.012.

Liu, Y.Q., Moy, B., Kong, Y-H., Tay, J-H., 2010. Formation, physical characteristics and microbial community structure of aerobic granules in a pilot-scale sequencing batch reactor for real wastewater treatment. Enzyme and Microbial Technology, v. 46, p. 520-525. https://doi.org/10.1016/j.enzmictec.2010.02.001.

Liu, Y.Q., Tay, J.H., 2008. Influence of starvation time on formation and stability of aerobic granules in sequencing batch reactors. Bioresource Technology, 99, 980-985. https://doi.org/10.1016/j.biortech.2007.03.011.

Liu, Y.Q., Tay, J.H., 2002. The essential role of hydrodynamic shear force in the formation of biofilm and granular sludge. Water Res. 36. 1653-1665. https://doi.org/10.1016/s0043-1354(01)00379-7.

Lopez-Vazquez, C.M., Hooijmans, C.M., Brdjanovic, D., Gijzen, H.J., Van Loosdrecht, M.C.M., 2009. Temperature effects on glycogen accumulating organisms. Water Res. 43 (11), 2852–2864. https://doi.org/10.1016/j.watres.2009.03.038.

Luo, J., Hao, T., Wei, L., Mackey, H.R., Lin, Z., Chen, G-H., 2014. Impact of influent COD/N ratio on disintegration of aerobic granular sludge. Water Res. 62, 127-135. https://doi.org/10.1016/j.watres.2014.05.037.

Magnus, B.S., 2019. Efeito da configuração de ciclo e rotas metabólicas na produção e emissão de óxido nitroso em reator em bateladas sequenciais com lodo granular. Thesis [s.l.]. Universidade Federal de Santa Catarina.

Makinia, J., 2010. Mathematical Modelling and Computer Simulation of Activated Sludge Systems, Mathematical Modelling and Computer Simulation of Activated Sludge Systems. IWA Publishing, London-New York. https://doi.org/10.2166/9781780409528

Maus, I., Kim, Y. S., Wibberg, D., Stolze, Y., Off, S., Antonczyk, S., Pühler, A., Scherer, P., Schlüter, A., 2017. Biphasic Study to Characterize Agricultural Biogas Plants by HighThroughput 16S rRNA Gene Amplicon Sequencing and Microscopic Analysis. J. Microbiol. Biotechnol. 27 (2), 321-334. https://doi.org/10.4014/jmb.1605.05083.

Martins Jr., A.C.O., Silva, M.C.A., Benetti, A.D., 2022. Evaluation and optimization of ASM1 parameters using large-scale WWTP monitoring data from a subtropical climate region in Brazil. Water Pract. Technol. 17 (1) 268. https://doi.org/10.2166/wpt.2021.109

Metcalf & Eddy, 2016. Wastewater Engineering: Treatment and Reuse. fifth ed. MacGraw-Hill Companies, New York.

Mino, T., van Loosdrecht, M.C.M., Heijnen, J.J., 1998. Microbiology and biochemistry of the enhanced biological phosphate removal process. Water Res. 32, 3193-3207. https://doi.org/10.1016/S0043-1354(98)00129-8.

Mishima, K., Nakamura, M., 1991. Self-immobilization of aerobic activated sludge - a pilot study of the aerobic upflow sludge blanket process in municipal sewage treatment. Water Sci. Technol. 23 (4–6), 981–990. https://doi.org/10.2166/wst.1991.0550.

Mohammadi, F., Bina, B., Rahimi, S., Janati, M., 2022. Modelling of micropollutant fate in hybrid growth systems: model concepts, Peterson matrix, and application to a lab-scale pilot plant. Environ Sci Pollut Res. https://doi.org/10.1007/s11356-022-20668-2.

Morais, J.C., Gavazza, S., Florêncio, L., Kato, M.t., 2013. Operational aspects of an anaerobic wastewater treatment plant. In: 13th World Congress on Anaerobic Digestion. Santiago de Compostela. IWA, v. 1. p. 1-6.

Morais, J.C., 2015. Remoção de matéria orgânica e nitrogênio em reator compartimentado anaeróbio/anóxico e aeróbio tratando esgoto doméstico. Thesis. [s.l.] Universidade Federal de Pernambuco.

Muda, K., Aris, A., Salim, M.R., Ibrahim, Z., 2013. Sequential Anaerobic-Aerobic Phase Strategy Using Microbial Granular Sludge for Textile Wastewater Treatment. Biomass Now – Sustainable Growth and Use. http://dx.doi.org/10.5772/54458.

Ni, B., Xie, W-M., Liu, S-G., Yu, H-Q., Wang, Y-Z., Wang, G., Dai, X.L., 2009. Granulation of activated sludge in a pilot-scale sequencing batch reactor for the treatment of low-

strength municipal wastewater. Water Research. v. 43. p. 751-761. https://doi.org/10.1016/j.watres.2008.11.009.

Ning, Y-F., Chen, Y-P., Shen, Y., Zeng, N., Liu, S-Y., Guo, J-S., Fang, F., 2014. A new approach for estimating aerobic–anaerobic biofilm structure in wastewater treatment via dissolved oxygen microdistribution. Chemical Engineering Journal. 255, 171-177. http://dx.doi.org/10.1016/j.cej.2014.06.042.

Ong, Y.H., Chua, A.S.M., Huang, Y.T., Ngoh, G.C., You, S.J., 2016. The microbial community in a high-temperature enhanced biological phosphorus removal (EBPR) process. Sustain. Environ. Res. 26, 1, 14-19 http://dx.doi.org/10.1016/j.serj.2016.04.001

Pasztor, I., Thury, P., Pulai, J., 2009. Chemical oxygen demand fractions of municipal wastewater for modelling of wastewater treatment. Int. J. Sci. Environ. Technol. 6 (1), 51-56. https://doi.org/10.1007/BF03326059.

Peyong, Y.N., Zhou, Y., Abdullah, A.Z., Vadivelu, V., 2012. The effect of organic loading rates and nitrogenous compounds on the aerobic granules developed using low strength wastewater. BioChem. Eng. J. 67, 52-59. https://doi.org/10.1016/j.bej.2012.05.009.

Ploug, H., Jørgensen, B. B., 1999. A net-jet flow system for mass transfer and microsensor studies of sinking aggregates. Mar. Ecol. Prog. Ser. 176, 279-290. https://doi.org/10.3354/meps176279.

Płuciennik-Koropczuk, E., Jakubaszek, A., Myszograj, S., Uszakiewicz, S., 2017. COD fractions in mechanical-biological wastewater treatment plant. Civil Environ. Eng. Rep. 24, 207–217. https://doi.org/10.1515/ceer-2017-0014.

Pronk, M., De Kreuk, M.K., De Bruin, B., Kamminga, P., Kleerebezem, R., Van Loosdrecht, M.C.M., 2015. Full-scale performance of the aerobic granular sludge process for sewage treatment. Water Res. 84, 207–217. https://doi.org/10.1016/j.watres.2015.07.011.

Reichert, P; Wanner, O., 1997. Movement of solids in biofilms: Significance of liquid phase transport. Water Sci. Technol. 36 (1), 321-328. https://doi.org/10.1016/S0273-1223(97)00339-9.

Reichert, P., 1994. Aquasim - A tool for simulation and data analysis of aquatic systems. Water Science and Technology. v. 30. p. 21-30. https://doi.org/10.2166/wst.1994.0025

Roeleveld, P.J., Van Loosdrecht, M.C.M., 2002. Experiences with guidelines for wastewater characterisation in the Netherlands. Water Science and Technology 45 (6), 77-87. https://doi.org/10.2166/wst.2002.0095

Roldán, D.M., Carrizo, D., Sanchez-García, ´L., Menes, R.J., 2022. Diversity and effect of increasing temperature on the activity of methanotrophs in sediments of fildes peninsula freshwater lakes, King George Island, Antarctica. Front. Microbiol. 13, 822552. https://doi.org/10.3389/fmicb.2022.822552.

Rollemberg, S.L.S., Barros, A.R.M., Firmino, P.I.M., Santos, A.B., 2018. Aerobic granular sludge: cultivation parameters and removal mechanisms. Bioresour. Technol. 270, 678-688. https://doi.org/10.1016/j.biortech.2018.08.130.

Rollemberg, S.L.S., Barros, A.R.M., de Lima, J.P.M., Santos, A.F., Firmino, P.I.M., dos Santos, A.B., 2019. Influence of sequencing batch reactor configuration on aerobic granules growth: Engineering and microbiological aspects. Journal of Cleaner Production, 238, 117906 C. https://doi.org/10.1016/j.jclepro.2019.117906.

Rollemberg, S., Ferreira, T.J.T., Firmino, P.I.M., dos Santos, A.B., 2020a. Impact of cycle type on aerobic granular sludge formation, stability, removal mechanisms and system performance. J. Environ. Manage. 256, 109970. https://doi.org/10.1016/j.jenvman.2019.109970

Rollemberg, S., de Oliveira, L.Q., Firmino, P.I.M., dos Santos, A.B., 2020b. Tecnologia de lodo granular aeróbio no tratamento de esgoto doméstico: oportunidades e desafios. Eng. Sanit. e Ambient. 25(3). https://doi.org/10.1590/S1413-4152202020190302

Saito, T., Brdjanovic, D., van Loosdrecht, M.C.M., 2004. Effect of nitrite on phosphate uptake by phosphate accumulating organisms. Water Res. 38, 17, 3760-3768. https://doi.org/10.1016/j.watres.2004.05.023.

Sales, M.A.M.P., Dantas, B.K.S.F., Gavazza, S., Kato, M.T., Florencio, L., 2018. Nutrient removal in aerobic granules treating low-strength wastewater under tropical conditions. IWA Biofilms: Granular Sludge System Conference. Anais… Delft, Holanda.

Santos, R.C.O., Barbosa Filho, O., Giordano, G., 2006. Proposta de um método racional para o dimensionamento de reatores de tratamento de esgotos por lodos ativados em bateladas para remoção de carga orgânica. Eng. Sanit. e Ambient.11 (2), 153-161. https://doi.org/10.1590/S1413-41522006000200008.

Sarma, S.J., Tay, J.H., Chu, A., 2017. Finding Knowledge Gaps in Aerobic Granulation Technology. Trends in Biotechnology. 35, 66-78. https://doi.org/10.1016/j.tibtech.2016.07.003.

Schambeck, C.M., da Costa, R.H.R., Derlon, N., 2021. Phosphate removal from municipal wastewater by alginate-likeexopolymers hydrogels recovered from aerobic granular sludge. Bioresour. Technol. 333, 125167. https://doi.org/10.1016/j.biortech.2021.125167

Schwarzenbeck, N., Erley, R., Wilderer, P.A., 2004. Aerobic granular sludge in a SBR-system trating wastewater rich in particulate matter. Water Science and Technology. v 49. p. 41-46. https://doi.org/10.2166/wst.2004.0799.

Sengar, A., Basheer, F., Aziz, A., Farooqi, I.H., 2018. Aerobic granulation technology: Laboratory studies to full scale practices. Journal of Cleaner Production. 197, 616–632. https://doi.org/10.1016/j.jclepro.2018.06.167.

Shanahan, J.W., Semmens, M.J., 2015. Alkalinity and pH effects on nitrification in a membrane aerated bioreactor: An experimental and model analysis. Water Research. 74, 10-22. https://doi.org/10.1016/j.watres.2014.12.055

Silva, P.M.J., 2017a. Avaliação das diferentes condições operacionais na formação de grânulos aeróbios utilizando Reatores em Bateladas Sequências na remoção de nitrogênio e fósforo de esgoto sanitário. Thesis. [s.l.] Universidade Federal de Pernambuco.

Silva, R.J., 2017b. Uso de esgoto doméstico tratado e lodo no cultivo de duas espécies de feijão: biofortificação dos grãos e redução na incidência de pragas. Thesis. [s.l.] Universidade Federal de Pernambuco.

Song, Y., Ishii, S. Rathnayake, L., Ito, T., Satoh, H., Okabe, S., 2013. Development and characterization of the partial nitrification aerobic granules in a sequencing batch airlift reactor. Bioresource Technology. 139, 285-291. https://doi.org/10.1016/j.biortech.2013.04.018

Stewart, P.S., 1998. A review of experimental measurements of effective diffusive permeabilities and effective diffusion coefficients in biofilms. Biotechnology and Bioengineering. 59, 261-272. https://doi. org/10.1002/(SICI)1097-0290(19980805)59:3<261::AID-BIT1>3.0. CO;2-9.

Stewart, P.S., 2003. Diffusion in biofilms. J. Bacteriol. 185(5), 1485-1491, https://doi.org/10.1128/JB.185.5.1485-1491.2003.

Sun, F., Lu, Y., Wu, J., 2019. Comparison of operational strategies for nitrogen removal in aerobic granule sludge sequential batch reactor (AGS-SBR): A model-based evaluation. J. Environ. Chem. Eng. 7, 103314. https://doi.org/10.1016/j.jece.2019.103314.

Światczak, P., Cydzik-Kwiatkowska, A., 2017. Performance and microbial characteristics of biomass in a full-scale aerobic granular sludge wastewater treatment plant. Environ. Sci. Pollut. Res. 25(2), 1655-69. https://doi.org/10.1007/s11356-017-0615-9.

Szabó, E., Liébana, R., Hermansson, M., Modin, O., Persson, F., Wilén, B-M., 2017. Microbial population dynamics and ecosystem function of anoxic/aerobic granular sludge in sequencing batch reactors operated at different organic loading rates. Front. Microbiol. 8, 201-07. https://doi.org/10.3389/fmicb.2017.00770.

Thans, F. C., 2008. Controle operacional de reator em bateladas seqüenciais (RBS): ajustes na concentração de oxigênio dissolvido visando a remoção de nutrientes. Dissertação. 105p. UFSC: Florianópolis.

Thwaites, B.J., Stuetz, R., Short, M., Reeve, P., Alvarez-Gaitan, J.P., Dinesh, N., Philips, R., van den Akker, B., 2021. Analysis of nitrous oxide emissions from aerobic granular sludge treating high saline municipal wastewater. Sci. Total Environ. 756, 143653. https://doi.org/10.1016/j.scitotenv.2020.143653.

Thwaites, B.J., Short, M.D., Stuetz, R.M., Reeve, P.J., Alvarez-Gaitan, J.P., Dinesh, N., Van den Akker, B., 2018. Comparing the performance of aerobic granular sludge versus conventional activated sludge for microbial log removal and effluent quality: implications for water reuse. Water Res. 145, 442–452. https://doi.org/10.1016/j.watres.2018.08.038.

Tomar, S.K., Kumar, R., Chakraborty, S., 2022. Simultaneous biodegradation of pyridine, indole, and ammonium along with phenol and thiocyanate by aerobic granular sludge. Journal of Hazardous Materials. 422, 126861. https://doi.org/10.1016/j.jhazmat.2021.126861.

Van den Berg, L., van Loosdrecht, M.C.M., de Kreuk, M.K., 2020. How to measure diffusion coefficients in biofilms: A critical analysis. Biotechnol. and Bioeng. 118, 1273-1285. https://doi.org/10.1002/bit.27650.

Van Haandel, A., Marais, G., 1999. O comportamento do sistema de lodo ativado: Teoria e aplicações para projetos e operação. Epgraf: Campina Grande.

Van Loosdrecht, M.C.M., Lopez-Vazquez, C.M., Meijer, S.C.F., Hooijmans, C.M., Brdjanovic, D., 2015. Twenty-five years of ASM1: past, present and future of wastewater treatment modelling. Journal of Hydroinformatics. 17(5), 697-718. https://doi.org/10.2166/hydro.2015.006

Volcke, E., Picioreanu, C., De Baets, B., van Loosdrecht, M. C.M., 2012. The granule size distribution in an anammox-based granular sludge reactor affects the conversion-

Implications for modeling. Biotechnol. Bioeng., 109, 7. https://doi.org/10.1002/bit.24443

Von Sperling, M., 2005. Introdução à qualidade das águas e ao tratamento de esgotos. 3ª Edição. Belo Horizonte: Editora UFMG.

Wagner, J., Da Costa, R.H.R., 2013. Aerobic Granulation in a Sequencing Batch Reactor using real Domestic Wastewater. J. Environ. Eng. 139, 1391-96. https://doi.org/10.1061/(ASCE)EE.1943-7870.0000760.

Wagner, J., Weissbrodt, D.G., Manguin, V., da Costa, R.H.R., Morgenroth, E., Derlon, N., 2015. Effect of particulate organic substrate on aerobic granulation and operating conditions of sequencing batch reactors. Water Res., 85, 158-166. http://dx.doi.org/10.1016/j.watres.2015.08.030.

Walder, C., Lindtner, S., Proesl, A., Klegraf, F., Weissenbacher, N., 2013. WWTP design in warm climates - guideline comparison and parameter adaptation for a full-scale activated sludge plant using mass balancing. Water Sci. Technol. (1), 224-231. https://doi.org/10.2166/wst.2012.559.

Wang, X., Li, J., Zhang, X., Chen, Z., Shen, J., Kang, J., 2021. Impact of hydraulic retention time on swine wastewater treatment by aerobic granular sludge sequencing batch reactor. Environ. Sci. Pollut. Res. 28(5), 5927-37. https://doi.org/10.1007/s11356-020-10922-w.

Wang, L., Zhan, H., Wu, G., Zeng, Y., 2020a. Effect of operational strategies on the rapid start-up of nitrogen removal aerobic granular system with dewatered sludge as inoculant. Bioresour. Technol. 315, 1-10. https://doi.org/10.1016/j.biortech.2020.123816.

Wang, Z., Yao, Y., Steiner, N., Cheng, H.-H., Wu, Y., Woo, S.-G., Criddle, C. S., 2020b. Impacts of nitrogen-containing coagulants on the nitritation/denitrification on anaerobic digester centrate. Environ. Sci.: Water Res. Technol. 6, 3451-3459. https://doi.org/10.1039/D0EW00938E.

Wang, Z., Chen, X-M., Ni, B-J., Tang, Y-N., Zhao, H-P., 2019. Model-based assessment of chromate reduction and nitrate effect in a methane-based membrane biofilm reactor. Water Res. 5, 100037. https://doi.org/10.1016/j.wroa.2019.100037.

Wang, H., Zhang, W., Ye, Z., He, Q., Zhang, S., 2018. Isolation and characterization of Pseudoxanthomonas sp. strain YP1 capable of denitrifying phosphorus removal (DPR). Geomicrobiol. J. 35 (6), 537-543. https://doi.org/10.1080/01490451.2017.1420710.

Wang, Q., Garrity, G.M., Tiedje, J. M., Cole, J. R., 2007. Naïve Bayesian Classifier for Rapid Assignment of rRNA Sequences into the New Bacterial Taxonomy. Appl. Environ. Microbiol.. 73(16), 5261-5267. https://doi.org/10.1128/AEM.00062-07.

Wanner, O., Eberl, H.J., Morgenroth, E., Noguera, D.R., Picioreanu, C. Rittmann, B.E. van Loosdrecht, M.C.M., 2006. Mathematical Modeling of Biofilms. IWA Publishing. Scientific Report No. 18.

Wanner, O., Reichert, P., 1996. Mathematical modelling of mixed-culture biofilms. Biotechnology & Bioengineering. 49, 172-184. https://doi.org/ 10.1002/(SICI)1097-0290(19960120)49:2<172::AID-BIT6>3.0.CO;2-N.

Wanner, O., 1995. New experimental findings and biofilm modelling concepts. Wat. Sci. Tech. 32 (8), 133-140. https://doi.org/10.1016/0273-1223(96)00017-0

Wanner, O., 1994. Modeling of mixed-population biofilm accumulation. In: Geesey, G., Levandowski, Z., Flemming, H.-C. (ed.). Biofouling and Biocorosion in Industrial Water Systems. p. 37-62. Lewis Publishers, Boca Raton.

Wanner, O., Gujer, W., 1986. A Multispecies Biofilm Model. Biotechnology and Bioengineering. v. 28. p. 314-328. https://doi.org/10.1002/bit.260280304

Wichern, M., Gehring, T., Lübken, M., 2018. Modeling of Biological Systems in Wasterwater Treatment. Reference Module in Earth Systems and Environmental Sciences. Elsevier. 8-Fev-18. https://doi.org/10.1016/B978-0-12-409548-9.10944-3.

Wichern, M., 2010. Simulation biochemischer Prozesse in der Siedlungswasserwirtschaft, ISBN 3835631799, Oldenbourg-Verlag, München.

Wichern, M., Lübken, M., Horn, H., 2008. Optimizing sequencing batch reactor (SBR) reactor operation for treatment of dairy wastewater with aerobic granular sludge. Water Sci. Technol. 58(6), 1199-1206. https://doi.org/10.2166/wst.2008.486.

Winkler, M.K.H., Straka, L., 2019. New directions in biological nitrogen removal and recovery from wastewater. Curr Opin Biotechnol. 57, 50-55. https://doi.org/10.1016/j.copbio.2018.12.007.

Winkler, M.K.H., Kleerebezem, R., de Bruin, L.M.M., Verheijen, P.J.T., Abbas, B., Habermacher, J., van Loosdrecht, M.C.M., 2013. Microbial diversity differences within aerobic granular sludge and activated sludge flocs. Applied Microbiology and Biotechnology. 97, 16, 7447-7458. https://doi.org/10.1007/s00253-012-4472-7.

Wu, L., Shen, M., Li, J.; Huang, S., Li, Z., Yan; Z., Peng, Y., 2019. Cooperation between partial-nitrification, complete ammonia oxidation (comammox), and anaerobic ammonia oxidation (anammox) in sludge digestion liquid for nitrogen removal. Environ. Pollut. 254 (A), 112965. https://doi.org/10.1016/j.envpol.2019.112965.

Xia, J., Ye, L., Ren, H., Zhang, X-X., 2018. Microbial community structure and function in aerobic granular sludge. Applied Microbiology and Biotechnology. 102, 3967-3979. https://doi.org/10.1007/s00253-018-8905-9.

Yamada, T., Sekiguchi, Y., 2018. Anaerolineaceae, in: Bergey's Manual of Systematics of Archaea and Bacteria, Major Reference Works. pp. 1-5. https://doi.org/10.1002/9781118960608.fbm00301.

Yuan, C., Peng, Y., Wang, B., Li, X., Zhang, Q., 2020. Facilitating sludge granulation and favoring glycogen accumulating organisms by increased salinity in an anaerobic/micro-aerobic simultaneous partial nitrification, denitrification and phosphorus removal (SPNDPR) process. Bioresour. Technol. 313, 123698. https://doi.org/10.1016/j.biortech.2020.123698

Zhang, L., Long, B., Wu, J., Cheng, Y., Zhang, B., Zeng, Y., Huang, S., Zeng, M., 2019. Evolution of microbial community during dry storage and recovery of aerobic granular sludge. Heliyon. 5 (12), Article e03023. https://doi.org/10.1016/j.heliyon.2019.e03023

Zhang, Q., Hu, J., Lee, D-J., 2016. Aerobic Granular Processes: Current Research Trends. Bioresource Technology. 210, 74-80. http://doi.org/10.1016/j.biortech.2016.01.098.

Zhu, T., Xu, B., Wu, J., 2018. Experimental and mathematical simulation study on the effect of granule particle size distribution on partial nitrification in aerobic granular reactor. Biochem. Eng. J. 134, 22-29. https://doi.org/10.1016/j.bej.2018.03.004.

APPENDIX A – Aquasim code

```
**********************************************************************
AQUASIM Version 2.1g (win/mfc) - Listing of System Definition
**********************************************************************
Date and time of listing:  25/09/2022  09:58:12


**********************************************************************
Variables
**********************************************************************
a01_CODsol:   Description:        Graphics: soluble COD
          Type:          Formula Variable
          Unit:          g COD/m^3
          Expression:        s_SS+s_SI+s_XS*i_CODsol_fXS
-----------------------------------------------------------------------
a02_CODtot:   Description:        Graphics: total COD
          Type:          Formula Variable
          Unit:          g COD/m^3
          Expression:        s_SS+s_SI+s_XS+s_XI+s_XH+s_XA
-----------------------------------------------------------------------
a03_TSS:      Description:        Graphics: simulated TSS
          Type:          Formula Variable
          Unit:          g COD/m^3
          Expression:
i_VSS_XI*s_XI+i_VSS_XS*s_XS+i_TSS_BM*(s_XH+s_XA)+i_VSS_Sto*s_XSto+s_XMI
-----------------------------------------------------------------------
a_BH_CODbio:  Description:        Fraction of biomass from biodegradable COD
          Type:          Constant Variable
          Unit:          -
          Value:         0.195
          Standard Deviation:  1
          Minimum:          0
          Maximum:          10
          Sensitivity Analysis: inactive
          Parameter Estimation: inactive
-----------------------------------------------------------------------
a_COD_VSS:    Description:        Ratio of COD to VSS
          Type:          Constant Variable
          Unit:          g COD / gTSS
          Value:         1.45
          Standard Deviation:  1
          Minimum:          0
          Maximum:          2
          Sensitivity Analysis: inactive
          Parameter Estimation: inactive
-----------------------------------------------------------------------
A_film:       Description:        Surface area of the biofilm
          Type:          Formula Variable
          Unit:          m^2
          Expression:        4*pi*n_g*(1e-009+z)^2
-----------------------------------------------------------------------
a_XTSS_COD:   Description:        Fraction TSS to COD
          Type:          Formula Variable
          Unit:          gTSS/gCOD
          Expression:        70/120
-----------------------------------------------------------------------
b_A:          Description:        Decay rate for autotrophs (endogenous respiration coefficient)
          Type:          Formula Variable
          Unit:          1/d
```

Expression: 0.18*exp(-0.105*(20-T))

----

b_H: Description: Decay rate for heterotrophs (endogenous respiration coefficient)

Type: Formula Variable

Unit: 1/d

Expression: 0.3*exp(-0.06952*(20-T))

DifLiq_Alk: Description: Diffusion coefficient of HCO3

Type: Formula Variable

Unit: m^2/d

Expression: DifLiq_Alk_25*0.0008891*(273.15+T)/(298.15*0.0008141)

DifLiq_Alk_25: Description: Diffusion coefficient of HCO3 in water at 25oC

Type: Constant Variable

Unit: m^2/d

Value: 6e-005

Standard Deviation: 1

Minimum: 0

Maximum: 0.0001

Sensitivity Analysis: inactive

Parameter Estimation: inactive

DifLiq_N2: Description: Diffusion coefficient of N2

Type: Formula Variable

Unit: m^2/d

Expression: DifLiq_N2_25*0.0008891*(273.15+T)/(298.15*0.0008141)

DifLiq_N2_25: Description: Diffusion coefficient of N2 in water at 25oC

Type: Constant Variable

Unit: m^2/d

Value: 0.00018

Standard Deviation: 1

Minimum: 0

Maximum: 0.001

Sensitivity Analysis: inactive

Parameter Estimation: inactive

DifLiq_NH4: Description: Diffusion coefficient of NH4

Type: Formula Variable

Unit: m^2/d

Expression: DifLiq_NH4_25*0.0008891*(273.15+T)/(298.15*0.0008141)

DifLiq_NH4_25: Description: Diffusion coefficient of NH4 in water at 25oC

Type: Constant Variable

Unit: m^2/d

Value: 0.00018

Standard Deviation: 0.00018

Minimum: 0

Maximum: 0.001

Sensitivity Analysis: inactive

Parameter Estimation: inactive

DifLiq_NO: Description: Diffusion coefficient of NO2

Type: Formula Variable

Unit: m^2/d

Expression: DifLiq_NO_25*0.0008891*(273.15+T)/(298.15*0.0008141)

DifLiq_NO_25: Description: Diffusion coefficient of NO2 in water at 25oC

Type: Constant Variable

Unit: m^2/d

Value: 0.00016
Standard Deviation: 0.00016
Minimum: 0
Maximum: 0.001
Sensitivity Analysis: inactive
Parameter Estimation: inactive

DifLiq_SO2:   Description: Diffusion coefficient of oxygen
            Type: Formula Variable
            Unit: m^2/d
            Expression: DifLiq_SO2_25*0.0008891*(273.15+T)/(298.15*0.0008141)

DifLiq_SO2_25: Description: Diffusion coefficient of oxygen in water at 25oC
            Type: Constant Variable
            Unit: m^2/d
            Value: 0.0002
            Standard Deviation: 0.00021
            Minimum: 0
            Maximum: 0.001
            Sensitivity Analysis: inactive
            Parameter Estimation: inactive

DifLiq_VFA: Description: Diffusion coefficient of VFA
            Type: Formula Variable
            Unit: m^2/d
            Expression: DifLiq_VFA_25*0.0008891*(273.15+T)/(298.15*0.0008141)

DifLiq_VFA_25: Description: Diffusion coefficient of VFA in water at 25oC
            Type: Constant Variable
            Unit: m^2/d
            Value: 6e-005
            Standard Deviation: 6e-005
            Minimum: 0
            Maximum: 0.001
            Sensitivity Analysis: inactive
            Parameter Estimation: inactive
----
etaHend: Description: Reduction factor for bH under anoxic conditions (0.33)
            Type: Constant Variable
            Unit: -
            Value: 0.5
            Standard Deviation: 1
            Minimum: 0
            Maximum: 1
            Sensitivity Analysis: inactive
            Parameter Estimation: inactive
----
etaHNO: Description: Reduction factor for denitrification
            Type: Constant Variable
            Unit: -
            Value: 0.7
            Standard Deviation: 0.5
            Minimum: 0
            Maximum: 1
            Sensitivity Analysis: inactive
            Parameter Estimation: inactive
----
etaNend: Description: Reduction factor for bA under anoxic conditions
            Type: Constant Variable
            Unit: -

```
            Value:          0.5
            Standard Deviation:  1
            Minimum:         0
            Maximum:          1
            Sensitivity Analysis: inactive
            Parameter Estimation: inactive
------------------------------------------------------------------------
frac_COD_bio: Description:       Fraction of biodegradable COD
            Type:           Formula Variable
            Unit:           mg COD/L
            Expression:      in_COD-f_S*in_COD-frac_X_COD*f_A
------------------------------------------------------------------------
frac_X_COD:  Description:       Fraction of biodegradable particulate COD
            Type:           Formula Variable
            Unit:           mg COD/L
            Expression:      frac_X_TSS*a_COD_VSS*(1-f_B)
------------------------------------------------------------------------
frac_X_TSS:  Description:       TSS fraction in COD
            Type:           Formula Variable
            Unit:           mg/L
            Expression:      a_XTSS_COD*in_COD
------------------------------------------------------------------------
f_A:       Description:       Fraction of inert COD from particulate COD
            Type:           Constant Variable
            Unit:           gCOD/gCOD
            Value:          0.3
            Standard Deviation:  1
            Minimum:         0.2
            Maximum:          0.35
            Sensitivity Analysis: active
            Parameter Estimation: active
------------------------------------------------------------------------
f_B:       Description:       Fraction of non-volatile TSS
            Type:           Constant Variable
            Unit:           -
            Value:          0.2
            Standard Deviation:  1
            Minimum:         0.2
            Maximum:          0.3
            Sensitivity Analysis: active
            Parameter Estimation: inactive
------------------------------------------------------------------------
f_CSB:      Description:       Fraction of SS from biodegradable COD
            Type:           Constant Variable
            Unit:           -
            Value:          0.2
            Standard Deviation:  1
            Minimum:         0.1
            Maximum:          0.3
            Sensitivity Analysis: active
            Parameter Estimation: inactive
------------------------------------------------------------------------
f_iSS_BM_prod: Description: Fraction of SS from biomass
            Type:           Constant Variable
            Unit:           -
            Value:          1
            Standard Deviation:  1
            Minimum:         0
            Maximum:          10
            Sensitivity Analysis: inactive
```

Parameter Estimation: inactive

----

f_S: Description: Fraction of inert soluble COD
          Type: Constant Variable
          Unit: -
          Value: 0.1
          Standard Deviation: 1
          Minimum: 0.05
          Maximum: 0.1
          Sensitivity Analysis: inactive
          Parameter Estimation: inactive

----

f_SI: Description: Production of SI in hydrolysis
          Type: Constant Variable
          Unit: g SS/g XS
          Value: 0
          Standard Deviation: 1
          Minimum: 0
          Maximum: 0.1
          Sensitivity Analysis: active
          Parameter Estimation: active

----

f_XI: Description: Fraction of inert COD generated in biomass lysis
          Type: Constant Variable
          Unit: gCOD/gCOD
          Value: 0.2
          Standard Deviation: 1
          Minimum: 0
          Maximum: 0.3
          Sensitivity Analysis: inactive
          Parameter Estimation: inactive

----

ic_SAlk: Description: Initial condition - SAlk concentration (biofilm)
          Type: Constant Variable
          Unit: mmol HCO3-/L
          Value: 8
          Standard Deviation: 1
          Minimum: 0
          Maximum: 10
          Sensitivity Analysis: inactive
          Parameter Estimation: inactive

----

ic_SI: Description: Initial condition - SI concentration (biofilm)
          Type: Constant Variable
          Unit: mg COD/L
          Value: 22.56
          Standard Deviation: 1
          Minimum: 0
          Maximum: 30
          Sensitivity Analysis: inactive
          Parameter Estimation: inactive

----

ic_SN2:   Description: Initial condition - SN2 concentration (biofilm)
          Type: Constant Variable
          Unit: mg N/L
          Value: 0.1
          Standard Deviation: 1
          Minimum: 0
          Maximum: 10
          Sensitivity Analysis: inactive

Parameter Estimation: inactive

----
ic_SNH: Description: Initial condition - SNH concentration (biofilm)
            Type: Constant Variable
            Unit: mg N/L
            Value: 26.59
            Standard Deviation: 1
            Minimum: 0
            Maximum: 30
            Sensitivity Analysis: inactive
            Parameter Estimation: inactive
----
ic_SNO: Description: Initial condition - SNO concentration (biofilm)
            Type: Constant Variable
            Unit: mg N/L
            Value: 0.3273244
            Standard Deviation: 1
            Minimum: 0
            Maximum: 10
            Sensitivity Analysis: inactive
            Parameter Estimation: inactive
----
ic_SO2:   Description: Initial condition - SO2 concentration (biofilm)
            Type: Constant Variable
            Unit: mg O2/L
            Value: 0.1
            Standard Deviation: 1
            Minimum: 0
            Maximum: 10
            Sensitivity Analysis: inactive
            Parameter Estimation: inactive
----
ic_SS: Description: Initial condition - SS concentration (biofilm)
            Type: Constant Variable
            Unit: mg COD/L
            Value: 31.45
            Standard Deviation: 1
            Minimum: 0
            Maximum: 35
            Sensitivity Analysis: inactive
            Parameter Estimation: inactive
----
ic_XA: Description: Initial condition - XA concentration (biofilm)
            Type: Constant Variable
            Unit: mg COD/L
            Value: 0.0001
            Standard Deviation: 1
            Minimum: 0
            Maximum: 500
            Sensitivity Analysis: inactive
            Parameter Estimation: inactive
----
ic_XH: Description: Initial condition - XH concentration (biofilm)
            Type: Constant Variable
            Unit: mg COD/L
            Value: 3085.6
            Standard Deviation: 1
            Minimum: 0
            Maximum: 30000
            Sensitivity Analysis: inactive

Parameter Estimation: inactive

----
ic_XI: Description: Initial condition - XI concentration (biofilm)
            Type: Constant Variable
            Unit: mg COD/L
            Value: 7714
            Standard Deviation: 1
            Minimum: 0
            Maximum: 50000
            Sensitivity Analysis: inactive
            Parameter Estimation: inactive

----
ic_XMI: Description: Initial condition - XMI concentration (biofilm)
            Type: Constant Variable
            Unit: mg COD/L
            Value: 580
            Standard Deviation: 1
            Minimum: 0
            Maximum: 14000
            Sensitivity Analysis: inactive
            Parameter Estimation: inactive

----
ic_XS: Description: Initial condition - XS concentration (biofilm)
            Type: Constant Variable
            Unit: mg COD/L
            Value: 110.2
            Standard Deviation: 1
            Minimum: 0
            Maximum: 1000
            Sensitivity Analysis: inactive
            Parameter Estimation: inactive

----
ic_XSto: Description: Initial condition - XSto concentration (biofilm)
            Type: Constant Variable
            Unit: mg COD/L
            Value: 1e-005
            Standard Deviation: 1
            Minimum: 0
            Maximum: 1
            Sensitivity Analysis: inactive
            Parameter Estimation: inactive

----
in_COD: Description: Real inflow COD concentration
            Type: Real List Variable
            Unit: mg COD/L
            Argument: t
            Standard Deviations: global
            Rel. Stand. Deviat.: 0
            Abs. Stand. Deviat.: 1
            Minimum: 0
            Maximum: 1e+009
            Interpolation Method: linear interpolation
            Sensitivity Analysis: inactive
            Real Data Pairs (17 pairs):
                0   273
                6   200.9
                13   210.6
                19   209.9
                25   387.5
                  .   .

```
            .         .
         102       203.9
         117       245.1
         132       167.9
         138       167.1
         147       225.6
```
----
in_CODsol: Description: Inflow soluble COD concentration
       Type: Formula Variable
       Unit: mg COD/L
       Expression: in_SS+in_SI+in_XS*i_CODsol_fXS
----
in_CODtot: Description: Inflow total COD concentration
       Type: Formula Variable
       Unit: mg COD/L
       Expression: in_SS+in_SI+in_XI+in_XS+in_XH+in_XA
----
in_FSS: Description: Real inflow FSS concentration
       Type: Real List Variable
       Unit: mg/L
       Argument: t
       Standard Deviations: global
       Rel. Stand. Deviat.: 0
       Abs. Stand. Deviat.: 1
       Minimum: 0
       Maximum: 1e+009
       Interpolation Method: linear interpolation
       Sensitivity Analysis: inactive
       Real Data Pairs (14 pairs):

```
          6        14.102564
         13         0.83333333
         19        19.565217
         25        10.294118
         39        27
         48        60
         55        20
         67         6
         83        24.545455
         96        20.714286
        102        58.730159
        117        48.75
        132         3.3333333
        138        51.818182
```
----
in_NH4:   Description: Real inflow concentration NH4
       Type: Real List Variable
       Unit: mg N/L
       Argument: t
       Standard Deviations: global
       Rel. Stand. Deviat.: 0
       Abs. Stand. Deviat.: 1
       Minimum: 0
       Maximum: 1e+009
       Interpolation Method: linear interpolation
       Sensitivity Analysis: inactive
       Real Data Pairs (17 pairs):

```
          0        21.54
          6        24.57
         13        17.15
         19        16.91
```

```
       25           29.15
        .             .
        .             .
      102           26.39
      117           36.07
      132           27.47
      138           22.83
      147           27.83
```
----
in_NTK: Description: Real inflow NTK concentration
            Type: Real List Variable
            Unit: mg N/L or g N/m^3
            Argument: t
            Standard Deviations: global
            Rel. Stand. Deviat.: 0
            Abs. Stand. Deviat.: 1
            Minimum: 0
            Maximum: 1e+009
            Interpolation Method: linear interpolation
            Sensitivity Analysis: inactive
            Real Data Pairs (14 pairs):
```
       13           32.5
       19           32.6
       25           39.7
       39           36.2
       48           36.5
       55           33.8
       67           32.6
       83           29.6
       96           34.4
      102           31.3
      117           46.6
      132           33.9
      138           31.5
      147           33.2
```
----
in_P: Description: Real inflow P concentration
            Type: Real List Variable
            Unit: mgP/L
            Argument: t
            Standard Deviations: global
            Rel. Stand. Deviat.: 0
            Abs. Stand. Deviat.: 1
            Minimum: 0
            Maximum: 1e+009
            Interpolation Method: linear interpolation
            Sensitivity Analysis: inactive
            Real Data Pairs (16 pairs):
```
        6            3.2
       13            3.8
       19            3.7
       25            5
       39            4.5
        .             .
        .             .
      102            3.5
      117            5
      132            3.7
      138            4.2
      147            3.5
```

```
------------------------------------------------------------------------
in_SAlk:     Description:        Inflow alkalinity
             Type:              Constant Variable
             Unit:              mg HCO3-/L
             Value:             8
             Standard Deviation:  1
             Minimum:           0
             Maximum:           10
             Sensitivity Analysis: inactive
             Parameter Estimation: inactive
------------------------------------------------------------------------
in_SI:       Description:        Inflow SI fraction
             Type:              Formula Variable
             Unit:              mg COD/L
             Expression:        in_COD*f_S
------------------------------------------------------------------------
in_SNH:      Description:        Inflow SNH fraction (NTK fractionation)
             Type:              Formula Variable
             Unit:              mg N/L
             Expression:
in_NTK-(i_N_SS*in_SS+i_N_XS*in_XS+i_N_SI*f_S*in_COD+i_N_XI*in_XI+i_N_BM*
    (in_XH+in_XA))
------------------------------------------------------------------------
in_SS:       Description:        Inflow SS fraction
             Type:              Formula Variable
             Unit:              mg COD/L
             Expression:        f_CSB*frac_COD_bio
------------------------------------------------------------------------
in_TSS:      Description:        Real inflow TSS concentration
             Type:              Real List Variable
             Unit:              mg/L
             Argument:          t
             Standard Deviations:  global
             Rel. Stand. Deviat.:  0
             Abs. Stand. Deviat.:  1
             Minimum:           0
             Maximum:           1e+009
             Interpolation Method: linear interpolation
             Sensitivity Analysis: inactive
             Real Data Pairs (14 pairs):
               6          0.124
              13          0.072
              19          0.121
              25          0.128
              39          0.132
              48          0.137
              55          0.082
              67          0.073
              83          0.096
              96          0.041
             102          0.102
             117          0.086
             132          0.087
             138          0.056
------------------------------------------------------------------------
in_TSS_frac: Description:        Inflow TSS fractionated
             Type:              Formula Variable
             Unit:              mg/L
             Expression:        i_VSS_XI*in_XI+i_VSS_XS*in_XS+i_TSS_BM*(in_XH+in_XA)
------------------------------------------------------------------------
```

in_VSS: Description: Inflow VSS fraction (TSS - FSS)
     Type: Formula Variable
     Unit: mg/L
     Expression: in_TSS-in_FSS

----

in_XA: Description: Inflow XA fraction
     Type: Formula Variable
     Unit: mg COD/L
     Expression: in_COD*0.0001

----

in_XH: Description: Inflow XH fraction
     Type: Formula Variable
     Unit: mg COD/L
     Expression: a_BH_CODbio*frac_COD_bio

----

in_XI: Description: Inflow XI fraction
     Type: Formula Variable
     Unit: mg COD/L
     Expression: f_A*frac_X_COD

----

in_XMI: Description:
     Type: Formula Variable
     Unit:
     Expression: frac_X_TSS*f_B-(in_XH+in_XA)*(i_TSS_BM-i_VSS_BM)

----

in_XS: Description: Inflow XS fraction
     Type: Formula Variable
     Unit: mg COD/L
     Expression: frac_COD_bio-in_SS-in_XA-in_XH

----

i_CODsol_fXS: Description: Fraction of soluvel (coloidal) do XS
     Type: Constant Variable
     Unit: -
     Value: 0.5
     Standard Deviation: 1
     Minimum: 0
     Maximum: 10
     Sensitivity Analysis: inactive
     Parameter Estimation: inactive

----

i_N_BM: Description: N content of biomass, XH, XA (HSG old 0.08)
     Type: Constant Variable
     Unit: gN/(gX_H or gX_A)
     Value: 0.07
     Standard Deviation: 1
     Minimum: 0
     Maximum: 0.1
     Sensitivity Analysis: active
     Parameter Estimation: inactive

----

i_N_SI: Description: N content of inert soluble COD (SI)
     Type: Constant Variable
     Unit: g N/g SI
     Value: 0.01
     Standard Deviation: 1
     Minimum: 0
     Maximum: 0.1
     Sensitivity Analysis: inactive
     Parameter Estimation: inactive

----

i_N_SS: Description: N content of readily biodegradable substrate
    Type: Constant Variable
    Unit: g N/g SS
    Value: 0.03
    Standard Deviation: 1
    Minimum: 0
    Maximum: 0.1
    Sensitivity Analysis: active
    Parameter Estimation: inactive

----

i_N_XI: Description: N content of inert particulate COD XI (HSG old 0.045)
    Type: Constant Variable
    Unit: g N/g XI
    Value: 0.04
    Standard Deviation: 1
    Minimum: 0
    Maximum: 0.1
    Sensitivity Analysis: inactive
    Parameter Estimation: inactive

----

i_N_XS: Description: N content of slowly biodegradable substrate
    Type: Constant Variable
    Unit: gN/g XS
    Value: 0.03
    Standard Deviation: 1
    Minimum: 0
    Maximum: 0.1
    Sensitivity Analysis: inactive
    Parameter Estimation: inactive

----

i_TSS_BM: Description: Conversion factor biomass in TSS
    Type: Formula Variable
    Unit: g TSS/g XSto
    Expression: 1/1.42

----

i_TSS_Sto: Description: Conversion factor XSto in TSS
    Type: Constant Variable
    Unit: g TSS/g XBio
    Value: 0.6
    Standard Deviation: 1
    Minimum: 0
    Maximum: 10
    Sensitivity Analysis: inactive
    Parameter Estimation: inactive

----

i_TSS_VSS_BM: Description: TSS to VSS ratio biomasse
    Type: Formula Variable
    Unit: g /g COD
    Expression: 1/0.92

----

i_TSS_XI: Description: Conversion factor XI in TSS
    Type: Constant Variable
    Unit: gTSS/g XI
    Value: 0.75
    Standard Deviation: 1
    Minimum: 0
    Maximum: 10
    Sensitivity Analysis: inactive
    Parameter Estimation: inactive

----

i_TSS_XS: Description: Conversion factor XS in TSS
        Type: Constant Variable
        Unit: gTSS/g XS
        Value: 0.75
        Standard Deviation: 1
        Minimum: 0
        Maximum: 10
        Sensitivity Analysis: inactive
        Parameter Estimation: inactive

----

i_VSS_BM: Description: VSS to COD ratio biomass
        Type: Constant Variable
        Unit: g /g COD
        Value: 0.70423
        Standard Deviation: 1
        Minimum: 0
        Maximum: 10
        Sensitivity Analysis: inactive
        Parameter Estimation: inactive

----

i_VSS_Sto: Description: VSS to COD ratio XSTO
        Type: Formula Variable
        Unit:
        Expression: 0.6

----

i_VSS_XI: Description: VSS to COD ratio XI
        Type: Formula Variable
        Unit: g /g COD
        Expression: 1/1.33

----

i_VSS_XS: Description: VSS to COD ratio XS
        Type: Formula Variable
        Unit: g /g COD
        Expression: 1/1.8

----

k_att: Description: Attachment constant
        Type: Constant Variable
        Unit: mm/(mg*d)
        Value: 0.001
        Standard Deviation: 0.001
        Minimum: 0
        Maximum: 1
        Sensitivity Analysis: inactive
        Parameter Estimation: inactive

----

k_det: Description: Detachment constant
        Type: Constant Variable
        Unit: mm/(mg*d)
        Value: 0
        Standard Deviation: 1
        Minimum: 0
        Maximum: 1
        Sensitivity Analysis: inactive
        Parameter Estimation: inactive

----

k_H: Description: Hydrolysis rate
        Type: Formula Variable
        Unit: gX_S/(gX_H*d)
        Expression: (9)*exp(-0.04*(20-T))

K_H_Alk: Description: Saturation coefficient for alkalinity (HCO3-)
         Type: Constant Variable
         Unit: moleHCO3-/m^3
         Value: 0.1
         Standard Deviation: 1
         Minimum: 0
         Maximum: 10
         Sensitivity Analysis: inactive
         Parameter Estimation: inactive

K_H_NH: Description: Saturation/inhibition coefficient for ammonium (nutrient)
         Type: Constant Variable
         Unit: g N/m^3
         Value: 0.008
         Standard Deviation: 0.005
         Minimum: 0
         Maximum: 10
         Sensitivity Analysis: inactive
         Parameter Estimation: inactive

K_H_NO: Description: Saturation/inhibition coefficient for nitrate
         Type: Constant Variable
         Unit: g N/m^3
         Value: 0.4
         Standard Deviation: 0.5
         Minimum: 0
         Maximum: 10
         Sensitivity Analysis: inactive
         Parameter Estimation: inactive

K_H_O2:   Description: Saturation/inhibition coefficient for oxygen, het. growth
         Type: Constant Variable
         Unit: g O2/m^3
         Value: 0.3
         Standard Deviation: 0.2
         Minimum: 0
         Maximum: 10
         Sensitivity Analysis: inactive
         Parameter Estimation: inactive

K_H_SS: Description: Saturation/inhibition coefficient for readily biodegradable substrates
         Type: Constant Variable
         Unit: g COD/m^3
         Value: 10
         Standard Deviation: 1
         Minimum: 0
         Maximum: 10
         Sensitivity Analysis: inactive
         Parameter Estimation: inactive

K_H_Sto: Description: Saturation coefficient for storage products
         Type: Constant Variable
         Unit: g COD/m^3
         Value: 1
         Standard Deviation: 1
         Minimum: 0
         Maximum: 10
         Sensitivity Analysis: inactive
         Parameter Estimation: inactive

```
---------------------------------------------------------------------------
K_N_Alk:    Description:        Saturation coefficient for alkalinity (HCO3-), aut. growth
            Type:          Constant Variable
            Unit:          mole HCO3-/m^3
            Value:          0.5
            Standard Deviation:   1
            Minimum:          0
            Maximum:          10
            Sensitivity Analysis: inactive
            Parameter Estimation: inactive
---------------------------------------------------------------------------
K_N_NH:     Description:        Saturation coefficient for ammonium (substrate), aut. growth
            Type:          Constant Variable
            Unit:          g N/m^3
            Value:          1
            Standard Deviation:   1
            Minimum:          0
            Maximum:          10
            Sensitivity Analysis: inactive
            Parameter Estimation: inactive
---------------------------------------------------------------------------
K_N_O2:     Description:        Saturation coefficient for oxygen, aut. growth
            Type:          Constant Variable
            Unit:          g O2/m^3
            Value:          0.5
            Standard Deviation:   0.5
            Minimum:          0
            Maximum:          10
            Sensitivity Analysis: inactive
            Parameter Estimation: inactive
---------------------------------------------------------------------------
k_Sto:      Description:        Storage rate
            Type:          Formula Variable
            Unit:          gS_S/(g_XH*d)
            Expression:        12*exp(-0.06952*(20-T))
---------------------------------------------------------------------------
K_X:        Description:        Hydrolysis saturation constant
            Type:          Constant Variable
            Unit:
            Value:          1
            Standard Deviation:   1
            Minimum:          0
            Maximum:          10
            Sensitivity Analysis: inactive
            Parameter Estimation: inactive
---------------------------------------------------------------------------
mu_A:       Description:        Maximum growth rate of XA
            Type:          Formula Variable
            Unit:          1/d
            Expression:        1.12*exp(-0.105*(20-T))
---------------------------------------------------------------------------
mu_H:       Description:        Maximum growth rate on substrate
            Type:          Formula Variable
            Unit:          g XS/(g XH*d) or 1/d
            Expression:        3*exp(-0.06952*(20-T))
---------------------------------------------------------------------------
n_g:        Description:        Number of granules
            Type:          Formula Variable
            Unit:          -
            Expression:        4.69214e+006
```

```
-------------------------------------------------------------------------
n_g_real:    Description:        Number of granules
             Type:          Real List Variable
             Unit:                -
             Argument:          t
             Standard Deviations: global
             Rel. Stand. Deviat.: 0
             Abs. Stand. Deviat.: 1
             Minimum:            0
             Maximum:          1e+009
             Interpolation Method: linear interpolation
             Sensitivity Analysis: inactive
             Real Data Pairs (14 pairs):
                6        2188613.6
               13        14447172
               19        3844269.6
               25        4993564.6
               39        11509495
               48        3118016
               55        723304.48
               67        2158783
               83        1858060.9
               96        4210218.6
              102        7417564.5
              117        2236163.4
              132        5054918.1
              138        1929773.2
-------------------------------------------------------------------------
on_aeration: Description:        (on/off) Aeration system drive
             Type:          Real List Variable
             Unit:              d
             Argument:            t
             Standard Deviations: global
             Rel. Stand. Deviat.: 0
             Abs. Stand. Deviat.: 1
             Minimum:            0
             Maximum:          1e+009
             Interpolation Method: linear interpolation
             Sensitivity Analysis: inactive
             Real Data Pairs (6076 pairs):
               0.0638889     0
               0.0645833     1
               0.15          1
               0.1506944     0
               0.2305556     0
                  .          .
                  .          .
              252.98403      0
              253.06389      0
              253.06458      1
              253.15         1
              253.15069      0
-------------------------------------------------------------------------
on_empty:    Description:        (on/off) Discharge drive
             Type:          Real List Variable
             Unit:              d
             Argument:            t
             Standard Deviations: global
             Rel. Stand. Deviat.: 0
             Abs. Stand. Deviat.: 1
```

```
            Minimum:            0
            Maximum:            1e+009
            Interpolation Method: linear interpolation
            Sensitivity Analysis: inactive
            Real Data Pairs (6076 pairs):
              0.1631944      0
              0.1638889      1
              0.1659722      1
              0.1666667      0
              0.3298611      0

                  .          .
                  .          .
              253           0
              253.16319      0
              253.16389      1
              253.16597      1
              253.16667      0
```

```
on_fill:    Description:        (on/off) Filling system drive
            Type:               Real List Variable
            Unit:               d
            Argument:           t
            Standard Deviations:  global
            Rel. Stand. Deviat.:  0
            Abs. Stand. Deviat.:  1
            Minimum:            0
            Maximum:            1e+009
            Interpolation Method: linear interpolation
            Sensitivity Analysis: inactive
            Real Data Pairs (6076 pairs):
              0            0
              0.0006944      1
              0.0013889      1
              0.0020833      0
              0.1666667      0

                  .          .
                  .          .
              252.83542      0
              253           0
              253.00069      1
              253.00139      1
              253.00208      0
```

P01_hydrolisis:Description: Hydrolisis rate
```
            Type:               Formula Variable
            Unit:               g/(m^3.d)
            Expression:         if s_XS>0 then
```
$k\_H*(s\_XS/s\_XH)/((s\_XS/s\_XH)+K\_X)*s\_XH$ else 0 endif

P02_aerobic_sto:
```
            Description:        Process rate: Aerobic storage of COD
            Type:               Formula Variable
            Unit:               g/(m^3.d)
            Expression:         k_Sto*s_SO/(s_SO+K_H_O2)*s_SS/(s_SS+K_H_SS)*s_XH
```

P03_anoxic_sto:Description: Process rate: Anoxic storage
```
            Type:               Formula Variable
            Unit:               g/(m^3.d)
            Expression:
```
$k\_Sto*etaHNO*K\_H\_O2/(s\_SO+K\_H\_O2)*s\_SS/(s\_SS+K\_H\_SS)*s\_SNO/$

(s_SNO+K_H_NO)*s_XH

P04_aerobic_growth:
        Description: Process rate: Aerobic growth
        Type: Formula Variable
        Unit: g/(m^3.d)
        Expression:
mu_H*s_SO/(s_SO+K_H_O2)*s_SNH/(s_SNH+K_H_NH)*s_SAlk/(s_SAlk+K_H_Alk)*s_XSto/
(s_XSto+K_H_Sto)*s_XH

P05_anoxic_growth:
        Description: Process rate: Anoxic growth
        Type: Formula Variable
        Unit: g/(m^3.d)
        Expression:
mu_H*etaHNO*K_H_O2/(K_H_O2+s_SO)*s_SNH/(K_H_NH+s_SNH)*s_SAlk/
(K_H_Alk+s_SAlk)*s_SNO/(K_H_NO+s_SNO)*s_XSto/(s_XSto+K_H_Sto)*s_XH

P06_aerobic_end_het:
        Description: Process rate: Aerobic endogenous respiration of heterotrophs
        Type: Formula Variable
        Unit: g/(m^3.d)
        Expression: b_H*s_SO/(K_H_O2+s_SO)*s_XH

P07_anoxic_end_het:
        Description: Process rate: Anoxic endogenous respiration of heterotrophs
        Type: Formula Variable
        Unit: g/(m^3.d)
        Expression:
b_H*etaHend*K_H_O2/(K_H_O2+s_SO)*s_SNO/(s_SNO+K_H_NO)*s_XH

P08_aerobic_resp_sto:
        Description: Process rate: Aerobic respiration of XSTO
        Type: Formula Variable
        Unit: g/(m^3.d)
        Expression: if s_XSto>0 then b_H*s_SO/(s_SO+K_H_O2)*s_XSto else 0 endif

----

P09_anoxic_resp_sto:
        Description: Process rate: Anoxic endogenous respiration of XSto
        Type: Formula Variable
        Unit: g/(m^3.d)
        Expression: if s_XSto>0 then
b_H*etaHend*K_H_O2/(K_H_O2+s_SO)*s_SNO/(s_SNO+K_H_NO)*s_XSto else 0 endif

----

P10_nitrification:
        Description: Nitrification rate
        Type: Formula Variable
        Unit: g/(m^3.d)
        Expression:
mu_A*s_SO/(s_SO+K_N_O2)*s_SNH/(s_SNH+K_N_NH)*s_SAlk/(s_SAlk+K_N_Alk)*s_XA

P11_aerobic_end_aut:
        Description: Process rate: Aerobic endogenous respiration of autotrophs
        Type: Formula Variable
        Unit: g/(m^3.d)
        Expression: b_A*s_SO/(s_SO+K_H_O2)*s_XA

P12_anoxic_end_aut:
        Description: Process rate: Aerobic endogenous respiration of autotrophs
        Type: Formula Variable

Unit: $g/(m^3.d)$
Expression:
$b\_A*etaNend*s\_SNO/(s\_SNO+K\_H\_NO)*K\_H\_O2/(s\_SO+K\_H\_O2)*s\_XA$

P13_aeration: Description: Aeration rate
        Type: Formula Variable
        Unit: $g/(m^3.d)$
        Expression: if (ZoneIndex=0) then on_aeration* $(1/24)*10000*(SOsat-s\_SO)$ else 0 endif

----

porosity: Description: Biofilm porosity
        Type: Dyn. Volume State Var.
        Unit: 0.8
        Relative Accuracy: 1e-006
        Absolute Accuracy: 1e-006

----

q_empty: Description: Discharge flow
        Type: Constant Variable
        Unit: m^3/d
        Value: 41.4
        Standard Deviation: 1
        Minimum: 0
        Maximum: 400000
        Sensitivity Analysis: active
        Parameter Estimation: inactive

----

q_fill: Description: Filling flow
        Type: Constant Variable
        Unit: m^3/d
        Value: 82.8
        Standard Deviation: 1
        Minimum: 0
        Maximum: 100000
        Sensitivity Analysis: inactive
        Parameter Estimation: inactive

----

real_efCODs: Description: Real filt. COD concentration in effluent
        Type: Real List Variable
        Unit: mg/L
        Argument: t
        Standard Deviations: global
        Rel. Stand. Deviat.: 0
        Abs. Stand. Deviat.: 1
        Minimum: 0
        Maximum: 1e+009
        Interpolation Method: linear interpolation
        Sensitivity Analysis: inactive
        Real Data Pairs (16 pairs):

6	56.795033
13	48.3916
19	64.8331
25	73.6019
39	51.6799
.	.
.	.
102	39.988167
117	51.6799
132	51.6799
138	45.1033
147	61.179433

----
real_efCODt: Description: Real total COD concentration in effluent
       Type: Real List Variable
       Unit: m/L
       Argument: t
       Standard Deviations: global
       Rel. Stand. Deviat.: 0
       Abs. Stand. Deviat.: 1
       Minimum: 0
       Maximum: 1e+009
       Interpolation Method: linear interpolation
       Sensitivity Analysis: inactive
       Real Data Pairs (16 pairs):

6	180.31435
13	156.9055
19	98.8122
25	150.3289
39	160.55917
.	.
.	.
102	117.4459
117	188.6924
132	109.7732
138	93.3317
147	90.0434

----
real_efNH4:   Description: Real NH4+ concentration in effluent
       Type: Real List Variable
       Unit: mg/L
       Argument: t
       Standard Deviations: global
       Rel. Stand. Deviat.: 0
       Abs. Stand. Deviat.: 1
       Minimum: 0
       Maximum: 1e+009
       Interpolation Method: linear interpolation
       Sensitivity Analysis: inactive
       Real Data Pairs (16 pairs):

6	19.80748
13	22.49324
19	23.6852
25	24.5196
39	23.961
.	.
.	.
102	14.27608
117	12.61316
132	0.68908
138	1.31824
147	3.77496

----
real_efNO: Description: Real NO concentration in effluent
       Type: Real List Variable
       Unit: mg/L
       Argument: t
       Standard Deviations: global
       Rel. Stand. Deviat.: 0
       Abs. Stand. Deviat.: 1
       Minimum: 0
       Maximum: 1e+009

Interpolation Method: linear interpolation
Sensitivity Analysis: inactive
Real Data Pairs (16 pairs):

6	0.11
13	0.01
19	0.1
25	0.18
39	0.21
.	.
.	.
102	2.78
117	4.01
132	4.1
138	4.2
147	11.23

----

real_efTSS: Description: Real TSS concentration in effluent
        Type: Real List Variable
        Unit: mg/L
        Argument: t
        Standard Deviations: global
        Rel. Stand. Deviat.: 0
        Abs. Stand. Deviat.: 1
        Minimum: 0
        Maximum: 1e+009
        Interpolation Method: linear interpolation
        Sensitivity Analysis: inactive
        Real Data Pairs (14 pairs):

6	0.142
13	0.098
19	0.0507
25	0.0585
39	0.074
48	0.0896
55	0.053
67	0.234
83	0.1255
96	0.0575
102	0.0865
117	0.066
132	0.048
138	0.0027

----

real_flocTSS: Description: Real flocculent TSS concentration in reactor (mixed liquor)
        Type: Real List Variable
        Unit: mg/L
        Argument: t
        Standard Deviations: global
        Rel. Stand. Deviat.: 0
        Abs. Stand. Deviat.: 1
        Minimum: 0
        Maximum: 1e+009
        Interpolation Method: linear interpolation
        Sensitivity Analysis: inactive
        Real Data Pairs (14 pairs):

6	93.259717
13	96.830618
19	165.78032
25	281.81262
39	183.47525

48	205.87711
55	21.162815
67	120.77697
83	389.74443
96	1220.3659
102	1365.2237
117	790.6375
132	1227.35
138	1164.6007

----

real_mlTSS: Description: Real TSS concentration in reactor (mixed liquor)

Type: Real List Variable

Unit: mg/L

Argument: t

Standard Deviations: global

Rel. Stand. Deviat.: 0

Abs. Stand. Deviat.: 1

Minimum: 0

Maximum: 1e+009

Interpolation Method: linear interpolation

Sensitivity Analysis: inactive

Real Data Pairs (14 pairs):

6	124
13	856
19	366.7
25	426
39	925.6
48	650
55	475.6
67	498.1
83	892.6
96	2555
102	2651.7
117	1653.3
132	3200
138	3466.7

Ret: Description: Empirical factor for solids retention

Type: Real List Variable

Unit: -

Argument: t

Standard Deviations: global

Rel. Stand. Deviat.: 0

Abs. Stand. Deviat.: 1

Minimum: -1000

Maximum: 1e+009

Interpolation Method: linear interpolation

Sensitivity Analysis: inactive

Real Data Pairs (14 pairs):

0	0
13	0.26434943
19	0.78097126
25	0.85154142
39	0.70695
48	0.68617311
55	0
67	0
83	0.76752775
96	0.96520606
102	0.95326566

```
          117        0.93913821
          132        0.970619
          138        0.99826441
```
----
rho_biofilm: Description: Biofilm density (after Wichern et al. 2008: 40 kg VSS/L)
              Type: Constant Variable
              Unit: mg COD/L
              Value: 58000
              Standard Deviation: 1
              Minimum: 0
              Maximum: 1000000
              Sensitivity Analysis: inactive
              Parameter Estimation: inactive

SOsat: Description: Oxigen at saturation
            Type: Formula Variable
            Unit: mg O2/L
            Expression: 13.89-T*0.3825+T*T*0.007311-T*T*T*6
                             .588e-005
----
start_SAlk: Description: Start condition - SAlk concentration
             Type: Constant Variable
             Unit: mmol HCO3-/L
             Value: 8
             Standard Deviation: 1
             Minimum: 0
             Maximum: 10
             Sensitivity Analysis: inactive
             Parameter Estimation: inactive
----
start_SI: Description: Start condition - SI concentration
            Type: Constant Variable
            Unit: mg COD/L
            Value: 22.56
            Standard Deviation: 1
            Minimum: 0
            Maximum: 100
            Sensitivity Analysis: inactive
            Parameter Estimation: inactive
----
start_SN2:   Description: Start condition - SN2 concentration
             Type: Constant Variable
             Unit: mg N/L
             Value: 0.1
             Standard Deviation: 1
             Minimum: 0
             Maximum: 10
             Sensitivity Analysis: inactive
             Parameter Estimation: inactive
----
start_SNH: Description: Start condition - SNH concentration
             Type: Constant Variable
             Unit: mg N/L
             Value: 26.59
             Standard Deviation: 1
             Minimum: 0
             Maximum: 30
             Sensitivity Analysis: inactive
             Parameter Estimation: inactive
----

start_SNO: Description: Start condition - SNO concentration
        Type: Constant Variable
        Unit: mg N/L
        Value: 0.2670122
        Standard Deviation: 1
        Minimum: 0
        Maximum: 10
        Sensitivity Analysis: inactive
        Parameter Estimation: inactive
----
start_SO: Description: Start condition - SO2 concentration
        Type: Constant Variable
        Unit: mg O2/L
        Value: 0.1
        Standard Deviation: 1
        Minimum: 0
        Maximum: 10
        Sensitivity Analysis: inactive
        Parameter Estimation: inactive
----
start_SS: Description: Start condition - SS concentration
        Type: Constant Variable
        Unit: mg COD/L
        Value: 21.33
        Standard Deviation: 1
        Minimum: 0
        Maximum: 30
        Sensitivity Analysis: inactive
        Parameter Estimation: inactive
----
start_XA: Description: Start condition - XA concentration
        Type: Constant Variable
        Unit: mg COD/L
        Value: 0.0001
        Standard Deviation: 1
        Minimum: 0
        Maximum: 10
        Sensitivity Analysis: inactive
        Parameter Estimation: inactive
----
start_XH: Description: Start condition - XH concentration
        Type: Constant Variable
        Unit: mg COD/L
        Value: 37.1
        Standard Deviation: 1
        Minimum: 0
        Maximum: 40
        Sensitivity Analysis: inactive
        Parameter Estimation: inactive
----
start_XI: Description: Start condition - XI concentration
        Type: Constant Variable
        Unit: mg COD/L
        Value: 42.75
        Standard Deviation: 1
        Minimum: 0
        Maximum: 50
        Sensitivity Analysis: inactive
        Parameter Estimation: inactive
----

start_XMI: Description: Start condition - XMI concentration
     Type: Constant Variable
     Unit: mg TSS/L
     Value: 29.58
     Standard Deviation: 1
     Minimum: 0
     Maximum: 30
     Sensitivity Analysis: inactive
     Parameter Estimation: inactive

----

start_XS: Description: Start condition - XS concentration
     Type: Constant Variable
     Unit: mg COD/L
     Value: 95.13
     Standard Deviation: 1
     Minimum: 0
     Maximum: 100
     Sensitivity Analysis: inactive
     Parameter Estimation: inactive

----

start_XSto: Description: Start condition - XSto concentration
     Type: Constant Variable
     Unit: mg COD/L
     Value: 0.001
     Standard Deviation: 1
     Minimum: 0
     Maximum: 1
     Sensitivity Analysis: inactive
     Parameter Estimation: inactive

----

s_SAlk: Description: Alkalinity as H_2CO_3
     Type: Dyn. Volume State Var.
     Unit: mmol HCO_3-/L
     Relative Accuracy: 1e-006
     Absolute Accuracy: 1e-006

----

s_SI: Description: Soluble inert organic matter
     Type: Dyn. Volume State Var.
     Unit: mg COD/L
     Relative Accuracy: 1e-006
     Absolute Accuracy: 1e-006

----

s_SN2:   Description: Dinitrogen - only product of denitrification
     Type: Dyn. Volume State Var.
     Unit: mg N/L
     Relative Accuracy: 1e-006
     Absolute Accuracy: 1e-006

----

s_SNH: Description: NH4(+) and NH3 nitrogen
     Type: Dyn. Volume State Var.
     Unit: mg N/L
     Relative Accuracy: 1e-006
     Absolute Accuracy: 1e-006

----

s_SNO: Description: Nitrate NO3-N and nitrite NO2-N nitrogen
     Type: Dyn. Volume State Var.
     Unit: mg N/L
     Relative Accuracy: 1e-006
     Absolute Accuracy: 1e-006

----

s_SO: Description: Dissolved oxygen
          Type: Dyn. Volume State Var.
          Unit: mg O2/L
          Relative Accuracy: 1e-006
          Absolute Accuracy: 1e-006
----
s_SS: Description: Readily biodegradable substrate
          Type: Dyn. Volume State Var.
          Unit: mg COD/L
          Relative Accuracy: 1e-006
          Absolute Accuracy: 1e-006
----
s_XA: Description: Autotrophic biomass
          Type: Dyn. Volume State Var.
          Unit: mg COD/L
          Relative Accuracy: 1e-006
          Absolute Accuracy: 1e-006
----
s_XH: Description: Heterotrophic biomass
          Type: Dyn. Volume State Var.
          Unit: mg COD/L
          Relative Accuracy: 1e-006
          Absolute Accuracy: 1e-006
----
s_XI: Description: Particulate inert organic matter
          Type: Dyn. Volume State Var.
          Unit: mg COD/L
          Relative Accuracy: 1e-006
          Absolute Accuracy: 1e-006
----
s_XMI: Description: Particulate mineral fraction
          Type: Dyn. Volume State Var.
          Unit: g/m^3
          Relative Accuracy: 1e-006
          Absolute Accuracy: 1e-006
----
s_XS: Description: Slowly biodegradable substrate
          Type: Dyn. Volume State Var.
          Unit: mg COD/L
          Relative Accuracy: 1e-006
          Absolute Accuracy: 1e-006
----
s_XSto: Description: Organic storage products of s_XH (but not included in their mass)
          Type: Dyn. Volume State Var.
          Unit: mg COD/L
          Relative Accuracy: 1e-006
          Absolute Accuracy: 1e-006

T: Description: Temperature
          Type: Real List Variable
          Unit: degree Celsius
          Argument: t
          Standard Deviations: global
          Rel. Stand. Deviat.:   0
          Abs. Stand. Deviat.:   1
          Minimum: 0
          Maximum: 1e+009
          Interpolation Method: linear interpolation
          Sensitivity Analysis: inactive
          Real Data Pairs (6 pairs):

```
        13          26.7
        25          27.5
        39          27.8
        48          27.6
        132         30.8
        138         30.5
```
----
t: Description: time
          Type: Program Variable
          Unit: day
          Reference to: Time
----
th_att_vel: Description: Attachment velocity of biofilm
          Type: Program Variable
          Unit: m/d
          Reference to: Attachment Velocity of Biofilm
----
th_biofilm: Description: Biofilm thickness
          Type: Program Variable
          Unit: mm
          Reference to: Biofilm Thickness
----
th_biofilm_in: Description: Initial biofilm thickness
          Type: Constant Variable
          Unit: m
          Value: 0.0002
          Standard Deviation: 1
          Minimum: 0
          Maximum: 10
          Sensitivity Analysis: inactive
          Parameter Estimation: inactive
----
th_biofilm_real:
          Description: Real biofilm thickness
          Type: Real List Variable
          Unit: m
          Argument: t
          Standard Deviations: global
          Rel. Stand. Deviat.: 0
          Abs. Stand. Deviat.: 1
          Minimum: 0
          Maximum: 1e+009
          Interpolation Method: smoothing
          Smoothing Width: 2
          Sensitivity Analysis: inactive
          Real Data Pairs (14 pairs):
            6   0.000213
            13   0.000331
            19   0.00033
            25   0.000271
            39   0.000354
            48   0.000461
            55   0.000756
            67   0.000494
            83   0.000572
            96   0.000608
            102   0.000498
            117   0.000646
            132   0.000651
            138   0.000945
```

-------------------------------------------------------------------------
th_biofilm_virtual:
        Description:      Virtual biofilm thickness
        Type:        Real List Variable
        Unit:        m
        Argument:       t
        Standard Deviations:  global
        Rel. Stand. Deviat.:  0
        Abs. Stand. Deviat.:  1
        Minimum:       0
        Maximum:       1e+009
        Interpolation Method: smoothing
        Smoothing Width:    2
        Sensitivity Analysis: inactive
        Real Data Pairs (14 pairs):

| 6 | 0.000165 |
| 13 | 0.000481 |
| 19 | 0.000309 |
| 25 | 0.000277 |
| 39 | 0.000478 |
| 48 | 0.000403 |
| 55 | 0.000405 |
| 67 | 0.000381 |
| 83 | 0.00042 |
| 96 | 0.000586 |
| 102 | 0.00058 |
| 117 | 0.000505 |
| 132 | 0.000668 |
| 138 | 0.000703 |

-------------------------------------------------------------------------
th_BLR:     Description: Thickness of the boundary layer resistance - 100 micrometers (Horn & Morgenroth, 2006; Lee et al., 2009)
        Type:        Constant Variable
        Unit:        m
        Value:       0.0001
        Standard Deviation:   0.0001
        Minimum:       0
        Maximum:       0.5
        Sensitivity Analysis: active
        Parameter Estimation: inactive
-------------------------------------------------------------------------
th_det_vel:  Description:    Detachment velocity of biofilm
        Type:        Program Variable
        Unit:        m/d
        Reference to:     Detachment Velocity of Biofilm
-------------------------------------------------------------------------
u_F:       Description:      Advective velocity in biofilm
        Type:        Program Variable
        Unit:        m/d
        Reference to:     Growth Velocity of Biofilm
-------------------------------------------------------------------------
V:        Description:     Reactor volume
        Type:        Program Variable
        Unit:        m^3
        Reference to:     Reactor Volume
-------------------------------------------------------------------------
V_biofilm:   Description: Biofilm volume
        Type:        Formula Variable
        Unit:
        Expression:      V-V_bulk

```
------------------------------------------------------------------------
V_bulk:      Description: Bulk volume
             Type:           Program Variable
             Unit:
             Reference to:     Bulk Volume
------------------------------------------------------------------------
v_e:         Description:       Volumetric exchange ratio
             Type:           Formula Variable
             Unit:           -
             Expression:     82/115
------------------------------------------------------------------------
water_fraction:Description: Water fraction within the biofilm
             Type:           Program Variable
             Unit: -
             Reference to:     Water Fraction
------------------------------------------------------------------------
water_fraction_probe:
             Description:     Water fraction probe
             Type:           Probe Variable
             Unit:
             Variable:        water_fraction
             Compartment:     b2_biofilm
             Zone:           Biofilm Matrix
             Space:          0
------------------------------------------------------------------------
Y_A:         Description:       Yield coefficient for autotrophs
             Type:           Constant Variable
             Unit:           mg COD/mg COD
             Value:          0.24
             Standard Deviation:  1
             Minimum:        0
             Maximum:        2
             Sensitivity Analysis: inactive
             Parameter Estimation: inactive
------------------------------------------------------------------------
Y_H_aer:     Description:       Yield coefficient for heterotrophs in aerobic growth
             Type:           Constant Variable
             Unit:           mg COD/mg COD
             Value:          0.63
             Standard Deviation:  1
             Minimum:        0
             Maximum:        10
             Sensitivity Analysis: inactive
             Parameter Estimation: inactive
------------------------------------------------------------------------
Y_H_ano:     Description:       Yield coefficient for heterotrophs in anoxic growth (Koch 0.65)
             Type:           Constant Variable
             Unit:           mg COD/mg COD
             Value:          0.54
             Standard Deviation:  1
             Minimum:        0
             Maximum:        1
             Sensitivity Analysis: inactive
             Parameter Estimation: inactive
------------------------------------------------------------------------
Y_Sto_aer:   Description:       Yield coefficient for STO in aerobic growth (0.8)
             Type:           Constant Variable
             Unit:           mg COD/mg COD
             Value:          0.8
             Standard Deviation:  1
```

Minimum: 0
Maximum: 1
Sensitivity Analysis: inactive
Parameter Estimation: inactive

Y_Sto_ano: Description: Yield coefficient for Sto in anoxic growth (Koch 0.7)
              Type: Constant Variable
              Unit: mg COD/mg COD
              Value: 0.8
              Standard Deviation: 1
              Minimum: 0
              Maximum: 2
              Sensitivity Analysis: inactive
              Parameter Estimation: inactive

----

z: Description: Space coordinate z
              Type: Program Variable
              Unit: mm
              Reference to: Space Coordinate Z

ZoneIndex: Description: ZoneIndex = 0 for bulk phase
              Type: Program Variable
              Unit: unit.
              Reference to: Zone Index
****

****
Processes
****

P01_hydrolysis:Description: Hydrolysis
              Type: Dynamic Process
              Rate: P01_hydrolisis
              Stoichiometry:
               Variable: Stoichiometric Coefficient
               s_SNH : -(1-f_SI)*i_N_SS-f_SI*i_N_SI+i_N_XS
               s_SI : f_SI
               s_SAlk : (i_N_XS-i_N_SI*f_SI-(1-f_SI)*i_N_SS)/14
               s_SS : 1-f_SI
               s_XS : -1

P02_aerobic_sto:
              Description: Aerobic storage of COD
              Type: Dynamic Process
              Rate: P02_aerobic_sto
              Stoichiometry:
               Variable: Stoichiometric Coefficient
               s_SO : Y_Sto_aer-1
               s_SS : -1
               s_SNH : i_N_SS
               s_SAlk : i_N_SS/14
               s_XSto : Y_Sto_aer

P03_anoxic_sto:Description: Anoxic storage
              Type: Dynamic Process
              Rate: P03_anoxic_sto
              Stoichiometry:
               Variable: Stoichiometric Coefficient
               s_SS : -1
               s_SNH : i_N_SS
               s_SNO : (Y_Sto_ano-1)/(40/14)

s_SN2 : -(Y_Sto_ano-1)/(40/14)
s_SAlk : (i_N_SS-(Y_Sto_ano-1)/(40/14))/14
s_XSto : Y_Sto_ano

P04_aerobic_growth:

    Description: Aerobic growth
    Type: Dynamic Process
    Rate: P04_aerobic_growth
    Stoichiometry:
    Variable: Stoichiometric Coefficient
    s_SO : 1-1/Y_H_aer
    s_SNH : -i_N_BM
    s_SAlk : -i_N_BM/14
    s_XH : 1
    s_XSto : -1/Y_H_aer

P05_anoxic_growth:

    Description: Anoxic growth
    Type: Dynamic Process
    Rate: P05_anoxic_growth
    Stoichiometry:
    Variable : Stoichiometric Coefficient
    s_SNH : -i_N_BM
    s_SNO : (1-(1/Y_H_ano))/(40/14)
    s_SN2 : -(1-(1/Y_H_ano))/(40/14)
    s_SAlk : (-i_N_BM-(1-(1/Y_H_ano))/(40/14))/14
    s_XH : 1
    s_XSto : -1/Y_H_ano

P06_aerobic_end_het:

    Description: Aerobic endogenous respiration of heterotrophs
    Type: Dynamic Process
    Rate: P06_aerobic_end_het
    Stoichiometry:
    Variable: Stoichiometric Coefficient
    s_SNH : -1*f_XI*i_N_XI+i_N_BM
    s_SAlk : (-1*f_XI*i_N_XI+i_N_BM)/14
    s_XI : f_XI
    s_XH : -1
    s_SO : -1*(1-f_XI)
    s_XMI : f_iSS_BM_prod*f_XI*i_VSS_BM*(i_TSS_VSS_BM-1)

P07_anoxic_end_het:

    Description: Anoxic endogenous respiration of heterotrophs
    Type: Dynamic Process
    Rate: P07_anoxic_end_het
    Stoichiometry:
    Variable: Stoichiometric Coefficient
    s_SNO : (f_XI-1)/(40/14)
    s_SNH : -1*f_XI*i_N_XI+i_N_BM
    s_SAlk : (-1*f_XI*i_N_XI+i_N_BM)/14
    s_XI : f_XI
    s_XH : -1
    s_SN2 : -(f_XI-1)/(40/14)
    s_XMI : f_iSS_BM_prod*f_XI*i_VSS_BM*(i_TSS_VSS_BM-1)

P08_aerobic_resp_sto:

    Description: Aerobic respiration of XSTO
    Type: Dynamic Process
    Rate: P08_aerobic_resp_sto

          Stoichiometry:
           Variable: Stoichiometric Coefficient
           s_XSto : -1
           s_SO : -1

P09_anoxic_resp_sto:
          Description: Anoxic endogenous respiration of XSto
          Type: Dynamic Process
          Rate: P09_anoxic_resp_sto
          Stoichiometry:
           Variable: Stoichiometric Coefficient
           s_SNO : -14/40
           s_SAlk : 1/40
           s_XSto : -1
           s_SN2 : 14/40

P10_nitrification: Description: Nitrification
          Type: Dynamic Process
          Rate: P10_nitrification
          Stoichiometry:
           Variable : Stoichiometric Coefficient
           s_SO : -64/14*(1/Y_A)+1
           s_SNH : -1/Y_A-i_N_BM
           s_SNO : 1/Y_A
           s_SAlk : (-1/Y_A-i_N_BM-1/Y_A)/14
           s_XA : 1

P11_aerobic_end_aut:
          Description: Aerobic endogenous respiration of autotrophs
          Type: Dynamic Process
          Rate: P11_aerobic_end_aut
          Stoichiometry:
           Variable: Stoichiometric Coefficient
           s_SO : -1*(1-f_XI)
           s_SNH : -1*f_XI*i_N_XI+i_N_BM
           s_SAlk : (-1*f_XI*i_N_XI+i_N_BM)/14
           s_XI : f_XI
           s_XA : -1
           s_XMI : f_iSS_BM_prod*f_XI*i_VSS_BM*(i_TSS_VSS_BM-1)

P12_anoxic_end_aut: Description: Aerobic endogenous respiration of autotrophs
          Type: Dynamic Process
          Rate: P12_anoxic_end_aut
          Stoichiometry:
           Variable: Stoichiometric Coefficient
           s_SNO : (f_XI-1)/(40/14)
           s_SNH : -1*f_XI*i_N_XI+i_N_BM
           s_SAlk : (-1*f_XI*i_N_XI+i_N_BM-(f_XI-1)/(40/14))/14
           s_XI : f_XI
           s_XA : -1
           s_SN2 : -(f_XI-1)/(40/14)
           s_XMI : f_iSS_BM_prod*f_XI*i_VSS_BM*(i_TSS_VSS_BM-1)

P13_aeration: Description: Aeration in compartments a1_sbr and a2_biofilm (Bulk phase)
          Type: Dynamic Process
          Rate: P13_aeration
          Stoichiometry:
           Variable: Stoichiometric Coefficient
           s_SO : 1
****

```
**********************************************************************
Compartments
**********************************************************************
```

a_afluente: Description:
        Type: Mixed Reactor Compartment
        Compartment Index: 0
        Active Variables: s_SAlk, s_SI, s_SN2, s_SNH, s_SNO,
                        s_SO, s_SS, s_XA, s_XH, s_XI, s_XS,
                        s_XSto, s_XMI
        Active Processes:
        Initial Conditions:
         Variable(Zone) : Initial Condition
         s_SAlk(Bulk Volume) : start_SAlk
         s_SI(Bulk Volume) : start_SI
         s_SN2(Bulk Volume) : start_SN2
         s_SNH(Bulk Volume) : start_SNH
         s_SNO(Bulk Volume) : start_SNO
         s_SO(Bulk Volume) : start_SO
         s_SS(Bulk Volume) : start_SS
         s_XA(Bulk Volume) : start_XA
         s_XH(Bulk Volume) : start_XH
         s_XI(Bulk Volume) : start_XI
         s_XS(Bulk Volume) : start_XS
         s_XSto(Bulk Volume) : start_XSto
         s_XMI(Bulk Volume) : start_XMI
        Inflow: v_e*on_fill*q_fill
        Loadings:
         Variable: Loading
         s_SI : v_e*on_fill*q_fill*in_SI
         s_SAlk : v_e*on_fill*q_fill*in_SAlk
         s_SNH : v_e*on_fill*q_fill*in_SNH
         s_SS : v_e*on_fill*q_fill*in_SS
         s_XA : v_e*on_fill*q_fill*in_XA
         s_XH : v_e*on_fill*q_fill*in_XH
         s_XI : v_e*on_fill*q_fill*in_XI
         s_XS : v_e*on_fill*q_fill*in_XS
         s_XMI : v_e*on_fill*q_fill*in_XMI
        Volume: 1e-005
        Accuracies:
         Rel. Acc. Q: 0.001
         Abs. Acc. Q: 0.001
         Rel. Acc. V: 0.001
         Abs. Acc. V: 0.001

----

b1_sbr: Description:
        Type: Mixed Reactor Compartment
        Compartment Index: 0
        Active Variables: s_SAlk, s_SI, s_SN2, s_SNH, s_SNO,
                        s_SO, s_SS, s_XA, s_XH, s_XI, s_XS,
                        s_XSto, s_XMI
        Active Processes: P13_aeration, P01_hydrolysis, P02_a
                        erobic_sto, P03_anoxic_sto, P04_aer
                        obic_growth, P05_anoxic_growth, P06
                        _aerobic_end_het, P07_anoxic_end_he
                        t, P08_aerobic_resp_sto, P09_anoxic
                        _resp_sto, P10_nitrification, P11_a
                        erobic_end_aut, P12_anoxic_end_aut
        Initial Conditions:
         Variable(Zone) : Initial Condition
         s_SAlk(Bulk Volume) : start_SAlk

```
                s_SI(Bulk Volume) : start_SI
                s_SN2(Bulk Volume) : start_SN2
                s_SNH(Bulk Volume) : start_SNH
                s_SNO(Bulk Volume) : start_SNO
                s_SO(Bulk Volume) : start_SO
                s_SS(Bulk Volume) : start_SS
                s_XA(Bulk Volume) : start_XA
                s_XH(Bulk Volume) : start_XH
                s_XI(Bulk Volume) : start_XI
                s_XMI(Bulk Volume) : start_XMI
                s_XS(Bulk Volume) : start_XS
                s_XSto(Bulk Volume) : start_XSto
           Inflow:           0
           Loadings:
           Outflow:          v_e*on_empty*q_empty
           Accuracies:
            Rel. Acc. Q:     0.001
            Abs. Acc. Q:     0.001
            Rel. Acc. V:     0.001
            Abs. Acc. V:     0.001
---------------------------------------------------------------------
b2_biofilm:   Description:       Biofilm reactor
              Type:              Biofilm Reactor Compartment
              Compartment Index:   0
              Active Variables:    s_SAlk, s_SI, s_SN2, s_SNH, s_SNO,
                        s_SO, s_SS, s_XA, s_XH, s_XI, s_XS,
                         s_XSto, s_XMI
              Active Processes:    P01_hydrolysis, P02_aerobic_sto, P0
                        3_anoxic_sto, P04_aerobic_growth, P
                        05_anoxic_growth, P06_aerobic_end_h
                        et, P07_anoxic_end_het, P08_aerobic
                        _resp_sto, P09_anoxic_resp_sto, P10
                        _nitrification, P11_aerobic_end_aut
                        , P12_anoxic_end_aut
              Initial Conditions:
               Variable(Zone) : Initial Condition
               s_SAlk(Bulk Volume) : start_SAlk
               s_SI(Bulk Volume) : start_SI
               s_SN2(Bulk Volume) : start_SN2
               s_SNH(Bulk Volume) : start_SNH
               s_SNO(Bulk Volume) : start_SNO
               s_SO(Bulk Volume) : start_SO
               s_SS(Bulk Volume) : start_SS
               s_XA(Bulk Volume) : start_XA
               s_XH(Bulk Volume) : start_XH
               s_XI(Bulk Volume) : start_XI
               s_XS(Bulk Volume) : start_XS
               s_XSto(Bulk Volume) : start_XSto
               s_XMI(Bulk Volume) : start_XMI
               s_SAlk(Pore Water) : start_SAlk
               s_SI(Pore Water) : start_SI
               s_SN2(Pore Water) : start_SN2
               s_SNH(Pore Water) : start_SNH
               s_SNO(Pore Water) : start_SNO
               s_SO(Pore Water) : start_SO
               s_SS(Pore Water) : start_SS
               s_XA(Biofilm Matrix) : ic_XA
               s_XH(Biofilm Matrix) : ic_XH
               s_XI(Biofilm Matrix) : ic_XI
               s_XS(Biofilm Matrix) : ic_XS
```

s_XSto(Biofilm Matrix) : ic_XSto
s_XMI(Biofilm Matrix) : ic_XMI
th_biofilm(Biofilm Matrix) : th_biofilm_in
Inflow: 0
Loadings:
Particulate Variables:
 s_XA:
   Density: rho_biofilm
   Surf. Att. Coeff.:k_att
   Surf. Det. Coeff.:k_det
   Vol. Att. Coeff.: 0
   Vol. Det. Coeff.: 0
   Layer Resist.:   0
   Pore Diffusivity: 0
   Matrix Diffusivity:
             0
 s_XH:
   Density: rho_biofilm
   Surf. Att. Coeff.:k_att
   Surf. Det. Coeff.:k_det
   Vol. Att. Coeff.: 0
   Vol. Det. Coeff.: 0
   Layer Resist.:   0
   Pore Diffusivity: 0
   Matrix Diffusivity:
             0
 s_XI:
   Density: rho_biofilm
   Surf. Att. Coeff.:k_att
   Surf. Det. Coeff.:k_det
   Vol. Att. Coeff.: 0
   Vol. Det. Coeff.: 0
   Layer Resist.:   0
   Pore Diffusivity: 0
   Matrix Diffusivity:
             0
 s_XS:
   Density: rho_biofilm
   Surf. Att. Coeff.:k_att
   Surf. Det. Coeff.:k_det
   Vol. Att. Coeff.: 0
   Vol. Det. Coeff.: 0
   Layer Resist.:   0
   Pore Diffusivity: 0
   Matrix Diffusivity:
             0
 s_XMI:
   Density: rho_biofilm
   Surf. Att. Coeff.:k_att
   Surf. Det. Coeff.:k_det
   Vol. Att. Coeff.: 0
   Vol. Det. Coeff.: 0
   Layer Resist.:   0
   Pore Diffusivity: 0
   Matrix Diffusivity:
             0
 s_XSto:
   Density: rho_biofilm
   Surf. Att. Coeff.:k_att
   Surf. Det. Coeff.:k_det

```
                    Vol. Att. Coeff.: 0
                    Vol. Det. Coeff.: 0
                    Layer Resist.:   0
                    Pore Diffusivity: 0
                    Matrix Diffusivity:
                              0
              Dissolved Variables:
               s_SAlk:
                 Layer Resist.:    th_BLR/DifLiq_Alk
                 Pore Diffusivity: DifLiq_Alk
               s_SI:
                 Layer Resist.:    th_BLR/DifLiq_VFA
                 Pore Diffusivity: DifLiq_VFA
               s_SN2:
                 Layer Resist.:    th_BLR/DifLiq_N2
                 Pore Diffusivity: DifLiq_N2
               s_SNH:
                 Layer Resist.:    th_BLR/DifLiq_NH4
                 Pore Diffusivity: DifLiq_NH4
               s_SNO:
                 Layer Resist.:    th_BLR/DifLiq_NO
                 Pore Diffusivity: DifLiq_NO
               s_SS:
                 Layer Resist.:    DifLiq_NO/DifLiq_VFA
                 Pore Diffusivity: DifLiq_VFA
               s_SO:
                 Layer Resist.:    th_BLR/DifLiq_SO2
                 Pore Diffusivity: DifLiq_SO2
              Reactor Type:        confined
              Reactor Volume:      0.033
              Pore Volume:         liquid phase only
              Biofilm Matrix:      rigid
              Detach. Velocity:    abs(u_F)*(th_biofilm/th_biofilm_virtual)^10
              Film Surface:        A_film
              Rate of epsFl:       0
              Num. of Grid Pts:    10
              Accuracies:
               Rel. Acc. Q:        0.001
               Abs. Acc. Q:        0.001
               Rel. Acc. V:        0.001
               Abs. Acc. V:        0.001
               Rel. Acc. Z:        0.001
               Abs. Acc. Z:        1e-009
               Rel. Acc. EPS:      0.001
               Abs. Acc. EPS:      1e-005
---------------------------------------------------------------------------
c_effluent:   Description:
              Type:           Mixed Reactor Compartment
              Compartment Index:   0
              Active Variables:    s_SAlk, s_SI, s_SN2, s_SNH, s_SNO,
                          s_SO, s_SS, s_XA, s_XH, s_XI, s_XS,
                          s_XSto, s_XMI
              Active Processes:
              Initial Conditions:
              Inflow:           0
              Loadings:
              Volume:           1e-005
              Accuracies:
               Rel. Acc. Q:       0.001
               Abs. Acc. Q:       0.001
```

```
          Rel. Acc. V:      0.001
          Abs. Acc. V:      0.001
**********************************************************************
```

```
**********************************************************************
Links
**********************************************************************
```

a_b: Type: Advective Link
          Link Index: 0
          Compartment In: a_afluente
          Connection In: Outflow
          Compartment Out: b1_sbr
          Connection Out: Inflow
          Bifurcations:
----

b_c: Type: Advective Link
          Link Index: 0
          Compartment In: b1_sbr
          Connection In: Outflow
          Compartment Out: c_effluent
          Connection Out: Inflow
          Bifurcations:
           Retention:
            Description:
            Compartment Out: b1_sbr
            Connection Out: Inflow
            Water Flow: 0
            Mass Loadings:
             Variable: Loading
             s_XA : Ret*on_empty*s_XA*v_e*q_empty
             s_XH : Ret*on_empty*s_XH*v_e*q_empty
             s_XI : Ret*on_empty*s_XI*v_e*q_empty
             s_XS : Ret*on_empty*s_XS*v_e*q_empty
             s_XSto : Ret*on_empty*s_XSto*v_e*q_empty
             s_XMI : Ret*on_empty*s_XMI*v_e*q_empty
----

c_out: Type: Advective Link
          Link Index: 0
          Compartment In: c_effluent
          Connection In: Outflow
          Compartment Out:
          Bifurcations:

Mixture: Type: Diffusive Link
          Link Index: 0
          Compartment 1:   b1_sbr
          Connection 1:   Bulk Volume
          Compartment 2:   b2_biofilm
          Connection 2:   Bulk Volume
          Exchange Coefficients:
           Variable: Exch. Coeff., Conv. Fact. 1
           s_SAlk : 1e+006, 1
           s_SI : 1e+006, 1
           s_SN2 : 1e+006, 1
           s_SNH : 1e+006, 1
           s_SNO : 1e+006, 1
           s_SO : 1e+006, 1
           s_SS : 1e+006, 1
           s_XA : 1e+006, 1
           s_XH : 1e+006, 1
```

s_XI : 1e+006, 1
s_XS : 1e+006, 1
s_XSto : 1e+006, 1
s_XMI : 1e+006, 1
****

****
Definitions of Calculations
****

Teste: Description:
            Calculation Number: 0
            Initial Time: 0
            Initial State: given, made consistent
            Step Size: 0.001
            Num. Steps: 147000
            Status: active for simulation
                                active for sensitivity analysis
----
Teste_rapido: Description:
            Calculation Number: 1
            Initial Time: 0
            Initial State: given, made consistent
            Step Size: 0.1
            Num. Steps: 230
            Status: active for simulation
                                inactive for sensitivity analysis
****

****
Calculation Parameters
****

Numerical Parameters: Maximum Int. Step Size: 1
                        Maximum Integrat. Order: 5
                        Number of Codiagonals: 1000
                        Maximum Number of Steps: 1000

                        Fit Method: secant
                        Max. Number of Iterat.: 100
****

APPENDIX B – COD influent fractionation (code)

- Matlab code for data processing and calculation of the f_A, f_B, and f_S

```matlab
% COD_filt Interpolation code
% COD_total and COD_filt effluent Database-based

c_COD_t=[]; % declaring COD_total
c_COD_ef_f=[]; % declaring COD_filt

M=xlsread('Fractionation','Sheet2','C3:Q139');

c_COD_t=[c_COD_t;M(:,3)];
c_COD_ef_f=[c_COD_ef_f;M(:,13)];

% Deleting NaN Data
c_COD_ef_f(isnan(c_COD_t))=[];
c_COD_t(isnan(c_COD_t))=[];
c_COD_t(isnan(c_COD_ef_f))=[];
c_COD_ef_f(isnan(c_COD_ef_f))=[];

int_COD_f=c_COD_ef_f;
int_COD=c_COD_t;

% Ascending arithmetic order based on COD_t
[int_COD, idx]=sort(int_COD);
int_COD_f=int_COD_f(idx);

% Check-plot
figure
hold on
plot(int_COD,int_COD_f,'Marker','o','LineStyle','None')
xlabel('Total COD')
ylabel('Dissolved COD')
title('Without Moving Average Filter')
set(gca,'fontsize', 18);
ax = gca;
ax.XGrid = 'off';
ax.YGrid = 'on';
ax.GridLineStyle = '-.';
figure
hold on;

% Moving average filter - 30 samples
A=movmean(int_COD_f,30);

% Check-plot
plot(int_COD,A,'Marker','o')
xlabel('Total COD')
ylabel('Dissolved COD')
title('Applying Moving Average Filter')
set(gca,'fontsize', 18);
ax = gca;
ax.XGrid = 'off';
ax.YGrid = 'on';
ax.GridLineStyle = '-.';
figure
```

```matlab
hold on
% Removing repeated COD_t data
int_M=[int_COD,A];
for n=1:(length(int_M)-1)
    if int_M(n,1)==int_M(n+1,1)
        int_M(n,2)=mean([int_M(n,2),int_M(n+1,2)]);
    end
end

[~, rows] = unique(int_M(:,1));
int_M_d = int_M(rows,:);

% Check-plot
plot(int_M_d(:,1),int_M_d(:,2),'Marker','o')
xlabel('Total COD')
ylabel('Dissolved COD')
title('Moving Average Filter without repetitions')
set(gca,'fontsize', 18);
ax = gca;
ax.XGrid = 'off';
ax.YGrid = 'on';
ax.GridLineStyle = '-.';
figure
hold on
% BOD_total Interpolation code
% COD_total and BOD_total Database-based

c_COD_t=[]; % declaring COD_total
c_BOD_t=[]; % declaring BOD_total

M=xlsread('Fractionation','Sheet2','C3:Q139');

c_COD_t=[c_COD_t;M(:,3)];
c_BOD_t=[c_BOD_t;M(:,5)];

% Deleting NaN Data
c_BOD_t(isnan(c_COD_t))=[];
c_COD_t(isnan(c_COD_t))=[];
c_COD_t(isnan(c_BOD_t))=[];
c_BOD_t(isnan(c_BOD_t))=[];

int_BOD=c_BOD_t;
int_COD=c_COD_t;

% Ascending arithmetic order based on COD_t
[int_COD, idx]=sort(int_COD);
int_BOD=int_BOD(idx);

% Check-plot
plot(int_COD,int_BOD,'Marker','o','LineStyle','None')
xlabel('COD')
ylabel('BOD')
title('Without Moving Average Filter')
set(gca,'fontsize', 18);
ax = gca;
ax.XGrid = 'off';
ax.YGrid = 'on';
ax.GridLineStyle = '-.';
figure
hold on;
```

```matlab
% Moving average filter - 10 samples
B=movmean(int_BOD,10);

% Check-plot
plot(int_COD,B,'Marker','o')
xlabel('Total COD')
ylabel('Total BOD')
title('Applying Moving Average Filter')
set(gca,'fontsize', 18);
ax = gca;
ax.XGrid = 'off';
ax.YGrid = 'on';
ax.GridLineStyle = '-.';
figure
hold on

% Removing repeated COD_t data
int_N=[int_COD,B];
for n=1:(length(int_N)-1)
    if int_N(n,1)==int_N(n+1,1)
        int_N(n,2)=mean([int_N(n,2),int_N(n+1,2)]);
    end
end

[~, rows] = unique(int_N(:,1));
int_N_d = int_N(rows,:);

% Check-plot
plot(int_N_d(:,1),int_N_d(:,2),'Marker','o')
xlabel('Total COD')
ylabel('Total BOD')
title('Moving Average Filter without repetitions')
set(gca,'fontsize', 18);
ax = gca;
ax.XGrid = 'off';
ax.YGrid = 'on';
ax.GridLineStyle = '-.';

% Parameterized Method
% COD and BOD data interpolation

M=xlsread('Fractionation','Sheet2','C3:Q139');
M(M==0)=NaN;

% Clean variables
clear VSS_TSS S_S X_S S_I X_I c_BOD_t c_BOD_bd ak COD_BOD

% Vectors with required data
c_COD_t=M(:,3);
c_BOD_t=M(:,5);
BOD_COD=M(:,10);
Temp=M(:,11);
c_COD_ef=M(:,12);
c_COD_ef_f=M(:,13);
c_FSS=M(:,14);
c_VSS=M(:,15);
COD_BOD=BOD_COD(:).^(-1);

% Linear interpolation c_COD_ef_f
for n=1:length(c_COD_t)
```

```matlab
    if isnan(c_COD_ef_f(n))>0
            c_COD_ef_f_int(n)=interp1(int_M_d(:,1),int_M_d(:,2),c_COD_t(n),'linear','extrap');
    else
        c_COD_ef_f_int(n)=c_COD_ef_f(n);
    end
end
c_COD_ef_f_int=c_COD_ef_f_int';

% Linear interpolation c_BOD_t
for n=1:length(c_COD_t)
    if isnan(c_BOD_t(n))>0
        c_BOD_t_int(n)=interp1(int_N_d(:,1),int_N_d(:,2),c_COD_t(n),'linear','extrap');
    else
        c_BOD_t_int(n)=c_BOD_t(n);
    end
end
c_BOD_t_int=c_BOD_t_int';

% Removing NaN
% BOD_t_int
c_COD_t(isnan(c_BOD_t_int))=[];
c_BOD_t_int(isnan(c_BOD_t_int))=[];
BOD_COD(isnan(c_BOD_t_int))=[];
Temp(isnan(c_BOD_t_int))=[];
c_COD_ef(isnan(c_BOD_t_int))=[];
c_COD_ef_f(isnan(c_BOD_t_int))=[];
c_FSS(isnan(c_BOD_t_int))=[];
c_VSS(isnan(c_BOD_t_int))=[];
COD_BOD(isnan(c_BOD_t_int))=[];

% COD_t
c_COD_t(isnan(c_COD_t))=[];
c_BOD_t_int(isnan(c_COD_t))=[];
BOD_COD(isnan(c_COD_t))=[];
Temp(isnan(c_COD_t))=[];
c_COD_ef(isnan(c_COD_t))=[];
c_COD_ef_f(isnan(c_COD_t))=[];
c_FSS(isnan(c_COD_t))=[];
c_VSS(isnan(c_COD_t))=[];
COD_BOD(isnan(c_COD_t))=[];

% VSS
c_COD_t(isnan(c_VSS))=[];
c_BOD_t_int(isnan(c_VSS))=[];
BOD_COD(isnan(c_VSS))=[];
Temp(isnan(c_VSS))=[];
c_COD_ef(isnan(c_VSS))=[];
c_COD_ef_f(isnan(c_VSS))=[];
c_FSS(isnan(c_VSS))=[];
c_VSS(isnan(c_VSS))=[];
COD_BOD(isnan(c_VSS))=[];

% COD_ef_f_int
c_COD_t(isnan(c_COD_ef_f_int))=[];
c_BOD_t_int(isnan(c_COD_ef_f_int))=[];
BOD_COD(isnan(c_COD_ef_f_int))=[];
Temp(isnan(c_COD_ef_f_int))=[];
c_COD_ef(isnan(c_COD_ef_f_int))=[];
c_COD_ef_f(isnan(c_COD_ef_f_int))=[];
c_FSS(isnan(c_COD_ef_f_int))=[];
```

```matlab
c_VSS(isnan(c_COD_ef_f_int))=[];
COD_BOD(isnan(c_COD_ef_f_int))=[];

% Fractionation
% Optimization using fgoalattain: BOD_t = (S_S + X_S) /1,684 (fun_BSB)

close all;

for j=1:length(c_COD_t)

    % Initial parameters as random numbers of the range
    f_A_in = (0.35-0.2)*rand(1,1)+0.2;
    f_S_in = 0.2*rand(1,1);
    f_B_in = (0.4-0.1)*rand(1,1)+0.1;
    x0 = [f_A_in,f_S_in,f_B_in]; % Initial Vector

    lb = [0.2,0,0.1];
    ub = [0.35,0.2,0.4];

    f_COD = 0.15;

    COD = c_COD_t(j);
    TS = (c_VSS(j)+c_FSS(j));
    ico = 1.6;

    fun_BOD = @(x)0.594*(COD*(1-x(2))-TS*ico*x(1)*(1-x(3)));

    Aeq = [0,COD,0]; % Restriction S_I=0.9*c_COD_ef_f
    beq = 0.9*c_COD_ef_f_int(j);

    [x,fval,attainfactor,exitflag] = fgoalattain(fun_BOD,x0,c_BOD_t(j),0,[],[],Aeq,beq,lb,ub);
    ak(j,1:3) = x;

    % Calculations

    X_COD(j,1)=TS*ico*(1-ak(j,3));
    S_COD(j,1)=c_COD_t(j,1)-X_COD(j,1);
    S_I(j,1)=c_COD_t(j,1)*ak(j,2);
    S_S_f(j,1)=S_COD(j,1)-S_I(j,1);
    X_I(j,1)=X_COD(j,1)*ak(j,1);
    X_S(j,1)=X_COD(j,1)-X_I(j,1);
    S_S(j,1)=(X_S(j,1)+S_S_f(j,1))*f_COD;
    S_XS(j,1)=S_S_f(j,1)-S_S(j,1);

    if (S_XS(j,1)>0)
        S_XS1(j,1)=S_XS(j,1);
    else
        S_XS1(j,1)=NaN;
    end

    c_COD_deg(j,1)=X_S(j,1)+S_S(j,1)+S_XS1(j,1);
    c_BOD_deg(j,1)=c_COD_deg(j,1)/1.684;

    anteil_X_I(j,1)=X_I(j,1)/COD*100;
    anteil_X_S(j,1)=X_S(j,1)/COD*100;
    anteil_S_I(j,1)=S_I(j,1)/COD*100;
    anteil_S_S(j,1)=S_S(j,1)/COD*100;
    anteil_S_XS(j,1)=S_XS(j,1)/COD*100;
end
```

```matlab
mean(ak)
std(ak)

% Plotting results
figure;
boxplot(ak,'labels',{'$$f_{A}$$','$$f_{S}$$','$$f_{B}$$'});
bp = gca;
set(gca,'fontsize', 26);
bp.Xaxis.TickLabelInterpreter = 'latex';
title('Fractionation coefficients');
set(gca,'fontsize', 26);
set(gca,'FontName','Times New Roman');
yticks(0.0:0.1:0.6);
set(gca,'yticklabel',num2str(get(gca,'ytick')','%.1f'))
ax = gca;
ax.Xgrid = 'off';
ax.Ygrid = 'on';
ax.GridLineStyle = '-.';
ax.GridColor = [0.1 0.2 0.9];

fractions=[anteil_X_I anteil_X_S anteil_S_XS anteil_S_S anteil_S_I]

figure;
boxplot(fractions,'labels',{'$$X_{I}$$','$$X_{S}$$','$$S_{XS}$$','$$S_{S}$$','$$S_{I}$$'});
bp = gca;
set(gca,'fontsize', 26);
bp.Xaxis.TickLabelInterpreter = 'latex';
title('Fractions');
set(gca,'fontsize', 26);
set(gca,'FontName','Times New Roman');
yticks(-60:20:100);
set(gca,'yticklabel',num2str(get(gca,'ytick')','%.0f'))
ax = gca;
ax.Xgrid = 'off';
ax.Ygrid = 'on';
ax.GridLineStyle = '-.';
ax.GridColor = [0.1 0.2 0.9];
```
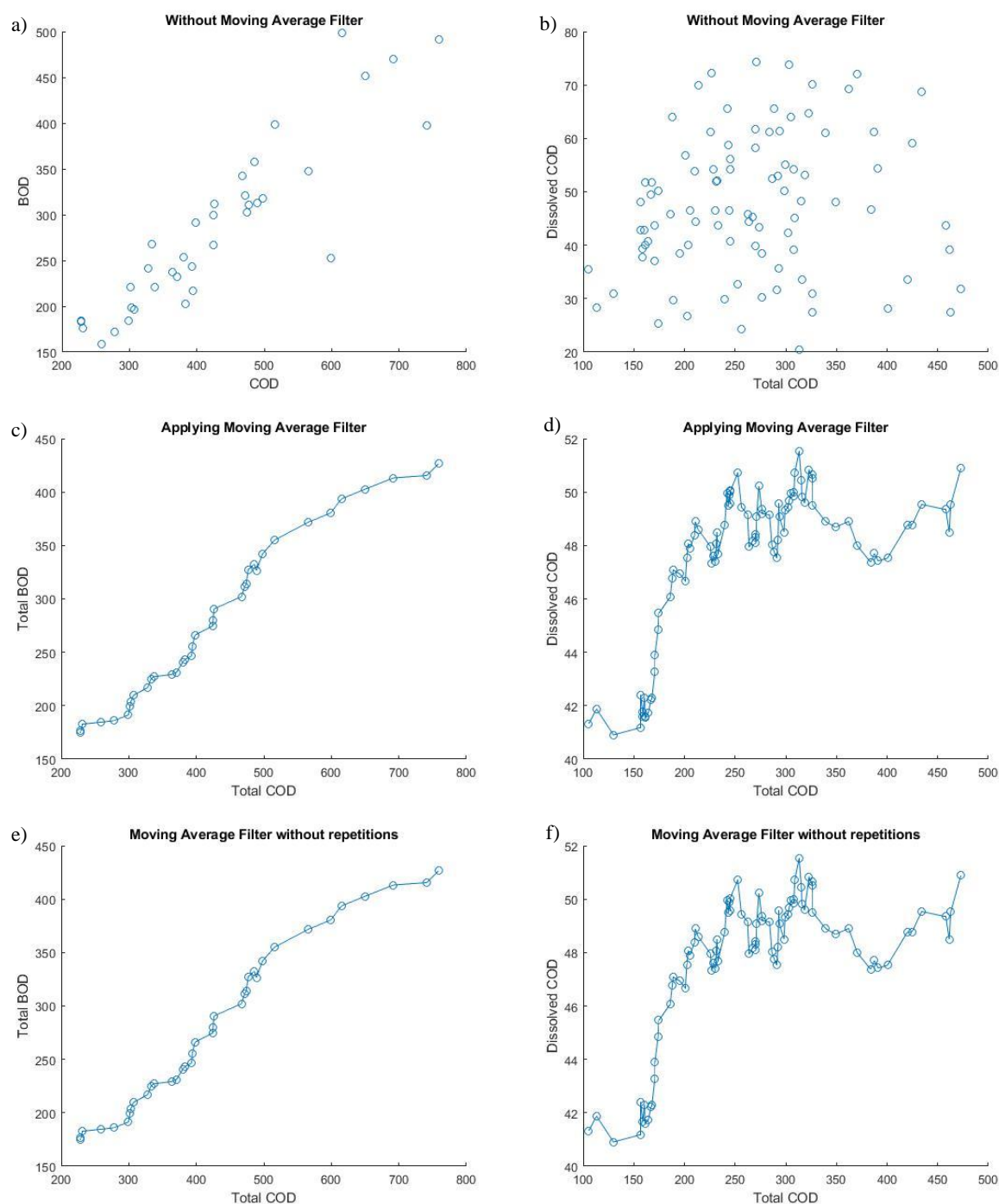
APPENDIX C – COD influent fractionation (graphics)

- Graphs generated during data processing with the code shown in Appendix B.

Figure 41. Graphs generated during data treatment for calculation of fractionation coefficients using data from WWTP Mangueira: Direct correlations between BOD_{total} and COD_{total} (a); between effluent $COD_{filtered}$ and affluent COD_{total} (b); correlation of BOD_{total} X COD_{total} using a moving average equal to 10 (c) and after removal of repeated values (e); correlation of effluent $COD_{filtered}$ X influent COD_{total} using a moving average of 50 (d) and after removal of repeated values (f).

Source: the author (2022).